

**EFFECT OF IMPELLER DESIGN ON DROP SIZES AND MASS
TRANSFER IN IMMISCIBLE LIQUID-LIQUID SYSTEM IN A
STIRRED VESSEL**

REZA AFSHAR GHOTLI

**FACULTY OF ENGINEERING
UNIVERSITY OF MALAYA
KUALA LUMPUR**

2018

**EFFECT OF IMPELLER DESIGN ON DROP SIZES AND
MASS TRANSFER IN IMMISCIBLE LIQUID-LIQUID
SYSTEM IN A STIRRED VESSEL**

REZA AFSHAR GHOTLI

**THESIS SUBMITTED IN FULFILMENT OF THE
REQUIREMENTS FOR THE DEGREE OF DOCTOR
OF PHILOSOPHY**

**FACULTY OF ENGINEERING
UNIVERSITY OF MALAYA
KUALA LUMPUR**

2018

UNIVERSITY OF MALAYA
ORIGINAL LITERARY WORK DECLARATION

Name of Candidate: Reza Afshar Ghotli

Registration/Matric No: KHA120085

Name of Degree: Doctor of Philosophy

Title of Project Paper/Research Report/Dissertation/Thesis (“this Work”):

EFFECT OF IMPELLER DESIGN ON DROP SIZES AND MASS TRANSFER IN
IMMISCIBLE LIQUID-LIQUID SYSTEM IN A STIRRED VESSEL

Field of Study: Chemical Engineering

I do solemnly and sincerely declare that:

- (1) I am the sole author/writer of this Work;
- (2) This Work is original;
- (3) Any use of any work in which copyright exists was done by way of fair dealing and for permitted purposes and any excerpt or extract from, or reference to or reproduction of any copyright work has been disclosed expressly and sufficiently and the title of the Work and its authorship have been acknowledged in this Work;
- (4) I do not have any actual knowledge nor do I ought reasonably to know that the making of this work constitutes an infringement of any copyright work;
- (5) I hereby assign all and every rights in the copyright to this Work to the University of Malaya (“UM”), who henceforth shall be owner of the copyright in this Work and that any reproduction or use in any form or by any means whatsoever is prohibited without the written consent of UM having been first had and obtained;
- (6) I am fully aware that if in the course of making this Work I have infringed any copyright whether intentionally or otherwise, I may be subject to legal action or any other action as may be determined by UM.

Candidate’s Signature

Date: 08.04.2018

Subscribed and solemnly declared before,

Witness’s Signature Date:

Name:

Designation:

EFFECT OF IMPELLER DESIGN ON DROP SIZES AND MASS TRANSFER IN IMMISCIBLE LIQUID-LIQUID SYSTEM IN A STIRRED VESSEL

ABSTRACT

Impeller design is one of the determinant factors for mixing performance in stirred vessels. In this work, performances of conventional and new impeller designs were evaluated for liquid-liquid dispersion. Drops size analysis and mass transfer characteristics studies were conducted at a specific energy input. The experiments were conducted in a standard cylindrical tank of 0.3 m diameter with a single impeller set-up. The impellers used were Rushton turbine, up-flow and down-flow pitched-blade turbines, half-circular blade turbine, elliptical blade turbine, parabolic blade turbine, hydrofoil impeller and double circular blades turbine that covers both the axial and radial flow impellers. Prior to mass transfer characteristics study and drop size analyses, the power number, mixing time and air entrainment speed were determined at various Reynolds numbers for all the impellers in a single phase system. Mixtures of palm-oil in water in a range of 1-10% v/v were selected as a liquid-liquid system. The power was measured using a suspended motor system and photographic method was used for drop size measurements. Mass transfer study was performed in a system with a hydrolysis reaction. The results showed that at the same energy dissipation rate, the hydrofoil impeller produced the largest mean drop size diameter (d_{32}) and the double curved blade turbine produced the smallest, about 37% lower. In the case of radial flow impellers, smaller drops size values were obtained for the impellers with larger curvature angle. Increasing the dispersed phase from 1 to 10% increased the d_{32} by about 20 to 40% due to higher collision frequency between drops. Therefore, higher interfacial areas were obtained using double curved blade impeller and pitched blade down flow turbine. Mass transfer coefficients were determined using Batchelor proposed correlation. The highest mass transfer coefficients were obtained at 1.08×10^{-5} and 1.02×10^{-5} (m.s^{-1}) for the

double curved blade impeller and pitched blade down flow turbine, respectively. This proved the suitability of these impellers for liquid-liquid dispersion within the Reynolds number range of 50×10^4 to 80×10^4 . In the case of reactive system, the experiments at the same energy dissipation rate ($\epsilon = 0.16 \text{ m}^2/\text{s}^3$) recorded the highest production rate in a range of 0.21×10^{-3} to 0.55×10^{-3} and 0.20×10^{-3} to 0.54×10^{-3} mole/ m^3 for double curved blade and pitched blade down flow impellers, respectively. This is due to the larger impeller swept area and longer residence time of vortices at the impeller tip speed which resulted in a higher mass transfer rate within the tank. In conclusion, for an energy efficient system, the pitched blade down flow turbine is the appropriate selection for the liquid-liquid systems whereas at the same energy consumption, the double curved blade impeller could be a suitable choice because of the better performance even in higher dispersed phase volume fraction.

Keywords: impeller design, impeller characterization, liquid-liquid mixing, drop size, mass transfer

**KESAN REKABENTUK PENGADUK KE ATAS SAIZ TITISAN DAN
PEMINDAHAN JISIM BAGI SISTEM CECAIR-CECAIR TAK TERLARUT
DALAM TANGKI TERADUK**

ABSTRAK

Rekabentuk pengaduk merupakan salah satu faktor penentu bagi pencapaian pengadukkan di dalam tangki teraduk. Di dalam kajian ini, pencapaian pengaduk konvensional dan pengaduk rekabentuk baru telah dinilai bagi penyerakan cecair-cecair. Bagi tujuan ini, analisa saiz titisan dan kajian ciri-ciri pemindahan jisim telah dijalankan pada masukan tenaga tertentu. Ujikaji telah dijalankan di dalam tangki silinder piawai, berdiameter 0.3 m, dengan pemasangan pengaduk tunggal. Pengaduk yang digunakan adalah turbin *Rushton*, turbin bilah-bercerun aliran atas dan turbin bilah-bercerun aliran bawah, turbin bilah separa bulat, turbin bilah bujur, turbin bilah parabola, pengaduk hidrofoil dan rekabentuk baru turbin bilah bulat berkembar yang merangkumi kedua-dua pengaduk aliran paksi dan pengaduk aliran jejarian. Sebelum menjalankan kajian ciri-ciri pemindahan jisim dan analisa saiz titisan, nombor kuasa, masa pengadukkan dan kelajuan pemerangkapan udara pada pelbagai nombor *Reynolds* bagi kesemua pengaduk telah dicirikan di dalam sistem fasa tunggal. Campuran air dan minyak sawit di dalam julat 1-10% v/v telah dipilih sebagai sistem cecair-cecair. Kuasa telah diukur menggunakan sistem motor tergantung dan kaedah fotografik telah digunakan bagi pengukuran saiz titisan. Kajian pemindahan jisim telah dijalankan di dalam sistem bersama tindakbalas hidrolisis. Keputusan menunjukkan bahawa pada kadar pelepasan tenaga yang sama, pengaduk hidrofoil memberikan diameter saiz titisan purata (d_{32}) terbesar manakala turbin bilah melengkung berkembar memberikan diameter terkecil, kira-kira 37% lebih rendah. Di dalam kes pengaduk aliran jejarian, saiz titisan yang lebih rendah telah diperolehi bagi pengaduk dengan sudut lengkungan yang lebih besar. Peningkatan fasa serakan dari 1 - 10% telah meningkatkan d_{32} kira-kira sebanyak 20 -

40%, disebabkan oleh kekerapan perlanggaran yang lebih tinggi di antara titisan. Maka, ruang antaramuka yang tinggi telah diperolehi bagi pengaduk bilah melengkung berkembar dan turbin bilah-bercerun aliran bawah. Pekali pemindahan jisim telah ditentukan menggunakan hubungkait *Batchelor* yang dicadangkan. Pekali pemindahan jisim tertinggi telah diperolehi bagi pengaduk bilah melengkung berkembar dan turbin bilah-bercerun aliran bawah, masing-masing pada 1.08×10^{-5} dan 1.02×10^{-5} ($\text{m}\cdot\text{s}^{-1}$). Ini membuktikan kesesuaian kesemua pengaduk ini bagi penyerakan cecair-cecair di dalam lingkungan julat nombor *Reynolds* 50×10^4 hingga 80×10^4 . Di dalam kes sistem bertindakbalas, ujikaji pada kadar pelepasan tenaga yang sama ($\epsilon = 0.16 \text{ m}^2\cdot\text{s}^{-3}$) mencatatkan kadar penghasilan tertinggi di dalam julat 0.21×10^{-3} hingga 0.55×10^{-3} dan 0.20×10^{-3} hingga $0.54 \times 10^{-3} \text{ mol}\cdot\text{m}^{-3}$ masing-masing bagi pengaduk bilah melengkung berkembar dan turbin bilah-bercerun aliran bawah. Ini disebabkan oleh ruang sapuan pengaduk yang lebih besar dan masa *residence* vorteks yang lebih lama pada hujung pengaduk, yang mengakibatkan kadar pemindahan jisim yang lebih baik dan tinggi di dalam tangki. Kesimpulannya, bagi sistem cekap tenaga, turbin bilah-bercerun aliran bawah merupakan pemilihan yang sesuai bagi sistem cecair-cecair, manakala pada penggunaan tenaga yang sama, pengaduk bilah melengkung berkembar boleh menjadi pilihan yang sesuai kerana pencapaian yang lebih baik walaupun di dalam pecahan isipadu fasa serakan yang lebih tinggi.

Kata kunci: rekabentuk pengaduk, pencirian pengaduk, pengadukkan cecair-cecair, saiz titisan, pekali jisim

ACKNOWLEDGMENTS

I am very grateful to God without his grace and blessing this degree would not have been possible. I would like to express my greatest gratitude to my supervisors Prof. Ir. Dr. Abdul Aziz Abdul Raman and Prof. Dr. Shaliza Ibrahim, for their encouragement and support throughout the course of this research. This work would not have been completed without their positive and methodological approach, constant encouragement and inspiration at times when I went astray. I truly appreciate the freedom given to me, to explore new ideas and their ability to keep me focused in the right direction.

My sincere appreciation goes to the University of Malaya High Impact Research Fund (HIR); “UM.C/625/1/HIR-MOHE/ENG/38” for financial support through this research work.

I am also grateful to all the faculty members of the Department of Chemical Engineering, my lab mates, my friends and everybody who helped me during my research work and for their useful suggestions, as well as expressing my apology that I could not mention personally one by one.

Last but definitely not least, I wanted to thank my wife, my parents and my brother for their endless love, support and encouragement to pursue this degree.

To all the above, and anyone who I may have missed, thank you.

Reza Afshar Ghotli

April 2018

TABLE OF CONTENTS

| | |
|--|----------|
| ABSTRACT | III |
| ABSTRAK | V |
| ACKNOWLEDGMENTS | VII |
| TABLE OF CONTENTS | VIII |
| LIST OF FIGURES | XI |
| LIST OF TABLES | XIII |
| LIST OF SYMBOLS AND ABBREVIATIONS | XIV |
| LIST OF APPENDICES | XX |
| CHAPTER 1: INTRODUCTION | 1 |
| 1.1 Background | 1 |
| 1.2 Problem Statement | 2 |
| 1.3 Objectives | 3 |
| 1.4 Significance of the Research | 4 |
| 1.5 Research Scopes | 5 |
| 1.6 Thesis outline | 5 |
| CHAPTER 2: LITERATURE REVIEW | 7 |
| 2.1 Review Approach | 7 |
| 2.2 Introduction | 8 |
| 2.3 Impeller Characterization | 9 |
| 2.3.1 Power Consumption | 9 |
| 2.3.2 Air entrainment point | 12 |
| 2.3.3 Mixing time | 13 |
| 2.3.4 Drop size distribution (DSD) | 16 |
| 2.3.5 Liquid- Liquid Mass Transfer | 28 |
| 2.3.5.1 Effect of liquid-liquid reaction | 28 |
| 2.3.5.2 Mass Transfer Models | 29 |
| 2.3.5.3 Mass Transfer Coefficient | 30 |
| 2.3.5.3.1 Continuous Phase Mass Transfer Coefficient | 38 |
| 2.3.5.3.2 Dispersed Phase Mass Transfer Coefficient | 42 |

| | | |
|--|--|-----------|
| 2.4 | Summary of Literature Review | 46 |
| CHAPTER 3: METHODOLOGY | | 48 |
| 3.1 | Introduction | 48 |
| 3.2 | Experimental Set up | 49 |
| 3.3 | Impellers..... | 50 |
| 3.4 | Materials..... | 52 |
| 3.5 | Analysis..... | 54 |
| 3.5.1 | Power and power number determination | 54 |
| 3.5.2 | Reynolds number | 55 |
| 3.5.3 | The point of air entrainment..... | 55 |
| 3.5.4 | Mixing time..... | 56 |
| 3.5.5 | Interfacial tension..... | 57 |
| 3.5.6 | Diffusivity measurement..... | 57 |
| 3.5.7 | Drop size measurement..... | 58 |
| 3.5.8 | Correlation study..... | 62 |
| 3.5.8.1 | Mixing time correlation..... | 62 |
| 3.5.8.2 | Drop size correlation..... | 63 |
| 3.5.9 | Mass Transfer Study | 63 |
| 3.5.10 | Impeller Efficiency in a Typical Reactive System..... | 64 |
| 3.5.10.1 | Determination of hydrolysis rate..... | 64 |
| 3.5.10.2 | Kinetic Mathematical Model..... | 65 |
| 3.6 | Safety Precautions..... | 67 |
| CHAPTER 4: RESULTS AND DISCUSSION | | 68 |
| 4.1 | Introduction..... | 68 |
| 4.2 | Impeller characterization..... | 68 |
| 4.2.1 | Power number | 68 |
| 4.2.2 | The effect of impeller off-bottom clearance on N_p | 70 |
| 4.2.3 | Air entrainment speed | 72 |
| 4.2.4 | Mixing time..... | 75 |
| 4.2.4.1 | Effect of various impeller type on mixing time | 75 |
| 4.2.4.2 | Effect of clearance on mixing time | 78 |
| 4.2.4.3 | Mixing time correlation..... | 79 |
| 4.2.5 | Mixing efficiency..... | 82 |

| | | |
|--|---|------------|
| 4.3 | Drop size evaluation..... | 84 |
| 4.3.1 | Spatial uniformity of dispersions | 84 |
| 4.3.2 | Equilibrium time | 84 |
| 4.3.3 | The effect of impeller types on drop size..... | 85 |
| 4.3.4 | Effect of dispersed phase volume fraction..... | 87 |
| 4.3.5 | Drop size correlation | 88 |
| 4.4 | Mass Transfer Study | 92 |
| 4.4.1 | Evaluation of mass transfer coefficient in non-reactive system..... | 92 |
| 4.4.2 | Impeller Performance in a Typical Reactive System..... | 94 |
| 4.4.2.1 | The effect of impeller type on the reaction rate | 94 |
| 4.4.2.2 | The effect of dispersed phase volume fraction on the reaction rate..... | 96 |
| 4.4.3 | Evaluation of mass transfer coefficient in reactive system..... | 98 |
| 4.4.3.1 | Kinetic Modeling | 99 |
| CHAPTER 5: CONCLUSION..... | | 101 |
| 5.1 | Conclusion | 101 |
| 5.2 | Recommended future works | 104 |
| REFERENCES..... | | 105 |
| LIST OF PUBLICATION AND PAPERS PRESENTED | | 118 |
| APPENDIX A..... | | 120 |
| APPENDIX B | | 121 |
| APPENDIX C | | 122 |
| APPENDIX D..... | | 130 |

LIST OF FIGURES

| Figure | Description | Page |
|------------|---|------|
| Figure 2.1 | Overview of literature study | 7 |
| Figure 2.2 | Schematic representation of drop break-up and coalescence in the liquid-liquid system. | 17 |
| Figure 3.1 | Overview of experimental methodology | 48 |
| Figure 3.2 | Experimental set up: 1. Motor; 2. Motor speed controller; 3. Power analyzer; 4. Impeller shaft; 5. Impeller; 6. Tank | 50 |
| Figure 3.3 | The Impeller used: (a) RT, (b) CB, (c) PBTU, (d) PBTD, (e) EB, (f) PB, (g) HE3, (h) DCB | 52 |
| Figure 3.4 | Mixing time measurement: A; Motor, B; Shaft, C; Impeller, D; Tank, E: Speed analyzer, F; Power analyzer, G1 and G2; Conductivity probes, H; Conductivity meter controller, I; Data logger, J; Computer, K; Injection point | 56 |
| Figure 3.5 | Overview of image processing procedure | 62 |
| Figure 4.1 | Comparison of NP values for DCB (\circ), RT (\blacklozenge), CB (\blacksquare), EB (\blacktriangle), PB (\bullet), PBTU (\diamond), PBTD (\blacktriangle) and HE3 (\square) at $C/T=1/3$ | 69 |
| Figure 4.2 | The effect of clearance on energy dissipation rate in various impellers and agitation speed; (a) 1.67 rps, (b) 3.33 rps, (c) 5 rps, (d) 6.67 rps, (e) 8.33 rps | 72 |
| Figure 4.3 | NE as a function of the impeller clearance and agitation speed for RT (\blacklozenge), CB (\blacksquare), PBTD (\blacktriangle), PBTU (\diamond), EB (\blacktriangle), PB (\bullet) and DCB (\circ) | 74 |
| Figure 4.4 | Mean energy dissipation rate at the point of air entrainment as a function of impeller clearance for RT (\blacklozenge), CB (\blacksquare), PBTD (\blacktriangle), PBTU (\diamond), EB (\blacktriangle), PB (\bullet) and DCB (\circ) | 75 |
| Figure 4.5 | Mixing time against Reynolds number for the studied impellers | 76 |
| Figure 4.6 | Comparison of the mixing time for different impellers at the same power consumption | 77 |
| Figure 4.7 | The effect of impeller clearance on mixing time at 5 rps | 79 |
| Figure 4.8 | Graphical evaluation of the fit of the experimental data to the proposed mixing time correlation for different impellers | 81 |
| Figure 4.9 | The efficiency of studied impellers in different agitation speed and clearance level | 83 |

| Figure | Description | Page |
|---------------|---|-------------|
| Figure 4.10 | Drops equilibrium time for each impeller in different agitation times and dispersed phase hold up | 86 |
| Figure 4.11 | Effect of dispersed phase volume fraction on dimensionless drop size (d_{32}/D) for all impellers | 88 |
| Figure 4.12 | Graphical evaluation of the proposed drop size correlation for different impellers | 91 |
| Figure 4.13 | The effect of different impeller designs on interfacial area in oil-in-water system with different dispersed phase volume fraction at $\epsilon=0.16 \text{ m}^2/\text{s}^3$ | 93 |
| Figure 4.14 | The effect of different impeller designs on mass transfer coefficient in oil-in-water system with different dispersed phase volume fraction at $\epsilon=0.16 \text{ m}^2/\text{s}^3$ | 94 |
| Figure 4.15 | The rate of FFA production for 1% oil in water mixture; Vs. time for various impellers: \circ DCB; \blacktriangle PBTD; \blacklozenge RT; \diamond PBTU; \blacksquare CB; \triangle EB; \bullet PB; \square HE3 at $\epsilon=0.16 \text{ m}^2/\text{s}^3$ | 96 |
| Figure 4.16 | The rate of FFA production for 3% oil in water mixture; Vs. time for various impellers: \circ DCB; \blacktriangle PBTD; \blacklozenge RT; \diamond PBTU; \blacksquare CB; \triangle EB; \bullet PB; \square HE3 at $\epsilon=0.16 \text{ m}^2/\text{s}^3$ | 97 |
| Figure 4.17 | The rate of FFA production for 5% oil in water mixture; Vs. time for various impellers: \circ DCB; \blacktriangle PBTD; \blacklozenge RT; \diamond PBTU; \blacksquare CB; \triangle EB; \bullet PB; \square HE3 at $\epsilon=0.16 \text{ m}^2/\text{s}^3$ | 97 |
| Figure 4.18 | The effect of different impeller designs on mass transfer coefficient in a reactive system with different dispersed phase volume fraction at $\epsilon=0.16 \text{ m}^2/\text{s}^3$ | 98 |
| Figure 4.19 | Comparison between experimental results and modeling for all studied impeller at 1% dispersed phase volume fraction | 100 |

LIST OF TABLES

| Table | Description | Page |
|--------------|---|-------------|
| Table 2.1 | Some of previous power number values for different impeller designs | 11 |
| Table 2.2 | Some of the published work on drop size measurements | 25 |
| Table 2.3 | Mass transfer coefficient equations in liquid-liquid mixing system | 33 |
| Table 3.1 | Geometrical details of the stirred vessel | 49 |
| Table 3.2 | Description of the impellers used | 51 |
| Table 3.3 | Physical properties of the dispersed and continuous phases | 54 |
| Table 4.1 | Calculated parameters of the proposed mixing time correlation and associated R^2 and Δq (%) for different impellers | 80 |
| Table 4.2 | Mean drop size diameter in a mixture of 1% palm oil in water at $P/V=160 \text{ W/m}^3$ | 84 |
| Table 4.3 | Calculated parameters of the proposed drop size correlation and associated R^2 and Δq (%) for different impellers | 89 |
| Table 4.4 | The reaction rate constants for all studied impellers with varying oil volume fraction | 99 |

LIST OF SYMBOLS AND ABBREVIATIONS

| | |
|----------------|--|
| a_v | Interfacial area per unit volume of dispersion, m^2/m^3 |
| B_n | Proportionally constant, dimensionless |
| C | Impeller off- bottom clearance, m |
| C_1 to C_8 | Dimensionless constant |
| $[C]$ | Concentration of reactive species, $g\ mole/cm^3$ |
| C^* | Solubility of the solute in the phase into which it is transferred, $gmole/cm^3$ |
| $C_{(t)}$ | Concentration of the trace at time (t) |
| C_0 | Initial concentration of the trace at time (0) |
| C_∞ | Final average concentrations of tracer |
| C_A | Bulk concentration of A, $mol\ m^{-3}$ |
| C_B | Bulk concentration of B, $mol\ m^{-3}$ |
| C_A/C_B | Concentration ratio of the reactants, dimensionless |
| C_{CB} | Equilibrium concentration of dispersed phase, mol/m^3 |
| \bar{C}_{CB} | Concentration of chlorobenzene, mol/m^3 |
| C/T | Ratio of impeller clearance to tank diameter, dimensionless |
| D | Diffusion coefficient of the solute in the phase into which it is transferred, $m^2\ s^{-1}$ |
| D_A | Molecular Diffusivity of A in continues phase, $m^2\ s^{-1}$ |
| D_{AB} | Molecular diffusion coefficient, $m^2\ s^{-1}$ |
| D_{oe} | Overall effective diffusivity, $m^2\ s^{-1}$ |

| | |
|--------------|---|
| D_d | Diffusion coefficient of the solute in the dispersed phase, $m^2 s^{-1}$ |
| d | Drop or particle diameter, m |
| d_i | Nominal diameter of drops, μm |
| d_I | Impeller diameter, m |
| d_I/T | Ratio of impeller diameter to tank diameter, dimensionless |
| d_{32} | Sauter mean diameter of droplets, μm |
| d_{max} | Maximum diameter, μm |
| Fr | Impeller Froude number ($N^2 D/g$), dimensionless |
| g | Gravitational acceleration, or breakage frequency, $m s^{-2}$ |
| g_c | Conversion factor, $kg m kg_f^{-1} s^{-2}$ |
| H | Liquid height, m |
| H_A | Hatta Number, dimensionless |
| k | Pseudo-first-order reaction rate constant, s^{-1} |
| k_2 | Second-order reaction rate constant, $m^3 mole^{-1} s^{-1}$ |
| k_d | Dispersed phase mass transfer coefficient, $m s^{-1}$ |
| k_c | Continuous phase mass transfer coefficient, $m s^{-1}$ |
| k_L | Overall mass transfer coefficient, $m s^{-1}$ |
| $k_L \alpha$ | Volumetric mass transfer coefficient, s^{-1} |
| l | Volume fraction of the phase within which A and B reacts (for this particular system, the continuous phase) |
| M | Mean molecular weight of phase under consideration, gr |
| m | Distribution coefficient among the phases ($m = C_{d,eq}/C_{c,eq}$) |

| | |
|------------|---|
| N | Impeller rotational speed, rps or rpm |
| N_{cd} | Minimum agitation speed, rps or rpm |
| N_Q | Gas flow number, dimensionless |
| n | A number, n |
| n_i | Number of drops, n |
| P | power required by the impeller, $\text{kg m}^2\text{s}^{-3}$ |
| P_0 | Impeller power number, dimensionless |
| P/V | power dissipation per unit volume, W/m^3 |
| R | Enhancement factor |
| R_a | Extraction rate per unit area, $\text{kg mol.cm}^{-2}\text{s}^{-1}$ |
| R' | Outer radius of continuous phase shell, m |
| Re | Impeller Reynolds number ($\rho_c N d_I^2 / \mu_C$), dimensionless |
| r | Rate of formation of products, mol s^{-1} |
| Sc | Viscous diffusion rate /Molecular (mass) diffusion rate, the Schmidt number ($\nu/D = \mu/\rho D$), dimensionless |
| Sh | Sherwood number, dimensionless |
| Sh_d | Dispersed phase Sherwood number, dimensionless |
| T | Tank diameter, m |
| t | Time, s |
| t_c | Circulation time, s |
| t_f | Single drop formation time, hr |
| $t_{F,95}$ | Time at which 95% of the possible mass transfer has occurred, s |

| | |
|----------|---|
| t_m | Mixing time, s |
| t_{95} | Mixing time to 95% reduction in variance, s |
| U | Mean drop velocity, relative to the surrounding media, $m s^{-1}$ |
| u_t | Droplet terminal velocity, $m s^{-1}$ |
| u | Mean drop velocity, $m s^{-1}$ |
| V | Filled volume of the tank, given by $(1 + \emptyset)V_C$ (L) |
| V_c | Continuous phase volume, dm^3 |
| V_i | Viscous number, dimensionless |
| W_{eT} | Weber Number, dimensionless |

Abbreviations

| | |
|------|--|
| B | Baffles |
| CB | Half-circle curved blade impeller |
| DCB | Dabble half-circle curved blade impeller |
| DSD | Drop size distribution |
| EB | Half-elliptical curved blade impeller |
| FFA | Free fatty acids |
| HE3 | Hydrofoil impeller |
| LPM | Liter per minute |
| O/W | Oil-in-Water dispersion |
| PBTD | Pitched blade down-flow turbine |
| PBTU | Pitched blade up-flow turbine |

| | |
|-----|--------------------------|
| PT | Parabolic blade impeller |
| RT | Rushton Turbine |
| W/O | Water-in-Oil dispersion |

Greek Letters

| | |
|--------------------|--|
| θ_c | Circulation time, s |
| θ_C | Time between coalescence, s |
| τ | Torque, N·m |
| φ | Dispersed phase volume fraction or holdup, % |
| ρ | Density, kg/m ³ |
| μ | Viscosity, kg/s m |
| λ_n | <i>n</i> th coefficient, dimensionless |
| ε_{av} | Energy dissipation rate per unit mass of fluid, m ² /s ³ |
| \emptyset | Dispersed phase volume fraction, % |
| $\Delta\rho$ | Density difference between phases, kg m ⁻³ |
| ρ_d | Dispersed phase density, kg m ⁻³ |
| ρ_c | Continuous phase density, kg m ⁻³ |
| μ_d | Dispersed phase viscosity, kg m ⁻¹ s ⁻¹ |
| K | Viscosity ratio (i.e., μ_d/μ_c) |
| ν | Kinematic viscosity, m ² s ⁻¹ |
| ν_c | Continuous phase kinematic viscosity, m ² s ⁻¹ |
| σ | Interfacial tension, N/m |

η Mixing efficiency

Subscripts

c Continuous phase

d Dispersed phase

University of Malaya

LIST OF APPENDICES

| | | |
|------------|--|-----|
| Appendix A | The effect of clearance on energy dissipation rate in various impellers and agitation speeds | 120 |
| Appendix B | The effect of clearance on power number in various impellers | 121 |
| Appendix C | The response of two conductivity sensors for various impellers at different speeds | 122 |
| Appendix D | Comparison between experimental results and modeling for all studied impeller at different dispersed phase volume fraction | 130 |

University of Malaya

CHAPTER 1: INTRODUCTION

1.1 Background

Liquid-liquid dispersion in stirred vessels is a key process in various industries such as chemical, biotechnological, pharmaceutical, and food processing. The objective of this unit is to generate essential interfacial area to support mass and heat transfer between phases. The efficiency of liquid-liquid mixing can be evaluated through the measurement of several parameters, such as power consumption, mixing time, circulation time, minimum agitation speed, break up and coalescence, drop size distribution, interfacial area and phase inversion. Changes in the input parameters, such as impeller design, impeller power number, impeller flow pattern, number of impellers, dispersed phase volume fraction and physical properties of phases (viscosity and density) can affect the liquid-liquid mixing efficiency.

The hydrodynamics in a stirred vessel have a strong influence on the mixing efficiency. Therefore, understanding agitation hydrodynamics is critical from the product quality and process economics points of views. This is necessary, to minimize investment and operating costs and to provide high yields and accordingly improving profitability. Generally, mixing of liquids by a mechanical agitation system in a stirred vessel is conducted by transfer of momentum from an impeller to the liquid. Therefore, various designs of impellers have been fabricated to achieve efficient mixing with the lowest power consumption for various applications in stirred vessels. Impeller selection commonly proceeds based on a number of parameters, such as viscosity of the fluid, operating conditions, system flow regime, etc. Several attempts have been carried out to evaluate the efficiency of mixing of liquid-liquid mixing in stirred vessels equipped with different designs of impellers. Although, several impellers have been designed and developed for better efficiency in many applications, Rushton turbine, pitched blade

turbines and propellers are the most common ones. Rushton turbine, which has been widely employed for gas-liquid dispersion has several disadvantages. For example, the flat blade generates pair of high speed and low pressure trailing vortices at the back side of the blades. Dispersion in mixing tanks is controlled by the turbulence flow, which is produced by the vortices. On the other hand, the trailing vortices results in high power number under un-aerated conditions, which cause high torque for each speed and consequently, increase the operating cost. Thus, the high power consumption and considerable drop at aerated conditions are some of the weakness of Rushton turbine. Therefore, it would be essential to find alternatives to the Rushton turbine.

1.2 Problem Statement

Several works found in the literature, discussed the efficiency of liquid-liquid mixing through different variables in mixing tanks. However, there is lack of information on the effect of impeller designs on immiscible liquid-liquid mixing vessels. Therefore, further studies are needed to investigate the effect of various impeller designs on drop size and mass transfer rate for immiscible liquid-liquid system. Also, hydrolysis of oil was found to be one of the important liquid-liquid processes to yield valuable high purity unsaturated fatty acids and glycerol. Many works have been conducted to increase the interfacial area and the efficiency of the process using stirred vessel equipped with Rushton turbine. However, these studies mainly focused on oil to water ratio, surfactant, additives and etc. The main limitation of these studies is that the role of agitation parameters such as impeller and tank designs, agitation speed and so on have not been considered. Furthermore, most of the experiments have been performed in small scale set-ups. This leads us to design the experiments based on semi-industrial scale set-up.

Therefore, in this work, drop size and mass transfer characterizations have been performed in oil in water system for various designs of impellers, including conventional and new impeller designs, namely Rushton turbine (RT), 45- up flow

pitched-blade turbine (PBTU), 45- down flow pitched-blade turbine (PBTU), semicircular blade turbine (CB), double circular blades turbine (DCB), elliptical blade turbine (EB), parabolic blade turbine (PB) and hydrofoil impeller (HE3). The impeller characterization was carried out through power consumption, mixing time and air entrainment point measurements in a single phase system at various clearances and agitation speeds. Drop size measurement performed for immiscible liquid-liquid system with different dispersed phase ratios and a drop size correlation developed based on the experimental results. Furthermore, the mass transfer coefficient was evaluated for all studied impellers in non-reactive immiscible liquid-liquid system (Oil-in-water) and in a reactive system with hydrolysis reaction inside the stirred vessel. It is expected to obtain better axial flow impeller efficiency compared with the radial flow impellers. Therefore, the main questions this work aims to quantify the efficiency of different design of impellers for liquid-liquid dispersion to improve the mixing performance. It is expected to obtain better axial flow impeller efficiency compared with the radial flow impellers. Therefore, the main questions this work is focused on are:

1. What is the effect of impeller blade design of mechanical stirring and off bottom clearance level on power number, air entrainment and mixing time?
2. What is the effect of impeller blade design of mechanical stirring and dispersed phase ratio on drop sizes in an immiscible liquid-liquid system?
3. What is the effect of impeller design of mechanical stirring and dispersed phase ratio on mass transfer rate in an immiscible liquid-liquid system?
4. Which is the best impeller for the liquid-liquid mixing?

1.3 Objectives

The following objectives were defined to find out a solution for the up-mentioned questions;

- 1) To characterize the various designs of impellers in a single phase. The activities to achieve this objective are as follows;
 - i. Power consumption measurements in a range of Reynolds number and clearance levels.
 - ii. Mixing time determination in a range of agitation speeds and clearance levels.
 - iii. Air entrainment point at different clearance levels.
- 2) To develop a new correlation to predict mixing time based on the energy dissipation rate and clearance in a single phase system.
- 3) To determine drop size and correlation study to predict drop size in an immiscible liquid-liquid system (oil- in-water) with different impeller designs and dispersed phase ratio and in various dispersed phase fraction. The activities to achieve this objective are as follows;
 - i. Determination of equilibrium condition for impellers at different dispersed phase ratio
 - ii. Drop size measurement for each impeller at different dispersed phase ratio.
- 4) To characterize mass transfer for each impeller at different dispersed phase ratio.

The following activities have been carried out to achieve this objective;

- i. The mass transfer coefficient calculation for each impeller in non-reactive immiscible liquid-liquid system.
- ii. The effect of impeller designs on reaction rate through hydrolysis reaction.

1.4 Significance of the Research

This study provides a comparative study on the effect of conventional and new impeller designs on drops sizes and mass transfer rates in an immiscible liquid-liquid system

with a semi-industrial scale set-up. A range of radial flow and axial flow impeller designs, in addition to a newly developed double curve blade impeller, were selected for the purpose of determining the most efficient impeller design in liquid-liquid system.

1.5 Research Scopes

1. Amongst different impeller designs, eight were selected to cover axial and radial flow impellers, up-flow and down flow impellers, and conventional and new impeller designs.
2. The characterizations of impellers were carried out in a single phase system.
3. Drop size measurement was performed in non-reactive oil-in-water system with the dispersed phase range of 1 to 10%.
4. The mass transfer rate was evaluated for a typical hydrolysis reaction with a dispersed range of 1 to 5%.
5. The experiment was conducted in batch mode at 1 atm pressure and selected temperature.

1.6 Thesis outline

Chapter 1: Introduction

This introductory chapter provides a brief overview to the research, research questions, problem statements, the aims, the objectives and important aspects of this study.

Chapter 2: Literature Review

The literature review chapter gives a comprehensive review on effective parameters for impeller characterizations. The role of impeller designs on mixing efficiency is explained. Moreover, a review on drop size and the mass transfer correlation in liquid-liquid mixing system is presented. Measurement techniques and the significance of results have been presented and discussed. The effects of input parameters on mixing efficiency were also investigated.

Chapter 3: Methodology

This chapter presents the research designs and methodologies to fulfill the research questions and objectives. The list of chemicals and materials used in this work are described. Detailed information on the experimental set-up and equipment, experimental procedure and analytical techniques and the analysis methods also provided.

Chapter 4: Results and Discussions

This chapter represents the experimental results and gives a comprehensive discussion. Experimental data including power consumption values in different clearance levels and Reynolds numbers, air entrainment points and mixing times in various clearance levels for a single phase system are presented and analyzed. The drop size results in immiscible liquid-liquid systems and reaction rate data for the oil hydrolysis reaction with various designs of impellers are described and analyzed. The correlations have been developed based on the experimental data for the drop size and mixing time.

Chapter 5: Conclusion and Recommendation for Future Work

The highlights of research results and findings are summarized in this chapter. The contribution of this study and recommendations for further research are also provided in this chapter.

CHAPTER 2: LITERATURE REVIEW

2.1 Review Approach

Liquid-liquid mixing performance can be evaluated by various parameters such as minimum agitation speed, mixing time, circulation time, power consumption, drop size distribution, break up and coalescence, interfacial area and phase inversion. These parameters can be affected by input parameters such as impeller design; impeller power number, number of impellers, and dispersed phase volume fraction, in addition to physical properties of phases such as viscosity and density. This section, aimed to investigate power consumption, mixing time, drop size distribution and mass transfer with the focus on the effect of impeller design. Furthermore, the most useful drop size and mass transfer correlation for liquid-liquid mixing system have been studied. The importance of liquid-liquid mixing parameters, the measurement methods and the results have been investigated briefly. Figure 2.1 presents the overview of literature study.

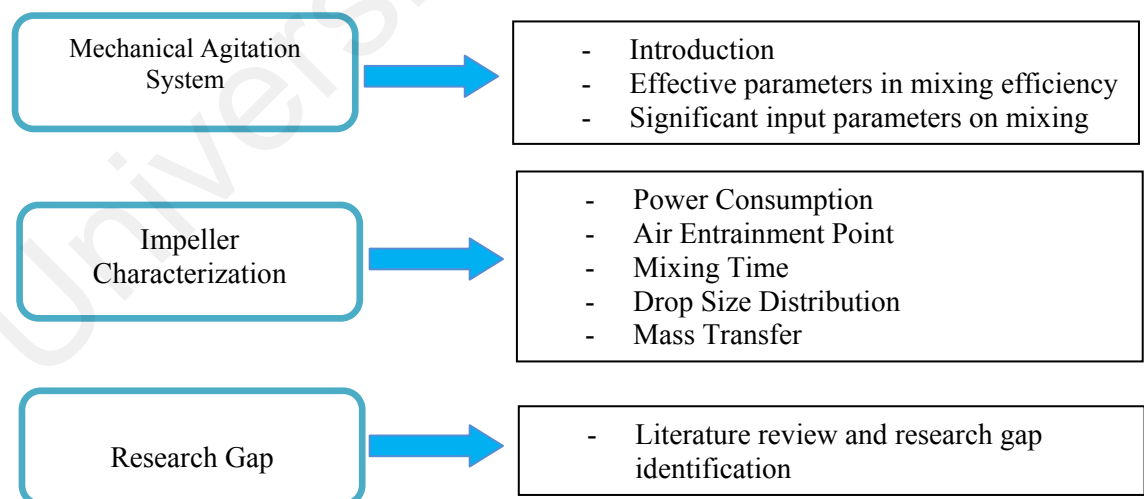


Figure 2.1: Overview of literature study

2.2 Introduction

Mixing is a key and common process to improve homogeneity and uniformity of systems. Mixing occurs when materials are moved from one area to another in the vessels (Chen et al., 2005; Rushton, 1956). Non-uniformity of systems can be explained as a gradient of properties such as concentration, viscosity, temperature, color, concentration, phase, temperature and etc. (Paul et al., 2004). Mixing operations can be divided into three main categories; gas-liquid, solid-liquid and liquid-liquid mixing.

Liquid-liquid mixing has been the subject of many industrial applications dealing with mass transfer such as solvent extraction, emulsification, multiphase reactions, distillation, humidification, liquid-liquid extraction, adsorption and ion exchange. It plays an important role in producing and increasing essential interfacial area to improve mass and heat transfer between phases (O'Rourke & MacLoughlin, 2005; Paul et al., 2004).

In general, mixing can be accomplished by mechanical agitation, rotor-stator mixer, static mixer, gas sparging, pumped circulation and extraction columns. Among these mixing facilities, the mechanical agitation system has proved to be the most efficient mixing device in terms of the average velocity throughout the whole tank per unit of power. Moreover, mixers can be employed either in batch or with continuous flow systems (Skelland & Moeti, 1990). Thus, wide range of impellers and mixers have been designed and created to achieve efficient mixing in various applications. Therefore, it is essential to understand the mechanism of mass transfer by certain types of impellers and mixers to optimize the design for more effective liquid-liquid dispersion. Impeller selection is depended on a number of factors, such as viscosity of fluid, operating

conditions, system flow regime, etc. (Paul et al., 2004). The most important parameters for impeller characterization will be described briefly in the following sections.

2.3 Impeller Characterization

2.3.1 Power Consumption

The amount of energy required per unit of time in a mechanically agitated tank bioreactor, chemical reactor, etc. is understood as power drawn or power consumption (Ascanio et al., 2004). The power number, a dimensionless group, has a significant effect on the definition of power consumption (Yapici et al., 2008). Therefore, it is one of the determinant factors in impeller selection. The vital role of the power drawn for the process and the mechanical design of mixing tank has been the subject of many studies since 1880 (Bujalski et al., 1987). Unwin in 1880 showed close relationships between power drawn (P) and tank diameter (T) and speed (N) for low-viscosity fluids (Bujalski et al., 1987);

$$P \propto N^3 d_I^5 \quad (2.1)$$

Experimentally, power consumption (P) is usually calculated directly from measurements of torque (τ) and impeller shaft speed (N):

$$P = 2\pi N\tau \quad (2.2)$$

Since, determination of power number is one of the impellers characterization tests, the present study tried to illustrate the relation between power and Reynolds number for various designs of impellers. The impeller power number is related to some dimensionless groups such a Reynolds number, Froude number and such geometrical ratios as d_I/T , C/T , H/T , etc. (Bujalski et al., 1987). Reynolds number (N_{Re}) is demonstrated in equation (2.3) which reveals the ratio of inertial forces to viscous forces.

$$N_{Re} = \frac{\rho N d_I^2}{\mu} \quad (2.3)$$

The central vortices can be eliminated and the Froude number is neglected For systems with a Reynolds number lower than 300 and for the baffled mixing tanks in the higher Reynolds number range (Paul et al., 2004). When a vortex occurs within the mixing tank, the Froude number, which is described in equation (2.4), becomes important.

$$\text{Fr number} = \frac{N^2 d_I}{g} \quad (2.4)$$

Under the same operating conditions, the geometrical ratios could also be neglected. Thus, impeller power number (N_p) is significantly related to Reynolds number (Chen et al., 2005):

$$N_p = \frac{P}{\rho_c N^3 d_I^5} \quad (2.5)$$

A comparison of different impellers would be helpful in determining the choice of an appropriate impeller for a dispersion process. Several works determined the power number of a wide range of impellers designs. Table 2.1 shows typical power number values for various designs of impellers.

Table 2.1: Examples power number values of different impeller designs

| Impeller design | Power Number Values | Reference |
|---|---------------------|------------------------------------|
| Down pumping 45° pitched blade turbines (PBT) | 1.7 | (Montante et al., 2005) |
| Down pumping 45° four pitched blade turbine | 0.99 | (El-Hamouz et al., 2009) |
| Down pumping 45° six pitched blade turbine | 1.77 | (Zhao et al., 2011) |
| Down pumping 45° six pitched blade turbine | 2.1 | (Ranade et al., 1992) |
| Sawtooth impeller | 0.32 | (El-Hamouz, 2009) |
| Concave blade (semi-circular) impeller | 2.8 | (Chen & Chen, 2000) |
| Concave blade (semi-circular) impeller | 3.8 | (Warmoeskerken & Smith, 1989) |
| Concave blade (semi-circular) impeller | 2.8 | (Karcz & Kaminska - Brzoska, 1994) |
| Concave blade (semi-circular) impeller | 3.0 | (Mhetras et al., 1994) |
| Lightnin A6000 impellers | 0.23 | (Weetman, 1988) |
| A310 fluidfoil impellers | 0.30 | (Weetman, 1988) |
| Propeller | 0.67 | (Shiue & Wong, 1984) |
| Propeller | 0.89 | (Ranade et al., 1992) |
| Curved pitched blade turbine | 2.41 | (Ranade et al., 1992) |
| Standard six blade Rushton turbine | 5.0 | (Pacek et al., 1999) |
| Convex pitched blade turbine | 2.29 | (Ranade et al., 1992) |
| Standard six blade Rushton turbine | 5.0 | (Bujalski et al., 1987) |
| Standard six blade Rushton turbine | 5.18 | (Rewatkar et al., 1990) |
| Standard six blade Rushton turbine | 6.0 | (Joanna Karcz & Major, 1998) |
| Standard six blade Rushton turbine | 5.58 | (Wu et al., 2001) |
| Standard six blade Rushton turbine | 5.4 | (Chen & Chen, 2000) |
| Standard six blade Rushton turbine | 5.77 | (Zhao et al., 2011) |

Turbines impellers are a good choice for dispersion of immiscible liquids even those that are quite viscous. Turbine impellers exhibit differing flow patterns and shear levels depending on whether they are axial flow, radial flow, hydrofoil or high shear designs.

Impeller flow patterns have considerable effect on mixing (Paul et al., 2004). The stirred vessel configuration has a direct effect on mixing parameters and consequent influence on operating cost and product quality (Houcine et al., 2000; Masiuk & Rakoczy, 2007; Ochieng & Onyango, 2008; Ochieng et al., 2008). Thus, the comparison of these parameters for various impeller designs gives valuable information about the performance of the agitation systems (Houcine et al., 2000; van de Vusse, 1955). Furthermore, it is also helpful to improve and develop the design of reactors especially when the geometrical design and the condition of experiments are comparable. However, achievement of desired level of mixing is expected with the lowest power consumption (Rewatkar & Joshi, 1991).

2.3.2 Air entrainment point

The impeller agitation speed at which air is first entrained from the surface of a stirred tank is the air entrainment point N_E (Bhattacharya et al., 2007). Therefore, when the N is larger than N_E then movement of liquid surface is resulted in large air entrainment inside the vessel (Bhattacharya et al., 2007). The air entrainment point is very important for several applications. In some applications air entrainment is not desirable and then a large N_E is needed whereas for the others air is needed for more efficient processes and therefore, a small N_E is desirable (Machado et al., 2012). On the other hand, prevention of air entrainment and/or the gas bubble removal from the viscous liquid is a great problem in many processes (Paul et al., 2004). The N_E characteristics let to perform a comparison on the amount of turbulence at the tank surface between different impeller geometries (Machado et al., 2012). However, the review surveys on liquid-liquid or single liquid systems proved that the most of experiments have just been defined the air entrainment point to avoid of any air entrainment and changes in the system. Chatzi et al. (1991) selected the maximum impeller speed of 300 rpm for a mixing vessel with six blade turbine (Chatzi et al., 1991). Angle et al. (2006) observed air entrainment at 1000

rpm for Rushton turbine, thus all of their experiments were performed below this speed (Angle & Hamza, 2006b). Bhattacharya studied air entrainment in a mixing tank deeply and checked the N_E for a system with PBTU and PBD in a baffled and baffled tank and different submergence (distance between the liquid surface and the impeller) levels. Machado et al. (2011) put air entrainment measurement as one of the impeller characterization parameters in their proposed protocol. Comparison of three bladed KPC hydrofoil impeller and four bladed PBT in a same impeller diameter showed smaller N_E for PBT the KPC. They found N_E in a range of 200 rpm to 1100 rpm in different submergence.

2.3.3 Mixing time

Mixing time is one of the most significant parameters in the liquid-liquid mixing and scale up because it is the time required obtaining a defined degree of uniformity (Jakobsen, 2008; Montante et al., 2005). It is the time required to achieve desirable mixing and homogeneity throughout the tank. Impeller speed, the diameter of the vessels and impellers, the number and placement of baffles, and fluid characteristics such as viscosity are the effective parameters for determining mixing time (Doran, 1995; Jakobsen, 2008). The dimensionless mixing time is independent of Reynolds number and Froude number in the turbulent regimes for single impeller mixing tanks (Khang & Levenspiel, 1976; Woziwodzki et al., 2010). All impellers obtain the similar mixing time at the same energy dissipation rate (ϵ) under turbulent conditions and the mixing time is independent of fluid density and viscosity (Woziwodzki et al., 2010).

Several mixing time correlations have already been developed to estimate the mixing time in different standard-baffled mixing vessels and with various designs of impellers such as Rushton turbine, pitched blade, propellers, etc. (Coker, 2001). However, comparison of the different researcher's results is not a simple task because

measurements and experimental methods, tank and impeller geometry, location of tracer injection and detection method, etc. vary widely from study to study (Jahoda et al., 2007). Van riet and Tramper (1991) derived a theoretical correlation to evaluate the mixing time (Nienow, 1997):

$$t_m N = 3(d_I / T)^{-3} N_p^{-1/3} \quad (2.6)$$

Ruszkowski (1994), Grenville et al. (1995) and Cooke et al. (1988), presented a correlation to calculate the mixing time at H=T;

$$t_m = A \left(\frac{1}{N} \right) \left(\frac{1}{N_p^{1/3}} \right) \left(\frac{d_I}{T} \right)^{-2} \quad (2.7)$$

The value of “A” was defined by Ruszkowski (1994), Grenville et al. (1995) at 0.53.

Thus;

$$t_m = 5.9 T^{2/3} (\epsilon_{av})^{-1/3} \left(\frac{d_I}{T} \right)^{-1/3} \quad (2.8)$$

Where “d_I” and “ε_{av}” show the impeller diameter (m) and the average energy dissipation rate (W/kg), respectively. Average energy dissipation rate is estimated through the following equation:

$$\epsilon_{av} = \frac{P}{\rho V} = \frac{N_p N^3 d_I^5}{V} \quad (2.9)$$

Where N_p is the impeller power number, N is the agitation speed; V is the liquid volume in the tank. Another correlation was also derived by Grenville and Nienow (2004) for the mixing time in miscible liquids to reach 95% homogeneity for single impellers in a turbulent regime as follows (Grenville & Nienow, 2004):

$$N_p^{1/3} N t_{95} \frac{d_I^2}{T^{1.5} H^{0.5}} = 5.20 \quad (2.10)$$

The experimental results of Hass and Nienow (1989) for the Prochem Maxflo T axial flow hydrofoil and Rushton turbine and Saito et al., (1992) for Scaba 6SRGT and Rushton turbine showed a good agreement with this equation. The experimental results those have been carried out with Shaw (1994) and Langheinrich et al. (1996) at low specific energy dissipation rate proofed a quite well agreement with this equation (Shaw, 1994).

Mixing time is mostly determined through the methods based on transient tracer concentration or temperature at different time (Masiuk & Rakoczy, 2007). The mixing time is experimentally defined by measurement of the concentration of injected tracer within the stirred vessel. Acids, bases and concentrated salt solutions are commonly used as tracers (Doran, 1995). Several methods such as the decolorization reaction of iodine and sodium thiosulfate in water (Hiraoka et al., 1990; Yeo et al., 2002), electrical conductivity probes (Kumaresan et al., 2005; Wesselingh, 1975), temperature pulse (Mayr et al., 1992), planar laser-induced fluorescence (PLIF) (Crimaldi, 2008; Zadghaffari et al., 2009), and acid-base neutralization reaction (Lamberto et al., 1996; Szalai et al., 2004) have been used for mixing time determination. Each technique measures a various degree of homogeneity; therefore, mixing time may different for each technique (Coker, 2001). Commonly, these methods are based on visual observation. A small amount of tracer is added to the bulk fluid and is monitored. Various types of tracers, principally hot water (Mayr et al., 1992), sodium chloride solution (Kumaresan et al., 2005), or fluorescent dye (Rhodamine) (Hu et al., 2010; Szalai et al., 2004) have been employed for determination of mixing time. The variety between the results is explained by the number and location of probes used to take samples as well as tracer injection time and location (Lamberto et al., 1999). In addition, geometrical and agitation parameters can also affect mixing time. Van de Vusse et al. (1995) demonstrated that at low stirrer speeds baffling has a little effect on mixing time.

Patwardhan and Joshi (1999) determined the mixing time for around 40 axial-flow impellers. The impellers were varied in angle, twist, width, diameter, location and pumping direction. The changes in blade angle showed that use of impellers with a blade angle of 50° resulted in the shortest mixing time studied. Mixing time decreased with each incremental increase in impeller blade width. Moreover, observation showed an increasing in the ratio of impeller diameter (d_i) to tank diameter (T) up to $d_i/T=1/2$ for a pitched-blade turbine (PBTD 45) impeller at impeller clearance $C = T/3$ caused the mixing time to decrease. However, if the d_i/T ratio was increased beyond $d_i/T=1/2$, mixing time began to increase. Further results showed that mixing time increased with clearance reduction. Under the same operating conditions, the mixing times for the pitch-blade down-flow impellers were larger than those for the up-flow ones. Reduction in impeller clearance and using a draft tube decreased the mixing time and resulted in better mixing (Ochieng & Onyango, 2008). Kumaresan et al. (2005) reported a considerable reduction in mixing time up to 60% for a hydrofoil impeller surrounded by using a long draft tube compared to a pitched-blade turbine. The axial mixing improved at low clearance because of the interaction between the flow stream and the bottom wall that produced a one-loop flow pattern (Montante et al., 2001). Increasing the axial velocity and the one-loop flow pattern caused increasing in the tracer transfer rate through the tank from the bottom to the top area. Subsequently, reduction in the mixing time resulted in better mixing (Ochieng & Onyango, 2008). The review showed that mixing time is strongly affected by any changes in geometrical ratio such as d_i/T , C/T and impeller design. The published work proved that axial impellers are the most energy efficient impellers.

2.3.4 Drop size distribution (DSD)

Drops size distribution is among the most important parameters to evaluate the dispersion stability and efficiency of the system operation. It plays an important role in

the mass transfer rate between the phases in liquid-liquid systems (Giapos et al., 2005; Maaß et al., 2007). The drop size distribution is a consequence of the dynamic equilibrium between the drop breaks up and coalesces (El-Hamouz, 2007; Sechremeli et al., 2006). Drop break up and coalescence occur at the same time. Fundamentally, drop breakage is initiated by the collision between droplets and eddies whereas coalescence caused by the collision between droplets. (Kraume et al., 2004). Figure 2.2 shows the schematic illustration of drop break-up and coalescence (Carlucci, 2010).

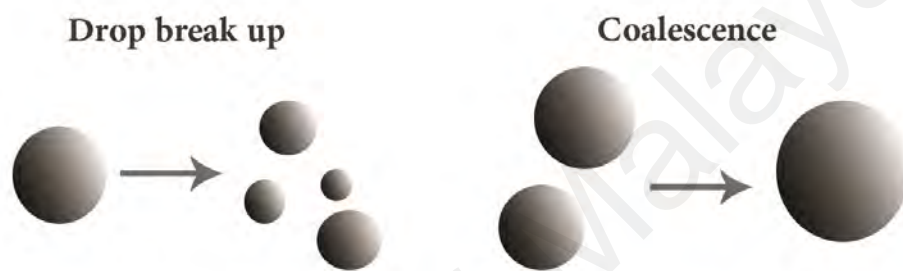


Figure 2.2: Schematic representation of drop break-up and coalescence in the liquid-liquid system

The maximum stability of drop diameter in the impeller region is the so-called maximum diameter, d_{\max} . Under steady conditions, drop size distribution is not a function of time. If a drop considerably larger than d_{\max} is formed by coalescence, it will normally break up in a short time. Furthermore, if a drop is notably smaller than the minimum droplet size, d_{\min} , it will coalesce. Consequently, dispersion is in dynamic equilibrium and a steady-state drop size distribution is maintained (Liu & Li, 1999). The exact mechanism of coalescence and break-up in a liquid-liquid agitation system is extremely complex and not very well understood (Zaldívar et al., 1996). Drops break-up generally occurs in high shear stress zones near the impeller blades. Moreover, turbulent velocity, viscous friction and pressure variations along the single drop surface also tend to break up drops while collision between droplets may consequently cause coalescence

(El-Hamouz, 2009; Kumar, 1983). Therefore, dispersion with uniform drop size within the mixing process is evidently unattainable (El-Hamouz, 2009).

Drop size distribution or granulometry of the emulsions is defined by a typical mean diameter based on statistical analysis. It is also convenient to introduce a mean or average drop diameter instead of having to specify the complete drop size distribution (Kreith & Berger, 1999). The average drop size, which is called Sauter mean diameter, d_{32} , is usually applied to evaluate drop size (Paul et al., 2004).

$$d_{32} = \frac{\sum n_i d_i^3}{\sum n_i d_i^2} \quad (2.11)$$

Where, n_i and d_i are the number of drops and the nominal diameter of drops, respectively. Average drop size is mostly used to calculate the interfacial area and many attempts have been done to relate d_{32} to d_{\max} (Lovick et al., 2005). The mean diameter is directly related to dispersed phase volume fraction (ϕ) and Interfacial area (a_v) by equation 2.12 (Paul et al., 2004):

$$d_{32} = \frac{6\phi}{a_v} \quad (2.12)$$

Whenever the interfacial area is a controlling factor for the mass transfer and chemical reactions, the mean surface diameter or Sauter Mean Diameter (SMD or d_{32}), becomes significant (Lemenand et al., 2003). Smaller drop sizes are more advantageous in mass transfer processes as they produce larger interfacial area and larger mass transfer areas around the impeller zone compared to larger drop size (Abdul Aziz et al., 2007; Patil & Kumar, 2010).

Different models and theories have been developed to predict drop size in turbulent liquid-liquid mixing in stirred vessels based on different parameters. Consideration on

the effect of impeller type on drop size is complicated due to the difficulties in drop coalescence modeling (Kichatov et al., 2003). When the inertial stress is greater than the interfacial tension stress in drop break up, the largest drop size in turbulent condition can be predicted by Kolmogorov's local isotropy theory (Kolmogorov, 1949; Nienow, 2004; Zaldívar et al., 1996). The maximum drop size (d_{\max}) is correlated to dimensionless Weber number (Calabrese, Wang, et al., 1986; Pacek et al., 1999).

$$\frac{d_{\max}}{d_I} = C_1 We^{-0.6} \quad (2.13)$$

Hinze (1955) was the first to express a model based on Kolmogorov theory and showed that drops in the inertial region of turbulence had the maximum size (d_{\max}) (El-Hamouz et al., 2009). Development of Hinze and Kolmogorov theory with the assumption of equilibrium condition results in a correlation between the maximum drop size diameter and a dimensionless impeller Weber number $d_{32} \propto We_e^{-0.6}$ (Calabrese et al., 1986; Pacek et al., 1999).

$$\frac{d_{\max}}{d_I} \propto \varepsilon_r^{-0.4} \propto We^{-0.6} \quad (2.14)$$

Where d_I is the impeller diameter, ε_{av} is the average energy dissipation rate and We is Weber number which is determined by:

$$We = \frac{\rho_c N^2 d_I^3}{\sigma} \quad (2.15)$$

Sprow (1967) stated that the sauter mean diameter is only depended on maximum drop size (Pacek et al., 1998). Since that, most of the published experimental works have reported that the maximum drop size is proportional to d_{32} due to the linear correlation between them (Calabrese et al., 1986; El-Hamouz et al., 2009; Sis et al., 2005; Sprow, 1967; Zhou & Kresta, 1998);

$$\frac{d_{32}}{d_l} = C_2 We^{-0.6} \quad (2.16)$$

Where C_2 is the dimensionless constant obtained experimentally depending on the tank geometry and impeller type (Podgórska, 2009). These expressions have been verified for the system with low dispersed phase hold up (<0.05) because of the assumption of equilibrium condition for both Hinze's and Kolmogorov's theories developed. In this condition the rate of coalescence can be neglected (Pacek et al., 1999; Podgórska, 2009; Zaldívar et al., 1996). The value of 0.5 is reported for C_2 (Angle & Hamza, 2006b). The modified form of Hinze model (1955) ($d_{32} \sim We^{-0.6}$) reported for most of the experimental works involved with dispersed phase hold up;

$$\frac{d_{32}}{d_l} = C_4(1 + C_3 \phi_d) We^{-a} \quad (2.17)$$

Where, C_3 and C_4 are depended on the coalescence tendency and the impeller type, respectively. C_3 is a coefficient particularly related to the liquid-liquid system (Angle & Hamza, 2006b). When the value of C_3 is high shows the tendency of system to coalesce easily whereas the low values show the slow coalesce systems. The values for C_3 have been reported in a range of 3 to 20 (Carlucci, 2010; Kraume et al., 2004; Pacek et al., 1994). The values for the C_4 have been reported in a range of 0.047 to 0.184 (Angle & Hamza, 2006b). Kraume et al. (2004) find out a very significant change in the Weber number exponent due to increase in phase ratio because of the effect of coalescence. In order to consider on the effect of viscosity, the following semi empirical equation was correlated by Calabrese et al. (1986) to predict d_{32} based on a large number of experimental data (Calabrese et al., 1986);

$$\frac{d_{32}}{d_l} = C_5(1 + C_6 \phi_d) We^{-0.6} \left[1 + C_7(1 - C_8 \phi_d) V_i \left(\frac{d_{32}}{d_l} \right)^{0.33} \right]^{0.6} \quad (2.18)$$

Where viscous number, V_i which shows the ratio of viscous to surface forces is evaluated from;

$$V_i = \frac{\mu_d N d_l}{\sigma} \left(\frac{\rho_c}{\rho_d} \right)^{0.5} \quad (2.19)$$

They reported the value of 0.054, 3, 4.42 and 2.5 for C_5 , C_6 , C_7 and C_8 , respectively.

Most of the available experimental works in liquid-liquid dispersion have been accomplished with Rushton turbine (O'Rourke & MacLoughlin, 2005; Pacek et al., 1999; Patil & Kumar, 2010; Quadros & Baptista, 2003). Although, using different design of impellers are attracting more attention recently, data for the other types of impellers are very limited (El-Hamouz et al., 2009; Maaß et al., 2012; Pacek et al., 1999; Quadros & Baptista, 2003).

Fernandes and Sharma (1967) observed the same interfacial area for paddles with straight, inclined and curved blades. Thus, it can be concluded that the average value of drop size for all the studied impellers was the same. Furthermore, their results showed greater interfacial area for a six-bladed disk turbine compared to an open-style impeller (Fernandes & Sharma, 1967; Sechremeli et al., 2006). Brown and Pitt (1974) proved un-significant effect of the ratio of impeller blade width to impeller diameter on drop sizes at the same impeller diameter and the agitation speed (Brown & Pitt, 1974). Study on the effect of dispersed phase hold up in different scale of stirred vessels equipped with Rushton turbine was established by Okufi et al. (1990) and resulted in an increase in droplet size with increasing the dispersed phase hold up for all investigated scales (Okufi et al., 1990). Drop size study in a very dilute liquid-liquid system was carried out by Zhou and Kresta (1998) with a Rushton turbine and three axial flow impellers without any reports on the comparison between the impellers (Zhou & Kresta, 1998). Beck (1998) reported much smaller drops for EKATO mizer-disk generated than a

Rushton turbine at the same diameter and specific power (Beck, 1998; El-Hamouz et al., 2009). Daglas and Stamatoudis (2000) found that the vertical position of impeller has a considerable effect on drop size distributions (Daglas & Stamatoudis, 2000). Pacek et al. (1999) studied on the effect of different type of impeller including Rushton turbine, disk turbine and four Chemineer impellers on drop size distribution. The results for viscous and non-viscous dispersed phases system with volume fraction of 1 and 5% showed that low-power impellers generated the same drop size at the same mean specific energy dissipation rate and it was much smaller than that of a Rushton turbine and disk turbine (Pacek et al., 1999). The low power number impellers generate smaller drop sizes due to shorter circulation time which can be led the drops to the impeller region regularly (Pacek et al., 1999). The other work on the effect of impeller design on drop size in immiscible liquid dispersions was performed by Musgrove et al (2000). The results showed smaller average drop size (d_{32}) for the hydrofoil impellers including Lightnin A310, Chemineer and HE3 than the turbine impellers (Rushton turbines and pitched-blade turbines) at the same power per unit volume and impeller diameter (Musgrove et al., 2000). Kraume et al. (2004) reported larger droplet size with increasing the dispersed phase hold up ($0.05 < \phi_d < 0.5$). They also stated that at higher dispersed phase ratios the relation between drop size and dispersed phase hold up is not linear and it has less effect of on drop size (Kraume et al., 2004). Giapos et al. (2005) performed a set of experiments to find the effect of number of blades in a disk turbine on drop size for a system of kerosene/distilled water with low dispersed phase hold up. They reported about 52% increasing in sauter mean diameter and wider drop size distribution with decrease in impeller blades number from 8 to 2. They correlated d_{32} with agitation speed and found a range of exponent values between 0.62 and 1.23 for the agitation speed due to different dispersed phase hold-ups. Lovick et al. (2005) evaluated the drop size distribution in mixtures of tap water and kerosene as the

dispersed phase using a six-bladed Rushton turbine for up to 60% dispersed phase at impeller speeds in the range of 350-550 rpm (Lovick et al., 2005). Their results revealed a reduction tendency in the maximum and the Sauter mean drop diameters with increasing impeller speed, which was in well agreement with the result of Mlynek and Resnick (1972). Lovick et al. (2005) also demonstrated that phase fractions did not greatly influence drop size. Comparing the drop size of the disk and open styles of six-flat blade impeller by Sechremeli et al (2006) implied 6 to 82% larger drop sizes for the open style impeller at the same impeller diameter and agitation speed for a system of distilled water and kerosene (Sechremeli et al., 2006). They argued that the larger power consumption generates greater turbulence and results in more drop breakage. The effect of different impellers including a Rushton disc turbine, a 4-bladed and 2-bladed 45° pitched blade turbines, a 4-bladed 60° degree pitched blade turbine, a Lightnin A310 and a Chemineer HE3 on drop size were performed by Podgórska (2009). Surprisingly, the results for low and high dispersed phase viscosity obtained much smaller droplets for the hydrofoil impeller at equal power input per mass (Podgórska, 2009). El-Hamouz (2009) compared the emulsification of oil with the viscosity of 242 mPas with the same diameter Sawtooth and PBT impellers. The higher power number results in higher mean energy and therefore smaller particle sizes. But, opposing to their expectation and the results of Pacek et al (1999) the smaller drop sizes have been observed for the impeller with the lower power number. This unexpected result might be specified a more significant role of local shear on drop breakage than turbulent shear. It should be mentioned that the pumping rate is much lower in the Sawtooth blade than the conventional impellers because of no radial flow pattern (El-Hamouz et al., 2009). El-Hamouz et al. (2009) reported that high concentration dispersed phase results in reducing the breakage rate and increasing the Sauter diameter increase. Moreover, they argued that increasing the dispersed phase hold up, does not have considerable effect on

the equilibrium d_{32} (El-Hamouz et al., 2009). They also stated a linear relation between Sauter mean diameter and dispersed phase hold up.

Various practical methods such as light transmission, in situ photography, and sample withdrawal have been employed to observe drop size distribution development in mixing vessels (O'Rourke & MacLoughlin, 2005; Paul et al., 2004). The main focus of these techniques was on the measurement of the final steady-state drop size distribution (O'Rourke & MacLoughlin, 2005). Direct photography is still used frequently by several researchers to measure drop size distribution (O'Rourke & MacLoughlin, 2005; Ribeiro et al., 2004; Zhao et al., 2011). However, in these techniques, when the holdup (volume fraction) is high or drop size is small, resolution is poor (Zhao et al., 1993). They are utilized typically for volume fractions less than 10% (O'Rourke & MacLoughlin, 2005). Table 2.2, shows some of the published work for determining drop size and drop size distribution.

Table 2.2: Some of the published work on drop size measurements

| Tank | Impeller type | System | Dispersed phase % | Surfactant | Method | Reference |
|-------------------------|---|--|-------------------|-----------------------------------|-------------------------------------|--------------------------------|
| Standard stirred vessel | -6-blade turbine | Styrene/Water | 1% | polyvinyl alcohol (PVA) | LDM | (Chatzi et al., 1991) |
| Standard stirred vessel | -Rushton turbine | Water/ organic phase | 0.8% | Sodium dodecyl sulfate (SDS) | PM | (Sathyagal et al., 1996) |
| Standard stirred vessel | -Rushton turbine | Distilled water / Xylene | 10% to 80% | 0.3% sodium dodecyl sulfate (SDS) | LDM | (Boye et al., 1996) |
| Standard stirred vessel | -Rushton turbine -HE3 -Pitched blade turbine -A310 | DIUF water/ Silicon oil | 0.03% | Not Used | LDM | (Zhou & Kresta, 1998) |
| Standard stirred vessel | -Rushton turbine -6-blade impeller (6DT) -HE3S -HE3L -CS2 | De-ionized water / Chlorobenzene and Sun flower oil | 1 and 5% | Not Used | VMS | (Pacek et al., 1999) |
| Standard stirred vessel | -Lightnin,A310 -Chemineer, HE3 -Rushton turbine -pitched blade turbine | -Silicone oil -Chlorobenzene -xylene -cyclohexane -Tri-butyl phosphate | 0.13% | Not Used | PM (Macro photography) | (Musgrove et al., 2000) |
| Standard stirred vessel | -Rushton turbine -Paddle impeller | Toluene-water | 1 and 10% | Not Used | Video camera system with microscope | (Ribeiro et al., 2004) |
| Standard stirred vessel | -Rushton turbine | Deionized water/ Silicone oils (Dow Corning 200) | 0.3% | Sodium dodecyl sulfate (SDS) | PVM | (O'Rourke & MacLoughlin, 2005) |
| Standard stirred vessel | - 6-blade turbine-type stirrer | Dodecane/ Distilled water | 0.1 % | Not Used | LDM | (Sis et al., 2005) |

Table 2.2: Continued

| Tank | Impeller type | System | Dispersed phase % | Surfactant | Method | Reference |
|-------------------------|--|---------------------------------------|--------------------------|---|---|---------------------------|
| Standard stirred vessel | -Rushton turbine | Kerosen /Water | 5 and 10% | Not Used | ORM | (Lovick et al., 2005) |
| Standard stirred vessel | Flat vertical disk style Impellers with 2,4,6,8 blades | Kerosen /Water | 1,2.5 and 7 % | Not Used | PM (photomicrography) | (Giapos et al., 2005) |
| Standard stirred vessel | -Rushton turbine | Heavy oil in Toluene | 25 % | Not Used | LDM | (Angle & Hamza, 2006a) |
| Standard stirred vessel | -6-blade disk style -6-blade open style | Distilled water and Kerosene | 1,2.5,5 and 10 % | Not Used | PM (Photomicrography) | (Sechremeli et al., 2006) |
| Esco mixing tank | -High shear Sawtooth | Silicon oil (Dow corning 200) / water | 1% | Sodium laureth sulfate (SLES) | LDM | (El-Hamouz, 2007) |
| Esco mixing tank | -Pitched blade turbine -Sawtooth | Silicon oil (Dow corning 200) / water | 1% | Sodium laureth sulfate (SLES) | LDM | (El-Hamouz et al., 2009) |
| Standard stirred vessel | -Rushton turbine | Toluene/water | 20% | Not Used | -2D optical reflectance techniques -FBR -FBRM -Endoscope technique | (Maaß et al., 2010) |
| Standard stirred vessel | -6-Blade Rushton turbine | Sugar syrup /Sunflower oil | 3% | Sodium dodecyl sulfata (SDS) | -LDM | (Patil & Kumar, 2010) |
| Mixing cell | - 6-Blade turbine | Water-in-crude oil emulsions | 15% water | Natural surfactant properties of the crude oils | -FBRM -PVM | (Boxall et al., 2011) |

Table 2.2: Continued

| Tank | Impeller type | System | Dispersed phase % | Surfactant | Method | Reference |
|-------------------------|--|---|-------------------|------------------------------|-----------------------------|--------------------------|
| Standard stirred vessel | -Retreat curve Impellers (RCI) | Distilled water/ Anisole, Cyclohexane, N-butyl chloride and Toluene | 5, 20 33, and 45% | Poly vinyl alcohol (PVA) | In-situ endoscope technique | (Maaß et al., 2012) |
| Batch reactor | -6-blade paddle -LR4 Silverson rotor-stator mixer | Aqueous solution of NaOH/ Solution of benzoic acid and ethyl chloroacetate in toluene | 1% | Not Used | LDM | (Jasińska et al., 2012) |
| Standard stirred vessel | 6-blade Rushton Turbine | Water/ silicone oils (20, 350, and 500 mPas) | 1% | Sodium dodecyl sulfate (SDS) | LDM | (Abidin et al., 2014) |

LDM; Laser Diffraction Method (Particle size analyzer)

PM; Photograph Method

ORM: Optical Reflectance Measurement

PVM: particle video microscope probe

FBRM: Focus beam reflectance measurement

FBR: Forward-backward ratio sensor

VMS: Video Microscope system

2.3.5 Liquid- Liquid Mass Transfer

The mass transfer rate between two liquids is strongly depended on the concentration difference, the interfacial area between the two liquids, and the mass-transfer coefficient (Skelland & Moeti, 1990). Other variables involved in mass transfer efficiency are molecular diffusivity, mixing conditions, rheology, chemical reactions, temperature and pressure (Vasquez & Bautista, 1997). Moreover, drop size distribution plays a crucial role to determine the mass transfer rate between the phases (Carlucci, 2010; Gäbler et al., 2006; Maaß et al., 2010)

2.3.5.1 Effect of liquid-liquid reaction

The mass transfer rate in liquid-liquid systems without reaction is defined by the mass transfer coefficients and interfacial area while in a system with reaction the effect of the chemical reactions on the overall transfer rate should also be taken into account (Bourne, 2003). Examples of industrial processes involving liquid-liquid reactions include production of caustic soda by reaction of sodium amalgam and water, nitration of organic compounds with aqueous nitric acid, sulphur removal from petroleum fraction by aqueous ethanalamines and treatment of petroleum products with sulphuric acid (Gavhane, 2009). In these systems, the mass transfer of chemical compounds between phases take places by diffusion and/or convection, simultaneous to reaction (Quadros & Baptista, 2003). Reaction is controlled by the mass transfer coefficient and interfacial area but in a multiphase reaction system the effect of the chemical reactions on the overall rate of conversion should also be considered (Bourne, 2003).

Very fast and very slow chemical reactions are considered as mass transfer controlled and kinetics controlled, respectively (Paul et al., 2004). If temperature causes considerable increase in the overall conversion, the rate is controlled by kinetics. On the other hand, different size of interfacial area or the flow rate change the system to mass

transfer controlled (Wales, 1989). However, simultaneous occurrence of mass transfer and chemical reaction which causes dynamic behavior of liquid-liquid reactions is complex (Zaldívar et al., 1996).

d_{32} is also a significant parameter in relation to liquid-liquid mass transfer and reactions. Small droplets increase mass transfer rate. The internal mass transfer coefficient is enhanced in a very small drop sizes because of the smaller diffusion length inside the drops. Moreover, inter-phase mass transfer which allows the reactants to come into contact is also an effective parameter in the liquid-liquid reaction process. Sufficient mass transfer for reaction occurs when the interfacial area is large enough for mass transfer between the reactants (Patil et al., 2004).

2.3.5.2 Mass Transfer Models

Several theoretical models such as film theory (Alopaeus, 2001; Hines, 1985), penetration theory (Higbie, 1935; Hines, 1985), and surface renewal theories (Danckwerts, 1951) have been derived and applied for developing the rate equation. These theories can be also combined, for example, Quadros (2004) employed both the film and penetration theories to model the liquid-liquid reaction of benzene nitration. However, theoretical reaction rate equations have mostly been derived based on “film theory” because of its simplicity to develop and comparison to other theories (Arai et al., 1977; Calabrese et al., 1986; Davies, 1985; Levenspiel, 1972; Nienow, 2004).

Moreover, several theoretical aspects and analysis methods in order to selection of reactions in mixing processes were presented by Baldyga and Bourne (1999). Fundamental theories and rate equations are commonly developed based on a second order chemical reaction (Bourne, 2003). Levenspiel (1979) described that several forms of reaction rate equation can be derived based on the rate constant k , mass transfer

coefficients of continuous phase (k_c) and mass transfer coefficients of dispersed phase (k_d), and concentration ratio of the reactants C_A/C_B .

Several empirical and theoretical correlations have been obtained for mass transfer coefficients involved in liquid-liquid mixing systems in either batch or continuous operations. These correlations have been derived through the specific liquid-liquid systems and based on different parameters and several assumptions.

2.3.5.3 Mass Transfer Coefficient

A deep understanding of the mixing process essentially needs accurate prediction of volumetric mass transfer coefficient ($k_L\alpha$) that can help in characterization and design of stirred and non-stirred reactors, performance optimization, economy and safety in industrial systems. Overall mass transfer coefficient, k_L , and interfacial area, α , are usually studied separately to set apart the influence of the design, operating conditions and the physical properties of the phases on each of the relevant parameter for better understanding of effects of various hydrodynamic and interfacial forces on mass transfer (Azizi & Al Taweel, 2012). The transfer flux in the liquid-liquid system is generally described by mass transfer coefficient, k_L (Jakobsen, 2008). The simplified form of the flux for liquid-liquid systems is presented by the following expression (Vasquez & Bautista, 1997):

$$\text{Transfer flux} = (k_L) \cdot (\alpha_v) \cdot (\Delta C) \quad (2.20)$$

Where k_L is the mass transfer coefficient, α is the interfacial area and ΔC is the concentration gradient.

Mass transfer coefficient consists of continuous phase mass transfer coefficient (k_c) and dispersed phase mass transfer coefficient (k_d). Several correlations have been derived for the liquid-liquid agitation batch and continuous flow systems based on experimental

and mathematical works by considering drop size distribution, break up and coalescence and interfacial area to calculate the mass transfer coefficient. Furthermore, the resistance of both dispersed and continuous phases in addition to any interfacial resistance to mass transfer has strong effect on the overall mass transfer coefficient, k_L .

When the film resistances are much larger than the interfacial resistance then the Whitman two-film theory can be employed:

$$\frac{1}{k_L} = \frac{m}{k_c} + \frac{1}{k_d} \quad (2.21)$$

where, m is the distribution coefficient among the phases ($m = C_{d,eq}/C_{c,eq}$). When m is very small, the dispersed phase resistance has significant effect on the overall mass transfer coefficient and continuous-phase resistance has less effect in the experimental results (Azizi & Al Taweel, 2012; Camurdan et al., 1989; Noh & Baird, 1984). There is also considerable influence of physical properties of phase also on mass transfer coefficient. When the viscosity of the dispersed phase is higher than the continuous phase, the mass transfer coefficient of dispersed phase is a controlling factor (Azizi & Al Taweel, 2012; Bart, 2003; Henschke & Pfennig, 1999). Furthermore, various designs in a mechanical system including the impellers and tanks produce different mass transfer efficiency. A number of new, modified impellers have been developed to improve the performance of conventional impellers in the last two decades. Typical examples are Hydrofoil impellers, such as Prochem Maxflow T and Lightnin A315 (McFarlane & Nienow, 1996) and the curved or hollow blade impellers, such as SCABA and concave blade turbines (Amanullah et al., 1998; Chen & Chen, 1999; Cooke & Heggs, 2005; Khare & Niranjana, 1999; Saito et al., 1992). It is essential to understand the mechanism of better mass transfer performance by certain types of impellers to optimize the impeller design for effective mixing process. Moreover, mode of operation also affects mass transfer efficiency. A batch system allows one to track the

mass transfer along time via mass transfer coefficient, drop size and interfacial surface area measurements from moment to moment for a single element dispersed phase. On the other hand, the continuous flow operation only gives average transfer conditions based on various elements of dispersed phase and about the mass transfer and drop breakup for given elements at different time. However, the time history of dispersed phase cannot be employed for proper modeling of the process (Skelland & Moeti, 1990).

Table 2.3 presents some of the correlations to predict the mass transfer coefficient in liquid-liquid mixing operations. They are based on different parameters such as hydrodynamic condition of the drop, condition of the system and physical properties.

University of Malaysia

Table 2.3: Mass transfer coefficient equations in liquid-liquid mixing system

| Tank | Impeller | Mixture | k_c/k_d | Equation | Remarks | Ref. |
|--|------------------------------|---|-----------|--|---|--------------------------------|
| Stirred tank | N/A | Benzoic acid - sperm oil Benzoic acid - cotton seed oil Benzoic acid - rape seed oil Benzoic acid - glycol Succinic acid - acetone Succinic acid - n-butanol Salicylic acid - benzene Salicylic acid - water Benzoic acid - water | k_c | $k_L = 0.13 \left[\frac{(P/V_c) \mu_c}{\rho_c^2} \right]^{1/4} \left[\frac{\mu_c}{\rho_c D_A} \right]^{-2/3}$ and $P = P_0 \rho_d N^3 d_I^5$ | -Applicable for both liquid-liquid and solid-gas mixing. (For just suspended small particles ($d < 0.6$ mm) in stirred tanks) | (Calderbank & Moo-Young, 1995) |
| Various sizes of baffled stirred tanks | Six flat bladed disk turbine | Continuous system o-xylene-water system | k_c | $k_c = \left(\frac{d_I^2 N}{\nu} \right) \left(\frac{d}{d_I} \right)^{0.33} \left(\frac{\Delta \rho}{\rho_d} \right)^{1.25} \left(\frac{\nu}{D_{AB}} \right)^{0.33} \left(\frac{D_{AB}}{d_I} \right)$ | -For droplet free motion | (Glen, 1965) |
| Baffled stirred tank | Turbine impeller | Continuous system Tetrachloride/iodine/water with dispersion of the organic phase and 0.1 percent aqueous solution of sodium thiosulphate/ carbon tetrachloride with dispersion of the aqueous phase | k_c | $k_c = 0.65 \left[\frac{D_{AB} u}{d} \right]^{1/2} \left[\frac{D_{AB}}{\nu_c} \right]^{1/6}$ | -For rigid spheres behavior for dispersed phase drops | (Boyadzhiev & Elenkov, 1966) |
| | | | k_c | $k_c = 1.13 \left(\frac{D_{AB} \mu}{d} \right)^{1/2}$ | -Based on Kolmogoroff's theory of local turbulent isotropy -For rigid spheres behavior for completely mobile interface -Based on Kolmogoroff's theory of local turbulent isotropy | |

Table 2.3: Continued

| Tank | Impeller | Mixture | k_c/k_d | Equation | Remarks | Ref. |
|---|---|--|-----------|--|--|----------------------------|
| Stainless steel beakers (T= 10.2, 14.7, 16.5 ,29.3, 40.0, 56.0, 86.0 cm) | (a) Six-bladed straight turbine (16 impellers with a range of D from 3.4 to 28.4 cm) (b) Four-bladed straight paddle (8 impellers with a range of D from 3.4 to 28.4 cm) (c) Four-bladed 45° inclined paddle (D= 9.7 cm) (d) Four-bladed curved paddle (D= 9.7 cm) (e) Six-bladed straight paddle (D= 9.7 cm) (f) Six-bladed curved paddle (D= 9.7 cm) (g) Three-bladed propeller. (5 impellers with a range of D from 7.0 to 28.4 cm) | continuous flow system of alkaline hydrolysis of methyl trichloroacetate | k_c | $R_a = \alpha C^* \sqrt{(Dk + k_c^2)}$ $k = k_2 [C]$ | -Equation of Danckwerts For Pseudo-first-order reaction (1.13-1.6) x 10 ⁻⁵ m s ⁻¹ | (Fernandes & Sharma, 1967) |

Table 2.3: Continued

| Tank | Impeller | Mixture | k_c/k_d | Equation | Remarks | Ref. |
|---|--|---|-----------|--|--|-----------------------------|
| Baffled and un-baffled stirred tank. (T= 24.13 cm.) | Six-flat bladed disk turbine (D= 7.62, 12.7 cm) | Continuous flow of ethyl acetate dispersed in water | k_c | $k_c = \frac{D_A R'}{(R' - r_p) d} + \sum_{n=1}^{\infty} \frac{2(R' - r_p)}{n^2 \pi^2 \theta_C} \left[1 - \exp \frac{-n\pi^2 D_A \theta_C}{(R' - r_p)^2} \right]$ | <ul style="list-style-type: none"> - Only molecular diffusion - No circulation of the fluid around the drop - No drop fluctuation, - No slip or variable velocities. - For single systems Low Reynolds number systems | (Schindler & Treybal, 1968) |
| Baffled stirred tank with various sizes (T=14.05, 19.76, 22.2 cm) | Six-bladed paddles (D= 4.49, 5.43, 6.27, 7.26, 7.66, 10.29, 11.83 cm) | Continuous flow of isooctane in water with o-nitrophenol as the solute | k_c | $N_{sh} = \frac{k_c d_I}{D_A} = 8.92 \times 10^{-4} N_{Re}^{1.36} T^{-0.5} d_I^{-0.36} - 336$ | <ul style="list-style-type: none"> -Turbulent boundary layers around the drops -No mixing within the dispersed phase | (Keey & Glen, 1969) |
| Baffled and un-baffled stirred tank mixing vessel T= 24.13 cm) | Six-flat bladed disk turbine (D= 12.7 cm for Baffled tank) (D= 7.6 cm for un-baffled tank) | The ethyl acetate as a dispersed phase and water as the continuous phase. | k_c | $k_c = 0.173 \left(\frac{d}{t_f M} \right) \left(\frac{\mu_d}{\rho_d D_\mu} \right)^{1.115} \left(\frac{\Delta \rho g d^2}{\sigma g_c} \right)^{1.302}$ | -Same particle size | (Mok & Treybal, 1971) |
| 500 ml round-bottomed threenecked Flask | Six-bladed paddle | Nitration of toluene | k_c | $k_L = 0.13 \left[\frac{(P/V_c) \mu_c}{\rho_c^2} \right]^{1/4} \left[\frac{\mu_c}{\rho_c D_A} \right]^{-2/3}$ and $P = P_0 \rho_d N^3 d_I^5$ | Applicable for both liquid-liquid and solid-gas mixing. $k_L = 1.03 \times 10^{-5} \text{ m s}^{-1}$. | (Chapman et al., 1974) |

Table 2.3: Continued

| Tank | Impeller | Mixture | k_c/k_d | Equation | Remarks | Ref. |
|---|---|---|-----------|---|--|--------------------------|
| Baffled stirred tank with two sizes (T= 0.210, 0.146 m) | Six flat bladed disk turbine with varying diameter (D=0.078 and 0.106 m) | Five different liquid-liquid systems with varying physical and transport properties | k_c | $\frac{k_c}{\sqrt{Nd_I}} = 2.932 \times 10^{-7} \phi^{-0.508} \left(\frac{d_I}{T}\right)^{0.548} (N_{Re})^{1.371}$ | -Based on penetration theory and penetration theory with Kolmogoroff's time scale | (Skelland & Lee, 1981) |
| Baffled cylindrical glass stirred vessel (T= 0.2135 m) | Six flat bladed disk turbine with two different of varying diameter (D=0.078 and 0.106 m) | Deionized water as the continuous phase Chlorobenzene and o-xylene as the disperse phase for high interfacial tension systems and benzaldehyde as the disperse phase for intermediate interfacial tension. | k_c | $\frac{k_c d_p}{D} = 1.237 \times 10^{-5} \left(\frac{\mu_c}{\rho_c D}\right)^{1/3} (N_{Re})^{2/3} \left(\frac{d_I N^2}{g}\right)^{5/12} \times \left(\frac{d_I}{d_p}\right)^2 \left(\frac{d_p}{T}\right)^{1/2} \left(\frac{\rho_d d_p^2 g}{\sigma}\right)^{5/4} \phi^{-1/2}$ | -The effect of diffusivity on the continuous phase mass transfer -The value of the exponent indicates the presence of stagnant internal small drops -Applicable for $\phi \leq 0.06$ | (Skelland & Moeti, 1990) |
| Baffled stirred tank (T= 0.213 m) | Six flat bladed disk turbine (D= 0.0667, 0.0762, and 0.1016 m) | -Deionized water as the continuous phase -Diisobutyl ketone (DBK) and mixtures of chlorobenzene and mineral oil, acetic acid, water as the dispersed phase. | K_d | $\frac{k_d}{\left[\left(\frac{d_I}{t_{F,95} - t_0}\right)\right]^{1/2}} = (5 \times 10^{-6}) \phi^{-0.0204} \left(\frac{d_I^2 N \rho_M}{\mu_M}\right)^{1.14} \left(\frac{\rho_c}{\Delta\rho}\right)^{0.518}$ | In a system without any reaction $0.0141 \leq \phi \leq 0.0909$ | (Skelland & Xien, 1990) |
| A stirred cell and Un-baffled stirred tank (T=0.035 m) | Two bladed straight paddle (D=0.03m) | Discontinuous system (Semi batch) Heterogeneous and fast reaction Nitration on benzene, toluene and chlorobenzene | k_c | $k_L = 0.13 \left[\frac{(P/V_c)\mu_c}{\rho_c^2}\right]^{1/4} \left[\frac{\mu_c}{\rho_c D_A}\right]^{-2/3}$ | -Applicable for both liquid-liquid and solid-gas mixing. | (Zaldívar et al., 1996) |
| RCI roppo calorimeter, Un- baffled (T=0.115 m) | Four-bladed 45° inclined paddle (D=0.059m) | | And | $P = P_0 \rho_{dis} N^3 D^5$ | | |

Table 2.3: Continued

| Tank | Impeller | Mixture | k_c/k_d | Equation | Remarks | Ref. |
|---|--|---|-----------|--|--|---------------------------|
| Glass beakers stirred-cell (T= 0.83 or 0.105 m) | Six flat bladed Rushton turbine (D=0.05 m) | Heptanoic acid solution with pure limonene. | k_c | $K_L a = -\text{slope} \left[\frac{V_c}{V} \right]$ | -Based on spherical drops and Kolmogoroff equation for the drop size | (Srivastava et al., 2000) |
| Baffled stirred tank (T=0.15 m) | Six flat bladed Rushton turbine (D=0.05 m) | Heptanoic acid as the continuous phase and pure limonene as the dispersed phase | | $\frac{k_c}{\sqrt{ND}} = 2.932 \times 10^{-7} \phi^{-0.508} \left(\frac{d_l}{T} \right)^{0.548} (N_{Re})^{1.371}$ | -System with surfactant | |
| Un-baffled glass reactor (T=0.1m) | Dual paddled impeller (D=0.05 m) | Mixture of chlorobenzene in sulfuric acid without any reaction. | K_d | $\frac{dC_{CB}^a}{dt} = k_L A (\bar{C}_{CB}^a - C_{CB}^a)$ | In a system without any reaction | (Ravikumar & Ghosh, 2011) |
| Batch reactor, Glass beaker (T=0.12 m) | -6 blade paddled -Silverson Rotor stator (D= 0.0312 m) | Aqueous solution of NaOH as the continuous phase and solution of benzoic acid and ethyl chloroacetate in toluene as the dispersed phase | k_c | $k_L a = \left[2 \frac{D_C}{d_d} + 0.689 \left(\frac{D_C^2}{d_d} \right)^{1/3} \left(\frac{\varepsilon_{av}}{\nu} \right)^{1/6} \right] \frac{6}{d_d}$ $d_d = 0.23 \frac{\sigma^{0.6}}{\varepsilon_{av}^{0.4} \rho_c^{0.6}}$ | -For spherical drops and based on Kolmogoroff equation for the drop size -Batch system -Instantaneous and the fast relative reaction -Dispersed phase volume = 1% vol | (Jasińska et al., 2012) |

The table shows that the correlations are divided based on continuous and dispersed phase mass transfer coefficient. Effects of drop size, interfacial area, physical properties and also hydrodynamic parameters have been incorporated into these models. Some of these equations are briefly described in the next section.

2.3.5.3.1 Continuous Phase Mass Transfer Coefficient

Molecular diffusion, natural and forced convection have effects on the continuous phase mass transfer around the drop. Besides, continuous phase mass transfer also depends on whether the drop is internally stagnant, circulating, or oscillating (Kumar & Hartland, 1999).

One of the useful equations to evaluate liquid-phase mass transfer coefficients was correlated by Calderbank and Moo-Young (1961) (Calderbank & Moo-Young, 1961; Rajapakse, 2007; Zaldívar et al., 1996) :

$$k_c = 0.13 \left[\frac{(P/V_c)\mu_c}{\rho_c^2} \right]^{1/4} \left[\frac{\mu_c}{\rho_c D_A} \right]^{-2/3} \quad (2.22)$$

where P/V is the power dissipation per unit volume (W/m^3). This equation shows good adoptability to determine continuous phase mass transfer coefficient in liquid-liquid systems (van Woezik & Westerterp, 2000; Zaldívar et al., 1996). Chapman et al. (1974) estimated the mass transfer coefficient using this equation at $1.03 \times 10^{-5} \text{ m.s}^{-1}$ for the toluene nitration experiments in a 500 ml round bottomed three-necked equipped with a paddled impeller as a reaction vessel (Chapman et al., 1974). This correlation was also employed by Van Woezik and Westerterp (2000) to evaluate mass transfer coefficient of ester in the continuous phase for $13 \times 10^{-6} \text{ m.s}^{-1}$. Their results were in a good agreement with the values of Fernandez and Sharma (1967). However, this equation does not mention impeller dimensions and particle size (Nagata, 1975; Rajapakse, 2007). Continuous phase mass transfer volumetric coefficient $k_L a$ was obtained at 5×10^7

⁵ 1/s through the hydrolysis of ester in the agitated tank equipped by six paddle impeller (Hiraoka et al., 1990). They found that the mass transfer behavior of tiny droplets was very similar to the solid spheres. The results were 2-5 and 2-3 times larger than those obtained through the equation 2.22 and experimental work of Schindler and Treybal (1968), respectively (Hiraoka et al., 1990).

Glen (1965) derived an equation to evaluate mass-transfer rates during droplet free motion. O-xylene-water system was employed for experiment in a baffled vessel with disk turbine. Several researchers such as Skelland and Moeti (1990), Ibemere (2005) and Ibemere and Kresta (2007) have claimed that this expression is the best to evaluate the mass transfer coefficient in droplet free motion in comparison with other correlations based on the experimental results (Ibemere & Kresta, 2007; Skelland & Kanel, 1992; Vasquez & Bautista, 1997) ;

$$k_c = \left(\frac{d_I^2 N}{\nu} \right) \left(\frac{d}{d_I} \right)^{0.33} \left(\frac{\Delta\rho}{\rho_d} \right)^{1.25} \left(\frac{\nu}{D_{AB}} \right)^{0.33} \left(\frac{D_{AB}}{d_I} \right) \quad (2.23)$$

The mass transfer coefficient depends on particle sizes with a range of exponents from -0.7 to 0.33 for both solid-liquid and liquid-liquid systems. Several correlations were derived through the experimental data due to the various operational conditions and particle sizes (Ibemere, 2005; Ibemere & Kresta, 2007).

Boyadzhiev and Elenkov (1966) claimed that when the continuous phase controlled the system, breakup-coalescence process did not considerably influence the transfer mechanism in a turbulent isotropic flow field with high interfacial tension for the dispersed phase volume fraction in a range of 0 to 0.06 (Boyadzhiev & Elenkov, 1966; Skelland & Moeti, 1990).

Fernandes and Sharma (1967) found mass transfer coefficient in a range of 11.3–16 ms for a system of alkaline hydrolysis of methyl trichloroacetate with different volume fraction in the range of 0.1 to 0.5 at constant agitator tip speed (Fernandes & Sharma, 1967). They employed various sizes of baffled stirred vessels and different impeller types including 6-bladed straight turbine, 4-bladed straight paddle, 4-bladed 45° inclined paddle, 4-bladed curved paddle; 6-bladed straight paddle, 6-bladed curved paddle and 3-bladed propeller. (Fernandes & Sharma, 1967; van Woezik & Westerterp, 2000). Schindler and Treybal (1968) found that increasing the Reynolds number and dispersed phase hold up by maintaining the same impeller power resulted in approximately 2.5 times larger mass transfer coefficients in the un-baffled vessel compared with the baffled vessels (Schindler & Treybal, 1968). As Schindler and Treybal (1968) and Keey and Glen (1969) did not consider on a range of physical properties and their correlations were restricted to their systems, Skelland and Lee (1981) attempted to develop and modify their works (Rajapakse, 2007). Liquid-liquid systems with various physical properties were employed in a batch mixing system to evaluate continuous phase mass transfer and total interfacial area for this purpose, the experiments were conducted using several vessel geometries and two six-bladed turbine impellers of varying diameter (Skelland & Lee, 1981). Based on the penetration theory and penetration theory with Kolmogoroff's time scale, the following expressions were derived through the experimental data (Skelland & Kanel, 1992; Skelland & Lee, 1981):

$$\frac{k_c}{\sqrt{Nd_I}} = 2.932 \times 10^{-7} \phi^{-0.508} \left(\frac{d_I}{T} \right)^{0.548} (\text{Re})^{1.371} \quad (2.24)$$

Investigation the effects of diffusivity on the continuous phase mass transfer by in the baffled vessel and six flat-blade turbine by Skelland and Moeti (1990) resulted in (Skelland & Moeti, 1990; Skelland & Xien, 1990):

$$\frac{k_c d}{D} = 1.237 \times 10^{-5} \left(\frac{\mu_c}{\rho_c D} \right)^{1/3} (\text{Re})^{2/3} \left(\frac{d_l N^2}{g} \right)^{5/12} \left(\frac{d_l}{d} \right)^2 \left(\frac{d}{T} \right)^{1/2} \left(\frac{\rho_d d^2 g}{\sigma} \right)^{5/4} \phi^{-1/2} \quad (2.25)$$

The constant value in equation (2.25) has been calculated from 180 experimental runs and the $\phi^{-1/2}$ shows the adoptability with the results of Skelland and Lee (1981) for $\phi \leq 0.09$. The term $\rho_d d^2 g / \sigma$ is known as a droplet Eotvos number to describe the reduced mobility of drop surfaces as a result of surface-active contamination in liquid-liquid systems (Clift et al., 1978; Skelland & Moeti, 1990).

Srivastava et al. (2000) characterized mass transfer properties of colloidal liquid aphrons (CLA) dispersions within transfer of heptanoic acid from water to limonene in both glass beakers stirred-cell and fully baffled stirred tank equipped with Rushton turbine. The unsteady state mass balance in the continuous phase was written as:

$$V_c \left(\frac{dC}{dt} \right) = k_L a_v V (C^* - C) \quad (2.26)$$

Integrating the initial time (t_0) and concentration (C_0) resulted in:

$$\ln \left[\frac{(C^* - C)}{(C^* - C_0)} \right] = - \left[k_L a_v \frac{V}{V_c} \right] (t - t_0) \quad (2.27)$$

The experimental data were plotted as $\log [(C^* - C)/(C^* - C_0)]$ against time. The value of $k_L a$ was then obtained from the slope of the graph:

$$k_L a = -\text{Slope} \left[\frac{V_c}{V} \right] \quad (2.28)$$

The interfacial area was calculated through equation (2.12). Although the continuous phase mass transfer coefficient correlation derived by Skelland and Lee (1985) was for systems without surfactants, the same correlation was used for the systems with surfactants (Srivastava et al. 2000).

Jasińska et al. (2012) examined mass transfer through the chemical reaction in a batch liquid-liquid stirred vessel using a six-blade paddle and Silverson rotor-stator mixer. An aqueous solution of NaOH and a solution of benzoic acid and ethyl chroacetate in toluene were used as a dispersed and continuous phase, respectively (Jasińska et al., 2012). The following equations were employed to determine the mass transfer coefficient:

$$k_L a = \left[2 \frac{D_A}{d} + 0.689 \left(\frac{D_A^2}{d} \right)^{1/3} \left(\frac{\varepsilon_{av}}{\nu} \right)^{1/6} \right] \frac{6}{d} \quad (2.29)$$

and

$$d = 0.23 \frac{\sigma^{0.6}}{\varepsilon_{av}^{0.4} \rho_c^{0.6}} \quad (2.30)$$

Their result showed that the Silverson rotor stator was not suitable for the mass transfer (Jasińska et al., 2012).

2.3.5.3.2 Dispersed Phase Mass Transfer Coefficient

Population balance model is one of the well-established tools to simulate dispersed phase because of its ability to describe drop breakage and coalescence processes based on physical and operational parameters. However, these models are associated with a significant weakness in simulation of multi fluid system such as liquid-gas or immiscible liquid-liquid systems and in the system with the assumption of uniform distribution of the dispersed phase holdup, drop size distribution through the mixing vessel (Azizi & Al Taweel, 2012). The dispersed phase mass transfer coefficient in liquid-liquid systems is dependent on the behavior of the droplets (Giles et al., 1971).

Molecular diffusion and natural/forced convection within drops are two significant affective factors on dispersed phase mass transfer. Plenty of models have been exhibited for laminar and creeping flow through stagnant, circulating, or oscillating drops. One of

the oldest equations for overall dispersed phase mass transfer in a liquid-liquid agitated vessel was derived by Grober (1925) assumed that each drop keeps its characteristics through the residence in the tank in the same residence time (Grober, 1925; Skelland & Kanel, 1992; Skelland & Moeti, 1990).

$$k_d = \frac{d}{6t_c} \ln \left[6 \sum_{n=1}^{\infty} B_n \exp \left[-\lambda_n^2 \frac{D_d t_c}{\left(\frac{d}{2}\right)^2} \right] \right] \quad (2.31)$$

Where B_n = Auxiliary functions (Constant), which is dimensionless and evaluated through:

$$B_n = \frac{L^2}{\lambda_n^2 [\lambda_n^2 + L(L-1)]} \quad (2.32)$$

Where λ_n is the Root of auxiliary is dimensionless

One of the most useful correlations for the dispersed phase mass transfer in turbulent regime has been expressed by Calderbank and Moo-Young (1961). The expression is given by Ravikumar and Ghosh (2011):

$$\frac{k_d d_{32}}{D_d} \propto \left[\frac{\rho_d^{1/3} (P/V_d)^{1/6} d^{2/3}}{\mu_d^{1/2}} \right]^{3/2} \left[\frac{\mu_d}{\rho_d D} \right]^{1/3} \quad (2.33)$$

Where the term of $\left[\frac{\rho_d^{1/3} (P/V_d)^{1/6} d^{2/3}}{\mu_d^{1/2}} \right]$ defines turbulence Reynolds number and

$\left[\frac{\mu_d}{\rho_d D} \right]$ shows the Schmidt number for the dispersed phase.

The mass transfer study in dispersed phase has been investigated through theoretical and semi empirical approaches (Vasquez & Bautista, 1997). Three time-dependent models were employed to evaluate drop phase mass transfer coefficients. In the first one, evaluation of drop side mass transfer coefficient in the rigid drops was performed mostly through the model developed by Newman (1931). In this model mass transfer is controlled by unsteady molecular diffusion in to the drops (Vasquez & Bautista, 1997).

$$k_d = -\frac{d}{6t} \ln \left\{ \frac{6}{\pi^2} \sum_{n=1}^{\infty} \frac{1}{n^2} \exp \left[\frac{-4n^2 \pi^2 D_d t}{d^2} \right] \right\} \quad (2.34)$$

If the overall effective diffusivity is used instead of molecular diffusivity in the Newman's expression, then the model can also be employed for the experimental results for the circulating drops. This model was demonstrated by Calderbank and Korchinski (1956) for the mass transfer into the stagnant drops and the dispersed phase mass-transfer coefficient as defined by equation 2.35 (Calderbank & Korchinski, 1956; Haghdoost et al., 2011; A. Kumar & Hartland, 1999):

$$k_d = -\frac{d}{6t} \ln \left[\frac{6}{\pi^2} \sum_{n=1}^{\infty} \frac{1}{n^2} \exp \left(-\frac{4n^2 \pi^2 D_{oe} t}{d^2} \right) \right] \quad (2.35)$$

and the overall effective diffusivity, D_{oe} was given by :

$$D_{oe} = \frac{\alpha d u_t}{2048(1+K)} \quad (2.36)$$

where K is the viscosity ratio (i.e., μ_d/μ_c) and α shows the effect of surfactant on the mass transfer coefficient in the dispersed phase.

Skelland and Hu Xien (1990) investigated the dispersed-phase mass-transfer rates in a baffled stirred vessel with six-flat-blade turbines and three liquid-liquid systems (Skelland & Xien, 1990). They used deionized water as the continuous phase, diisobutyl

ketone (DBK), two mixtures of chlorobenzene and mineral oil, acetic acid and water as the dispersed phase. The following correlation has been derived through the 55 runs for $d_i/T = 0.3582$.

$$\frac{k_d}{\left[\left(\frac{D}{t_{F,95} - t_0}\right)\right]^{1/2}} = (5 \times 10^{-6}) \phi^{-0.0204} \left(\frac{d_i^2 N \rho_M}{\mu_M}\right)^{1.14} \left(\frac{\rho_c}{\Delta\rho}\right)^{0.518} \quad (2.37)$$

Where μ_M and ρ_M are obtained through these following equations (Hu et al., 2007; Laity & Treybal, 1957; Skelland & Xien, 1990):

$$\rho_M = \phi \rho_d + (1 - \phi) \rho_c \quad (2.38)$$

$$\mu_M = \frac{\mu_C}{1 - \phi} \left(1 + \frac{1.5 \mu_d \phi}{\mu_d + \mu_C}\right) \quad (2.39)$$

Equation (2.37) shows that k_d is proportional to $D^{0.5}$ (Skelland & Xien, 1990). The results of the model show 9.8% mean absolute deviation with the experimental data.

Ravikumar et al. (2011) determined the dispersed phase mass transfer coefficients in an un-baffled glass reactor with a mixture of chlorobenzene in sulfuric acid without any reaction. The tank was equipped with two paddled impellers. The mass transfer coefficient was evaluated through same procedure of Srivastava et al. (2000). The mass balance equation is given as follows (Cussler, 1997);

$$\frac{dC_{CB}^a}{dt} = k_L \alpha (\bar{C}_{CB}^a - C_{CB}^a) \quad (2.40)$$

Integration of this equation with assumption of $C_{CB}^a=0$ at the zero time resulted in:

$$-\ln\left(1 - \frac{C_{CB}^a}{\bar{C}_{CB}^a}\right) = k_L \alpha t \quad (2.41)$$

Plotting the left hand of Equation (2.56) against the time resulted in a linear graph. The value of k_{La} was then obtained from the slope of the graph. They found that the increase in the concentration of sulfuric acid, temperature and stirring speed caused mass increase in the transfer coefficient.

Although, continuous phase turbulence has significant effect on the dispersed phase coefficient for some industrial application, it was studied only by Young and Korchinsky (1989) (Azizi & Al Taweel, 2012). Though these models yield reasonable results, they cannot cover the experimental results over a wide range of physical properties, designs and operating conditions of the system.

2.4 Summary of Literature Review

Literature review verifies the significant role of impeller designs on mixing performance. Mixing performance can be evaluated through power consumption, air entrainment speed, mixing time, drop size and mass transfer. On the other hand, input parameters such as impeller design; impeller power number, number of impellers, and dispersed phase volume fraction, in addition to physical properties of phases such as viscosity and density can be affected on the mixing performance parameters. On the basis of the literature review, most of the experimental works have been concentrated on the effect of physical properties and experimental condition on mixing efficiency. This section, aimed to investigate power consumption, mixing time, drop size distribution and mass transfer with the focus on the effect of impeller design. Furthermore, the most useful drop size and mass transfer correlation for liquid-liquid mixing system have been studied. The importance of liquid-liquid mixing parameters, the measurement methods and the results have been investigated briefly. Rushton turbine and pitched blade turbines were the most common used impellers through the experimental studies. Therefore, there is no information on comparison between different designs of

impellers. On the other hand, most of the literature studies have been performed in laboratory scale experimental set-up which causes many limitations in semi-industrial and industrial scales. Therefore, knowledge of hydrodynamic characteristics and mixing behavior is important for choosing the appropriate impeller for different processes. To achieve this aim, a range of axial and radial flow impeller in addition to one new design impeller were selected to evaluate the mixing performance in semi-industrial scale mixing vessel.

University of Malaya

CHAPTER 3: METHODOLOGY

3.1 Introduction

The purpose of this chapter is to serve the details on materials, experimental set up and analysis methods to study on the efficiency of various designs of impellers through different parameters including power consumption, mixing time, drop size distribution and mass transfer in stirred tank. Specification of experimental setup and impellers are described in detail. Figure 3.1 shows the overview of experimental methodology.

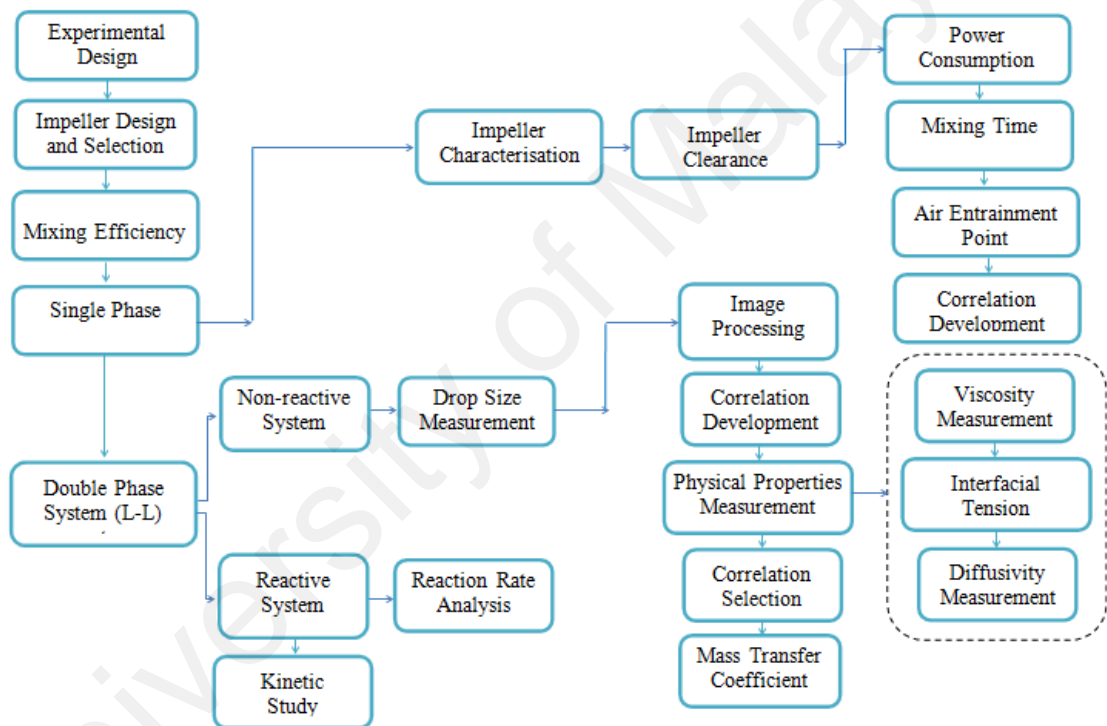


Figure 3.1: Overview of experimental methodology

3.2 Experimental Set up

Standard Stirred vessel and tank geometries were followed to design the experimental set-up. A photograph and a schematic of the experimental set up and detailed configuration of the components is shown in Figure 3.2. A flat-bottomed agitated vessel with a volume of 22 L and an internal diameter of 0.3 m were used for all the measurements. Four removable wall mounted baffles (B) of width, $B = T/10$, were fitted equally spaced. The 1.5 kW motor was installed vertically above the stirred vessel to impart the rotational motion to the shaft and impeller. The motor equipped with a precise speed controller system to adjust the rotational speed with a maximum speed of 1200 rpm. Accuracy of the system has been verified through the speed measurement using digital photoelectric tachometer. The accuracy of the instrument is 0.04% ± 2 digits. Table 3.1 shows the complete geometrical details of the stirred vessel.

Table 3.1: Geometrical details of the stirred vessel

| Description | Dimension (m) |
|--------------------------|----------------------|
| Tank height, H | 0.5 |
| Inside diameter, T | 0.3 |
| Liquid height, H | 0.3 |
| Baffle width, B | 0.028 |
| Baffle length, X | 0.4 |
| Impeller clearance, C | 1/3, 1/6, 1/4T |
| Impeller diameter, d_i | 0.1 |

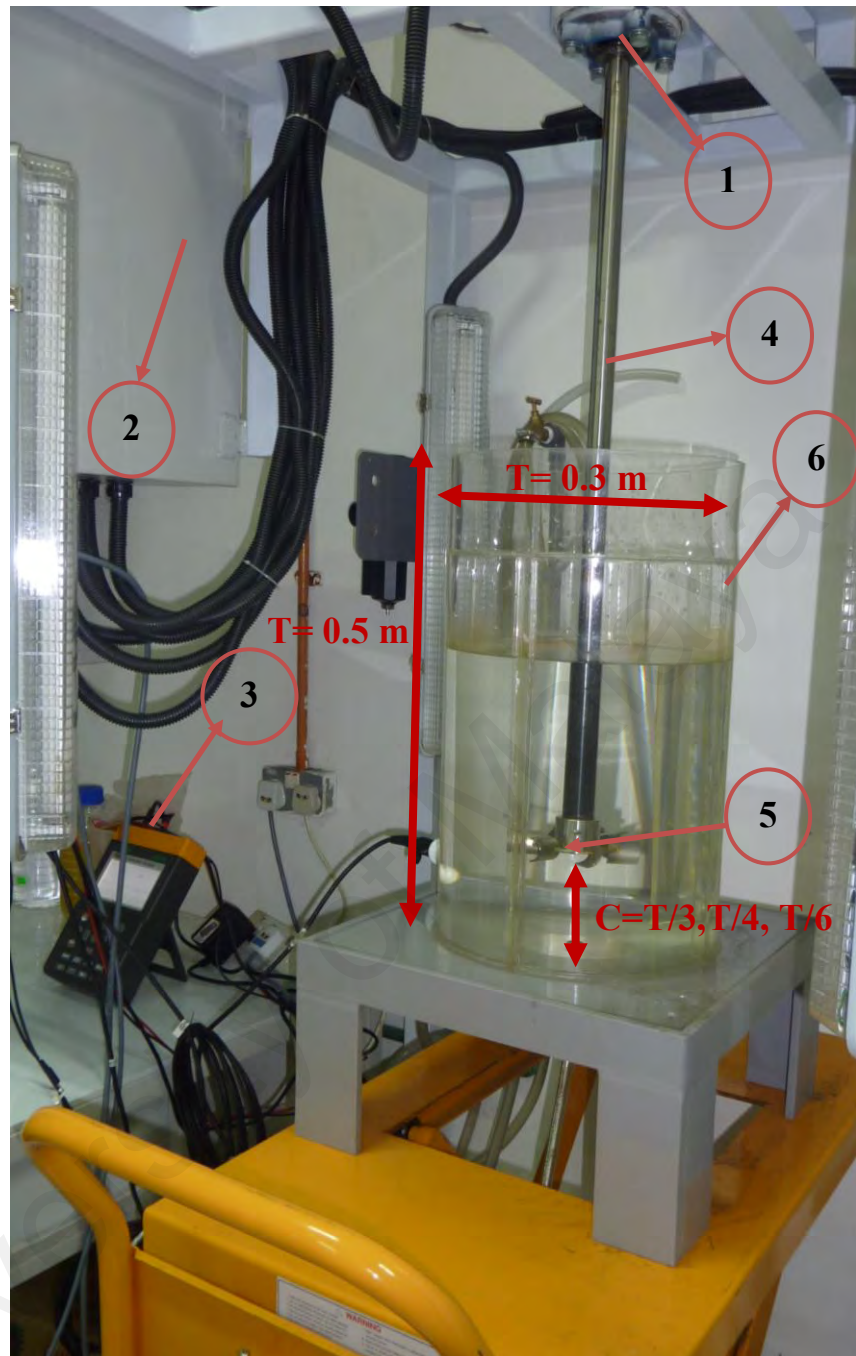


Figure 3.2: Experimental set up: 1. Motor; 2. Motor speed controller; 3. Power analyzer; 4. Impeller shaft; 5. Impeller; 6. Tank

3.3 Impellers

In order to make a detailed comparison between different designs of impeller, a series of impellers including Rushton turbine (RT), pitched-blade up flow turbine (PBTU), pitched-blade down flow turbine (PTBD), half-circle curved blade turbine (CB), parabolic blade turbine (PB), axial flow hydrofoil impeller (HE3) and new design

double circular blade turbine (DCB) have been employed. Rushton turbine, up and down flow pitched blade turbines have been commonly used through the past decades. On the other hand, curved blade, elliptical blade, parabolic blade and 3-blade hydrofoil impeller have been tried recently and the last one, double curved blade impeller have not been employed. The hydrofoil design is disclosed in European Patent EP 0 465 636 B1. The double curved blade impeller designed and developed by our team. Descriptions and schematic of employed impellers are demonstrated in Table 3.2 and Figure 3.3. The hydrofoil impeller and pitched-blade turbines are axial flow impellers. These impellers provide suction and pumping in a direction parallel to the shaft axis. The hydrofoil impeller is designed in 3-bladed impeller while the pitched blade turbines have 6-blade with 45° angle. Besides, the Rushton turbine, semicircular blade, double circular blade, parabolic blades are belonging to the radial flow impellers. The suction flow is in a direction parallel to the shaft axis while pumping is normal to the shaft. All of the radial impellers are provided in six-bladed designs. The impeller diameter was equal to $T/3$ for all of the impellers.

Table 3.2: Description of impellers used

| No. | Impeller design | Number of blades | Outer Dia. (d_1) | Central disk Size (m) | Blade length (m) | Blade thickness (m) | D/T |
|-----|-----------------|------------------|----------------------|-----------------------|------------------|---------------------|-----|
| 1 | RT | 6 | T/3 | 0.064 | 0.025 | 0.002 | 1/3 |
| 2 | PBTU | 6 | T/3 | N/A | 0.035 | 0.002 | 1/3 |
| 3 | PBTD | 6 | T/3 | N/A | 0.035 | 0.002 | 1/3 |
| 4 | CB | 6 | T/3 | 0.064 | 0.025 | 0.002 | 1/3 |
| 5 | EB | 6 | T/3 | 0.064 | 0.025 | 0.002 | 1/3 |
| 6 | PB | 6 | T/3 | 0.064 | 0.025 | 0.002 | 1/3 |
| 7 | DCB | 6 | T/3 | 0.064 | 0.025 | 0.002 | 1/3 |
| 8 | HE3 | 3 | T/3 | N/A | 0.035 | 0.002 | 1/3 |

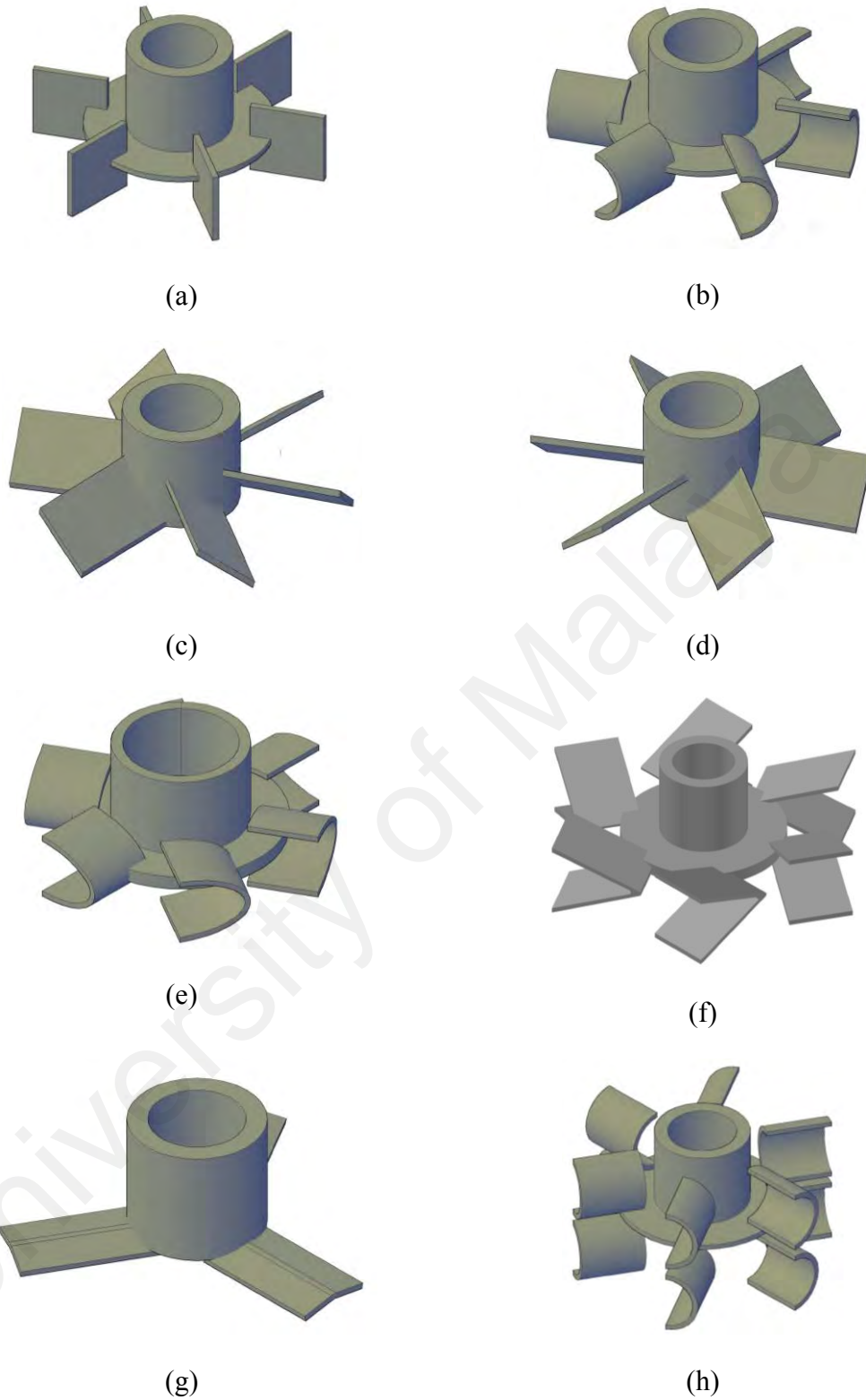


Figure 3.3: The Impeller used: (a) RT, (b) CB, (c) PBTU, (d) PBTU, (e) EB, (f) PB, (g) HE3, (h) DCB

3.4 Materials

Distilled water has been used for the single phase experimental part and RBD palm oil was added as a dispersed phase in the double phase system. Used water was drained and

the tank filled with fresh distilled water regularly before each experiments. The mass transfer rate was studied through the reaction between palm oil and water (hydrolysis reaction). For this purpose, enzyme solution was added to oil-water mixture to start the reaction. RBD Palm oil is obtained from refined, bleached and deodorized (RBD) crude palm oil which can be used for cooking application. Palm-oil was purchased from Sik Cheong Edible Oil SDN. BHD, Malaysia. The viscosities of the palm-oil and water were obtained at 84.5 and 1.0 mPa,S in room temperature, using a Brookfield DV-II +Pro EXTRA instrument. Densities of the fluids were measured using a DMA 4500 vibrating tube density/specific gravity meter (Anton Paar, Austria). Furthermore, the refractive indexes of the fluids were determined using an RE50 refractometer (Mettler-Toledo, US) with the accuracy of ± 0.00005 . The total volume of the reaction mixture was 0.022 m³ (22 liters) at the beginning of each run consisted of a mixture of distilled water and different percentage of palm-oil. Using high volume of oil results in low-quality photos and makes image processing difficult. Another problem that is mainly encountered in the hydrolysis of oils is the occurrence of substrate inhibition when the phase ratio of oil and aqueous phase is larger than 3-5% (v/v) (Noor et al., 2003).”The temperature was at about 25-27 °C ± 1 (room temperature). Sodium chloride was procured from R&M Chemical Co., Canada to prepare NaCl solution as a tracer in mixing time measurements. The surfactant used was sodium dodecyl sulfate (SDS) in powder form, supplied by Merck Chemicals Co., Germany. Ammonium Chloride, Sodium Dihydrogen Phosphate Monohydrate, Disodium Hydrogen Phosphate and Potassium Chloride were also purchased from Merck to prepare a pH 7.0 buffer solution (100 mM Sodium phosphate). Potassium hydroxide solution in ethanol (0.1 and 0.5 N) was used for FFA% evaluation using automatic Titrator, which was also provided from Merck Chemicals Co., Germany. Enzyme solution was prepared by a mixture of Lipase (Type-VII) from *Candida Rugosa* with the specific activity of 225,000 U.g⁻¹ obtained

from Sigma Chemical Co., Japan. Analytical grade Iso-propanol and Toluene were provided from R&M Chemicals Co., Canada. The physical properties of continuous and dispersed phase are presented in Table 3.3.

Table 3.3: Physical properties of the dispersed and continuous phases

| Fluid | Viscosity (kg/ms) | Density (kg.m ⁻³) | Refractive index | Interfacial tension (mN m ⁻¹) |
|--------------|----------------------|----------------------------------|---------------------|--|
| Water | 0.001 | 998.00 | 1.3325 | 71.90 |
| RBD palm-oil | 0.08198 | 890.00 | 1.4645 | 31.44 |

3.5 Analysis

3.5.1 Power and power number determination

The power consumptions were directly measured using a suspended motor system. Power analyzer system Model 6830A Prova (Taiwan) with the accuracy of 1% was selected. Data collections were performed for the agitation speeds in a range of 5 to 15 rps to provide the turbulent system. The power number of impellers is evaluated using the following expression;

$$N_p = \frac{P}{\rho N^3 D_a^5} \quad (3.1)$$

Where “P” is Power required by the impeller, kg m²/s³; N is impeller rotational speed, rev/s, ρ is liquid density, kg/m³ and D_a is impeller diameter, m.

Accuracy of the present procedure has been checked by standard Rushton turbine. The power number value of 5.55 for the Rushton turbine in standard geometries was in a good agreement with results of Pacek et. al (1999), Bujalski et al. (1987), Rewatkar et. al (1990), Joanna Karcz and Marta Major (1998) and Wu et. al (2001) in a range of 5.0 to 6. The uncertainty of these measurements varied between 2 and 10% for the higher

and lower agitation speeds, correspondingly, but only the data with uncertainties less than 5% were used for further evaluations.

Moreover, the effect of clearance on impeller power consumption was also investigated through 1/3T, 1/4T and 1/6T clearance levels. The mean specific energy or power consumption per unit of mass can be obtained through the following expression;

$$\bar{\varepsilon} = \frac{P}{V_T \rho} = \frac{N_p N^3 D^5}{V_T} \quad (3.2)$$

where V_T is the liquid volume.

3.5.2 Reynolds number

In the same geometrical systems, Reynolds number (Re), has a critical relation with power consumption because of its dependency to flow regimes, whether it is laminar or turbulent. In other words, the power drawn is extremely dependent on Reynolds number. Reynolds number (N_{Re}) is demonstrated in equation 3.3 which reveals the ratio of inertial forces to viscous forces.

$$N_{Re} = \frac{\rho N D^2}{\mu} \quad (3.3)$$

Where “ ρ ” is density, kg/m^3 ; D is the diameter of impeller, m, and “ μ ” is viscosity, kg/s m .

3.5.3 The point of air entrainment

Air entrainment is taken place by interaction between the interfacial tensions and the turbulent eddies at the surface of stirred vessel. The N_E characteristics lets to perform a comparison on the amount of turbulence at the tank surface between different impeller geometries. In the current study, air entrainment point was determined through direct observation of the liquid surface.

3.5.4 Mixing time

The mixing time is experimentally defined by measurement of the concentration of injected tracer within the stirred vessel. The concentration in the mixing tank is changed by tracer injection and macromixing or bulk blending time is defined when the concentration at the measuring points reach to 95% ΔC . The conductivity is the most common method to measure the mixing time. Therefore, it was applied to measure the mixing time in current study. In this method an electrolyte is added through the vessel as a tracer to monitor the local conductivity against the time. Solution of NaCl is used as an electrolyte commonly. 10 mL of NaCl Solution (250g/L) was injected to the tank through the liquid surface, 30 mm from the wall through a syringe. Two conductivity Suntex, EC.430 probes (Taiwan) with the accuracy of $\pm 1\% \pm 1$ were fitted to the wall; one was located at the opposite position of the injection point 80 mm lower than the liquid surface and the other one was 80 mm over the bottom. Figure 3.4 illustrates the schematic of mixing time measurements;

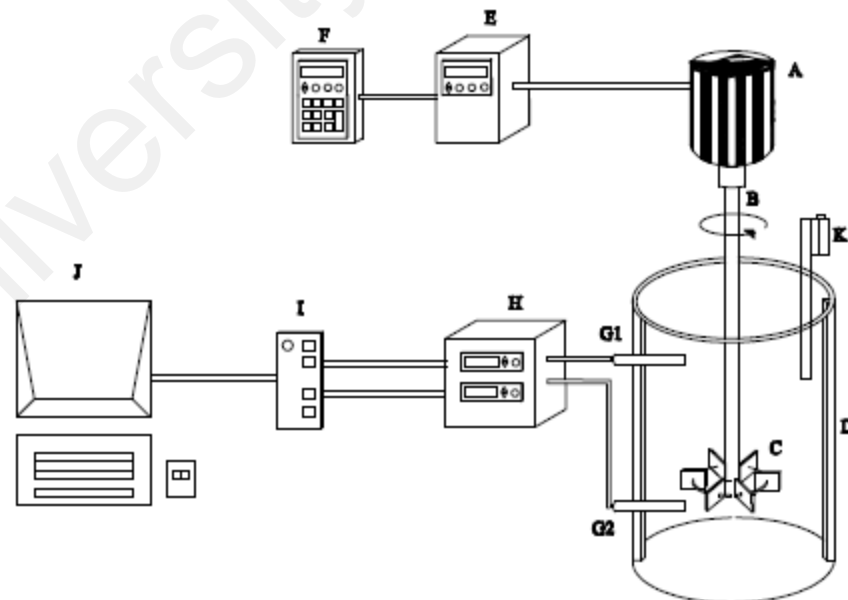


Figure 3.4: Mixing time measurement: A; Motor, B; Shaft, C; Impeller, D; Tank, E; Speed analyzer, F; Power analyzer, G1 and G2; Conductivity probes, H; Conductivity meter controller, I; Data logger, J; Computer, K; Injection point

The conductivity outputs are used to evaluate the mixing time. The time elapsed between the addition of tracer and the moment when the instant conductivity reached to 95% of its final value was defined as the mixing time for each probe;

$$Y = \left| \frac{C_{(t)} - C_0}{C_\infty - C_0} \right| \quad (3.4)$$

where $C_{(t)}$ is the concentration of the trace at time (t), C_0 is the initial and C_∞ is the final average concentrations of tracer. Each tests repeated 3 times to get an average of the mixing time. Mean concentration of 2.5 times the uniform concentration was resulted in a 3.5% measurement uncertainty.

The mixing value (η) of the system can be obtained through the calculation of mixing time (t_m) and mean specific energy dissipation rate (ε_{av}). The mixing value (η) for the single phase system can be found through the following expression:

$$\eta = \varepsilon_{av} t_m \quad (3.5)$$

It can be seen that the lower mixing values verify the higher mixing efficiency through the stirred vessel.

3.5.5 Interfacial tension

All interfacial tension measurements were carried out with a dynamic contact angle measuring instrument and tensiometer (data physics, Model DCAT 11EC, Australia). The most common method to evaluate the surface/interfacial tension is the Wilhelmy plate method. An iridium–platinum (Wilhelmy) plate was then suspended vertically from a sensitive force transducer. The accuracy of the instrument is about ± 0.01 mN/m.

3.5.6 Diffusivity measurement

In order to measure the diffusion coefficient, the electrochemical impedance spectroscopy (EIS) measurements were conducted using the frequency response module

of the potentiostat (Alpha Analytical SP-300 with EC-Lab V10.12 software, France) under ambient pressure and temperature. Chronoamperometric method was used to measure diffusion coefficient at voltage -0.5 V. In chronoamperometric studies, the current corresponding to the electrochemical reaction of solution onto an electrode surface is described by Cottrell equation (Ajeel et al., 2015):

$$I = \frac{nFAD^{1/2}C_o}{(\pi t)^{1/2}} \quad (3.6)$$

where “I” , “n” , “A” , “F” , “D” and “C_o” represent the current (A), number of electrons (1), active area of the electrode (cm²), the Faraday constant (96.487 C/mol), diffusion coefficient (cm²/s) and the bulk concentration (mol/cm³), respectively. Since the precise value of the surface area is well known, the diffusion coefficient is estimated by plotting I against t^{-1/2} and the slope of the linear segment is used to calculate the surface area.

A composite electrode based on MnO₂ and carbon nanotube (CNT) was prepared by mixing MnO₂ (50 mg), CNT (50 mg), Nafion binder (5 μL) and isopropanol (5 ml). The mixture was then ultrasonically agitated for 30 minutes. A rectangular copper sheet (1cm×1cm) was used as the current collector. The entire surface of the copper sheet was coated several times using the already-prepared MnO₂/CNT (50/50 wt%) ink. The composite electrode was dried under ambient conditions (25°C, 1atm) and was employed in the subsequent experiments. All experiments were carried out in an electrochemical cell using three electrodes, a Pt wire as the counter electrode and an Ag/AgCl (sat. KCl) as reference electrode at room temperature and ambient pressure.

3.5.7 Drop size measurement

In order to investigate the effects of different designs of impellers on Sauter mean diameter (d₃₂), a series of experiments were carried out at atmospheric pressure and a constant temperature of 26 °C. Distilled water was used as a continuous phase and

liquid height was equal to the tank diameter (T). Commonly, low dispersed-phase system and surfactant are used to reduce and eliminate coalescence. Surfactants are used to reduce the interfacial tension to eliminate or decrease coalescence. Polyvinyl alcohol (PVA) and sodium dodecyl sulfate (SDS) were two common surfactants used experiments. The latter is an anionic surfactant used in many cleaning and hygiene products. In this study, a required amount of SDS was diluted in the water.

After a short period of agitation (around 30 minutes), required amount of oil was added slowly into the mixture of water and surfactant. The effect of dispersed phase ratio on drop size distribution was studied in a range of 1 to 10 % oil in water. All the experiments carried out at the same power consumption. The experiments conditions were chosen to prevent surface aeration during drop size measurements. The mixing was conducted for two hours in order to reach the equilibrium condition.

Samples were withdrawn from the dispersed phase and analyzed. The sampling points were the same for all measurements, which were 0.02 m above the impeller level. This sampling point was chosen considering higher drop break-up rate around the impeller region compared to the other points in the stirred vessel. A vacuum pump was used to take the sample from the tank. 200 mL of sample was taken after 20, 40, 60, 80, 100 and 120 minutes of mixing. Samplings were repeated at the same time interval to prevent any changes on Sauter mean diameter with time. Samples were analyzed under a microscope connected to a camera. The tanks and sampling tubes were taken apart and washed with detergent and acetone after the experiments. They were then repeatedly washed with water to remove any trace contaminants.

The extracted samples from the stirred vessel are analyzed under the microscopic method. This method is capable to detect drops in the range of 17-1000 μm depends on the microscope Lens. Leica optical camera microscope (DF290) made by Germany at a

magnification of 20X and 10X was used to visually analyze drop sizes. In this work, for each time period, the taken images were analyzed using image processing tools in MATLAB®. Using this measurement technique for the droplet size distribution, the uncertainty of the mean drop size was evaluated to be 3.0 to 6.0 %. In the digital world, images are described in three main colors (red, green and blue (RGB)) and pixels where each pixel carries an RGB matrix and its location in an image. In order to analyze the images, the first step is to remove the background color as defined the more repeated color in an image which is described as an RGB matrix. Therefore, the image contrast has to be elevated and the background color matrix is subtracted from the main image. Afterwards, the images need to be converted to the binary format which only two colors exist: “black” and “white”. Finally, the image quality should be enhanced by filling in the small white gaps (less than 5 pixels) that leads in a better depiction of the drops. The drops appear as circles in the two dimensional view and there are multiple technique to define the drop sizes. Eventually, the droplet diameters are obtained in pixels and based on the reference scale provided by the microscope, the drop diameters are computed. Figure 3.5 present the required procedure for image processing.

The following equation is applied to evaluate the Sauter mean diameter, d_{32} for all impellers;

$$d_{32} = \frac{\sum n_i d_i^3}{\sum n_i d_i^2} \quad (3.7)$$

Where, n_i and d_i show the number of drops and the nominal diameter of drops, respectively.

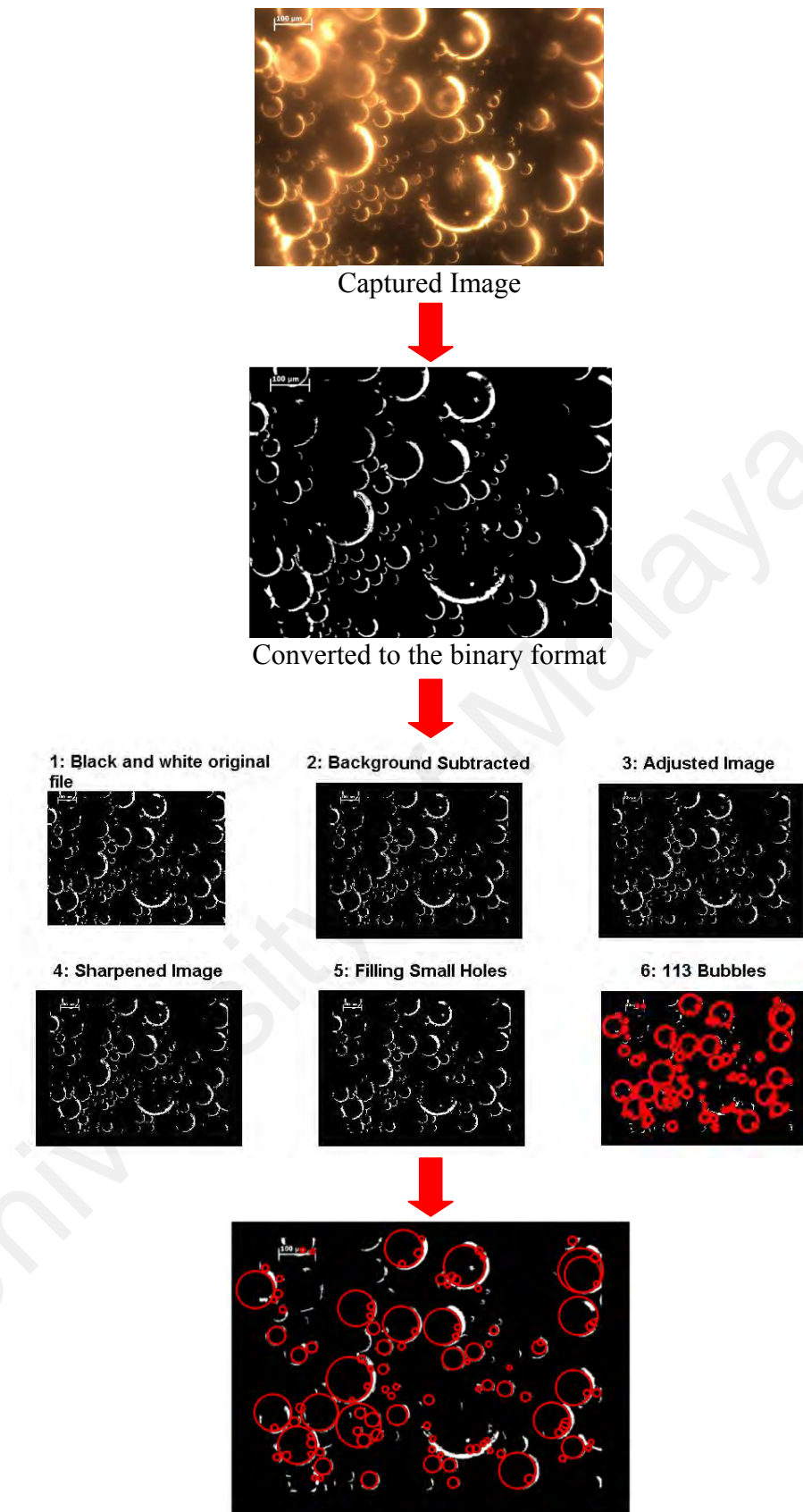


Figure 3.5: Overview of image processing procedure

3.5.8 Correlation study

3.5.8.1 Mixing time correlation

Mixing time and power consumption were measured for each impeller at three different off-bottom clearances (T/3, T/4 and T/6) and a range of speed from 1.67 rps to 15 rps. The general form of the relation between the mixing times, energy dissipation rate and impeller clearance in single phase liquid system was derived from the literature as follow;

$$t_m = \alpha (\bar{\varepsilon})^\beta \left(\frac{C}{T} \right)^\gamma \quad (3.8)$$

The experimental mixing time data were fitted to the abovementioned mixing time model and the corresponding parameters for each impeller were then estimated. The parameters associated with clearance and energy dissipation rate variables in the mixing time correlation were achieved by non-linear regression analysis using the Marquardt–Levenberg algorithm employed in SigmaPlot software version 12.0 (Systat Software Inc., USA), through a user-defined equation added to the Regression Wizard. Two different error functions, the normalized standard deviation (Δq) and the nonlinear coefficient of determination (R^2), were applied to evaluate the suitability of the abovementioned model (Equation 3.8) to the experimental data and adjust each set of mixing time model parameters. The normalized standard deviation, which measures the deviation between the experimental data and the fitted model values, was evaluated through to the following expression;

$$\Delta q (\%) = 100 \times \sqrt{\frac{\sum [(t_m)_{meas} - (t_m)_{cal}] / (t_m)_{meas}]^2}{n-1}} \quad (3.9)$$

where n is the number of data points at a given clearance, and subscripts “*meas*” and “*cal*” show the measured and calculated values of t_m , respectively. The coefficient of

determination, which determines how well the data points fit the model, was calculated as follows;

$$R^2 = 1 - \left(\frac{\sum_{i=1}^n (t_{m(meas)} - t_{m(cal)})^2}{\sum_{i=1}^n (t_{m(meas)} - \overline{t_{m(meas)}})^2} \right) \cdot \left(\frac{n-1}{n-p} \right) \quad (3.10)$$

where $\overline{t_{m(meas)}}$ is the average value of the experimental data; and p is the number of parameters of the model.

3.5.8.2 Drop size correlation

Drop size distribution and power consumption were measured for each impeller at different dispersed phase ratio at the same agitation speed. The relation between the drop size, Weber number and dispersed phase ratio was correlated through the modified form of Hinze model (1955) ($d_{32} \sim We^{-0.6}$) reported for most of the experimental works involved with dispersed phase hold up;

$$\frac{d_{32}}{d_I} = C_4 (1 + C_3 \phi_d) We^{-a} \quad (3.11)$$

Therefore, the experimental drop size data were fitted to equation (3.11) and the corresponding parameters for each impeller were then estimated. The non-linear regression method was also applied for this part. The normalized standard deviation was also followed the same basic principles in section 3.5.8.1.

3.5.9 Mass Transfer Study

Many correlations were presented in literature study to evaluate the mass transfer coefficient in liquid-liquid system. But only the limited ones considered on the effect of energy dissipation rate and drop size on mass transfer coefficient, simultaneously. With the assumption of spherical drops in the tank, Batchelor (1980) proposed a correlation

to evaluate the mass transfer coefficient as a function of the energy dissipation rate and the system properties. The physical properties were obtained through direct analytical measurements as described in 3.5.5 and 3.5.6;

$$k_L a = \left[2 \frac{D_A}{d} + 0.689 \left(\frac{D_A^2}{d} \right)^{1/3} \left(\frac{\varepsilon_{av}}{\nu} \right)^{1/6} \right] \frac{6}{d} \quad (3.12)$$

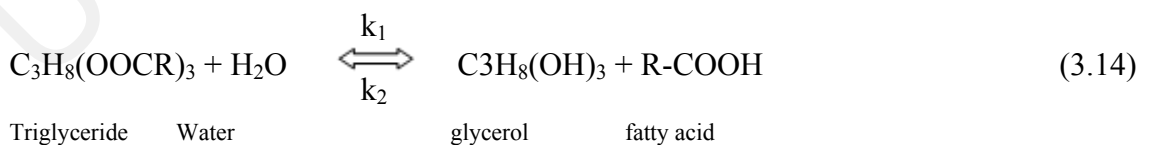
The effective Interfacial area (a_v) was also directly evaluated through the following equation:

$$d_{32} = \frac{6\phi}{a_v} \quad (3.13)$$

3.5.10 Impeller Efficiency in a Typical Reactive System

3.5.10.1 Determination of hydrolysis rate

Hydrolysis is one of the common reactions to produce fatty acids and glycerol. This reaction is typically occurs at room temperature and atmospheric pressure in the presence of enzyme as a catalyst for producing high value-added products or heat sensitive fatty acids. Fatty acids almost found in the form of esters of glycerol in triglycerides. The overall reversible reaction which is happened in hydrolysis of fats is illustrated as follows:



Required amount of solid lipase powder was dissolved in 100 ml of distilled water and pH buffer solution 7 to prepare the enzyme solution. The enzyme solution was then added to the oil and water mixture in the stirred vessel to start the reaction. The reaction was continued for 2 hours at defined agitation speed. Samples were taken from the

vessel every 10 minutes. In smaller intervals the variance of FFA% was not considerable. A peristaltic pump was used to collect the samples from the tank. The pump was connected to a steel tube by a poly-ethylene tube. The steel tube was immersed to an impeller region to extract samples of the vessel mixtures, at various stages of the dispersion process. The sampling point is located in the plane of the impeller at a distance of 10 cm from the axis of the impeller for all the experimental tests. This point was chosen due to the higher turbulence and therefore better mixing in a region of impellers. Prior to each experiment, these sampling tubes were cleaned with acetone and air dried. The samples were mixed with a mixture of isopropanol and toluene as a solvent to prepare a solution of 1.0 gram sample per 50 ml of solution. Titration method was used to determine the fatty acids produced from enzymatic hydrolysis of oil. Therefore, the fatty acid amounts were analyzed through Auto Titrator (Metrohm 716 DMS Titrino, Swaziland). Potassium hydroxide solution in ethanol (0.1N) was used as a titrant and the percentage of FFA against sample time was made for each impeller to find out the rate of reaction. The same processes were performed for all dispersed phase volume fractions. The mole fraction of produced FFA in a mixing tank was calculated based on the average molecular weight of 269.6 kg/kmol and 847.3kg/kmol for the FFA and Palm oil, respectively. Thereafter, the results for FFA

3.5.10.2 Kinetic Mathematical Model

The sequential reactions can be forward reactions, reversible or equilibrium depending on the experimental conditions including the catalyst and volume fraction of water and oil. Since, oil and water are immiscible, two phases are generated at the initial step and therefore the kinetic is controlled by the mass transfer at this step. The rate constants in the mathematical model are determined numerically from the experimental results. This model can be used to predict the rate of hydrolysis in a batch reactor based on the FFA

production. The overall reaction rate and mass balance equation can be expressed as follows;

$$\frac{dC_F}{dt} = -r_a \quad (3.15)$$

In the case of exothermic reaction, the reaction rate constant (k) can be represented by Arrhenius law (Levenspiel, 1972);

$$k = k_0 e^{-E_a/RT} \quad (3.16)$$

Where E_a is an activation energy (cal/mol), R is a gas constant (1.987 cal/mol•K) and T is the temperature. Therefore, the reaction rate can be expanded in the following form;

$$r_a = k_1 \exp\left(\frac{-E_a}{R(T+460)}\right) \times C_A - k_2 \exp\left(\frac{-E_a}{R(T+460)}\right) \times C_F \quad (3.17)$$

and

$$\frac{dC_F}{dt} = -k_1 \exp\left(\frac{-E_a}{R(T+460)}\right) \times C_A + k_2 \exp\left(\frac{-E_a}{R(T+460)}\right) \times C_F \quad (3.18)$$

Where;

$$E_a = 7.5 \times 10^7 \text{ (kg m}^2\text{/kmol s}^2\text{)}$$

$$\rho = 982 \text{ kg/m}^3$$

$$V = 0.022 \text{ m}^3$$

$$R = 156484.2 \text{ (kg m}^2\text{/kmol s}^2\text{ }^\circ\text{C)}$$

$$T = 24 \text{ }^\circ\text{C}$$

$$C_A = \text{Triglyceride concentration (kmol/m}^3\text{)}$$

$$C_F = \text{Fatty acid concentration (kmol/m}^3\text{)}$$

Consequently, kinetic model was solved and kinetic parameters were obtained using MATLAB software.

3.6 Safety Precautions

This project was involved with safety hazards, ergonomic hazards and chemical hazards, based on the hazard categories presented by the Occupational Safety and Health Administration (OSHA). The main hazards in each category are defined briefly as follows;

- Safety hazards: Electrical hazard is the main hazard in this category due to use of electrical laboratory equipment.
- Ergonomic hazards: Lifting the tank and waste material containers.
- Chemical hazards: Using chemicals for conducting the experiments.

Therefore, the personal protective equipment (PPE), Material Safety Data Sheets (MSDS) and manufacturer guidelines were followed to minimize hazards those cause serious injuries and illnesses through this project..

CHAPTER 4: RESULTS AND DISCUSSION

4.1 Introduction

This chapter presents and discusses the results obtained for impeller characterization, the measurement of power consumption, mixing time, air entrainment point at different clearances and agitation speeds. It also presents a correlation for the mixing time as a function of average energy dissipation rate and impeller clearance in a single-phase system. The obtained results on drop sizes in different dispersed phase ratios for all the impellers in an immiscible liquid-liquid system are presented and a correlation is developed to estimate the drop sizes. The mass transfer coefficients are also evaluated for all the impellers. The efficiencies of all studied impellers are defined through the hydrolysis reaction.

4.2 Impeller characterization

4.2.1 Power number

The power number of each impeller was determined through direct measurement of the required power, P , to drive the impeller. The accuracy of the measurement method was verified by determining the power number for commonly used impellers including Rushton turbine, Pitched blade up and down in addition to curved blade impeller. The variations of power number with Reynolds number for given impellers in this work at $T=1/3$ are illustrated in Figure 4.1. All the experiments were carried out in a Reynolds number range of 5.0×10^4 to 15.0×10^4 . The results showed that for the same geometry and agitation speed, the HE3 has the lowest power number. The power number (N_p) for the hydrofoil impeller (HE3) at $T=1/3$ was 0.36 whereas for PBTU, PB, EB and CB were 1.19, 1.75, 2.28, 2.96 and 3.25, respectively. The DCB and RT are ranked last with the values of 6.76 and 5.55.

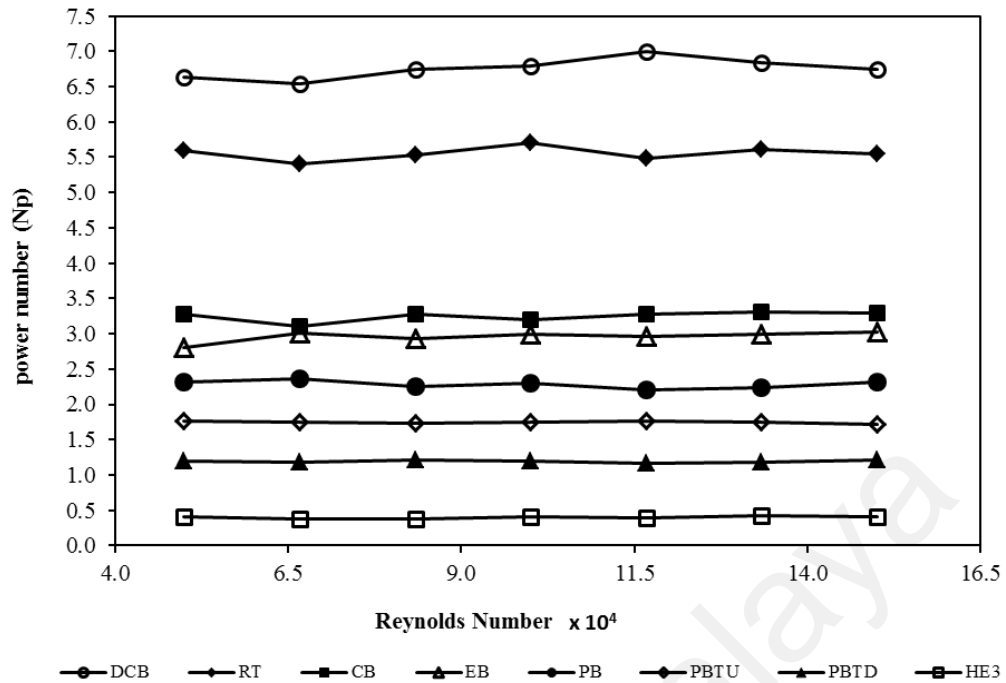


Figure 4.1: Comparison of N_p values for DCB (○), RT (◆), CB (■), EB (△), PB (●), PBTU (◇), PBD (▲) and HE3 (□) at $C/T=1/3$

The value of the impeller power number for HE3 was obtained at 0.3 by Pacek et al. (1999) and Nienow et al. (2004) due to different blade shapes (Nienow, 2004; Pacek et al., 1999). The results proved the power number of DCB and RT are almost 10 times than that of the hydrofoil impeller. If the impeller designs are categorized in axial, and radial flow impellers then the results indicated that the down flow impellers such as pitched blade down flow turbine and HE3, have the lowest power number values among the impellers. The radial flow impellers mostly have higher power number values than the axial flow impellers. The results clearly indicate a reduction in the power number values for the radial flow impellers as the blade curvature increases. Moreover, the disk turbines have higher power number values than the impellers without central disk. The experiments show that for a given impellers with the same geometric configuration the power number did not vary with the Reynolds number in a turbulent regime. However, slight changes can be seen due to instability of the measurement device. The flow pattern has a significant role on power consumption and any changes on flow direction

affect the power number value (Rewatkar et al., 1990). A tendency of the bubbles to accumulate at the low pressure area leads to extend the gas cavity effect and consequences in a higher power values under un-aerated condition (Nienow, 1996). The effect of this phenomenon is lower in HE3 impeller than the others. Moreover, the high volume of air bubbles was observed around the impeller region for the RT and DCB which leads to increase in the cavity effect and higher power consumption in higher Reynolds number. However, the radial jets of RT and DCB are more intense and powerful than those of the other types of the studied impellers. On the other hand, the HE3 has the weakest radial jet. Thus, any parameter that causes a change in the flow or turbulence, changes the power consumption.

4.2.2 The effect of impeller off-bottom clearance on N_p

The effect of clearance on impeller power consumption was also investigated. Three common clearance levels including $1/3T$, $1/4T$ and $1/6T$ were tested. The effect of clearance on mean energy dissipation rate for all impellers at different agitation speed, from 1.67 to 8.33 rps, were examined and plotted. Figure 4.2 illustrates a typical impellers trend at 5 rps while the other agitation speeds can be found in Appendix (A). In case of disk turbines, the value of impeller power number decreased with reduction in the clearance level from $T/3$ to $T/6$. The disc causes higher kinetic energy in the entrained flow at a clearance of $T/3$ compared with the lower clearance. The turbulent energy dissipation rate increases with an increase in the path length in a turbulent flow, which improves the impeller pumping and reduction in the power consumption (Rewatkar et al., 1990). For the RT, CB, EB, PBTU and PB a decrease in the off-bottom clearance from $T/3$ to $T/6$ led to lower power number value whereas an increase was observed in the power number values for PBTU and HE3. Also, a decrease in the clearance level led to shorter loops for return flows in the up flow turbines. Therefore, the flow has a higher energy which leads to better impeller pumping and further

reduction in impeller power number. Rewatkar and Joshi (1991) reported the same trend for the pitched blade down and up turbines. In the case of PBTU, a decrease in clearance level from T/3 to T/6 caused an increase in power number values. Rao and Joshi (1988) reported the power number values of 5.18 and 4.40 for DT at clearance of T/3 and T/6, respectively. They also found an increase in the power number values at 1.29, 1.35, and 1.61, while decreasing the clearance level from T/3 to T/4 and T/6, for PBTU (Raghav Rao & Joshi, 1988). Rewatkar et al. (1990) and Zhao et al. (2011) also reported the same trends for PBTU and PBTU with decreasing clearance level. The reduction in clearance leads to an increase in cross flows below the impeller area and higher velocity rate (Rewatkar et al., 1990). In lower clearances, the impeller output flow hits the tank bottom and changes the flow direction significantly, consequently leading to higher energy dissipation rate and higher power number in down flow impellers. The hydrofoil impeller did not provide strong pumping within the vessel. Therefore, the obtained results for HE3 at different clearances were mostly the same. The obtained results for the DCB impeller at different clearance levels showed a significant reduction in power number at level T/6.

Furthermore, it can be seen that the values of ϵ_{av} for DCB and RT were higher than the others, due to the higher power number obtained with these two impellers. For example, the mean energy dissipation rate for the CB and EB configurations were 42% and 29% larger than the PB at T=1/3 and 5 rps. The mean specific energies for the PBTU were 42%, 28% and 3% larger than the PBTU at T/3, T/4 and T/6, respectively. Moreover, the lowest values were found for the HE3 than the others.

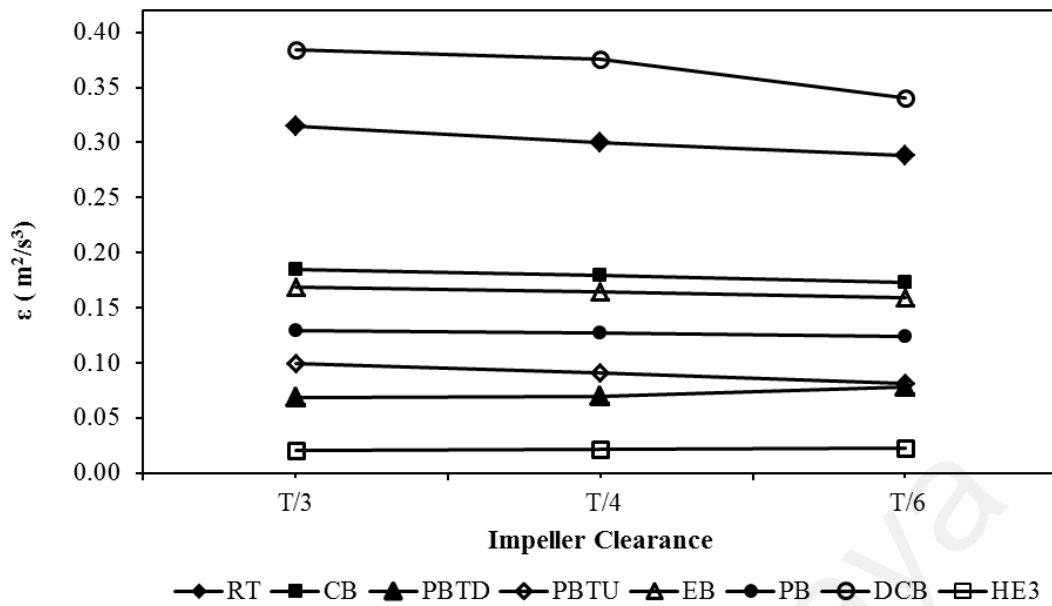


Figure 4.2: The effect of clearance on energy dissipation rate in various impellers at 5 rps

4.2.3 Air entrainment speed

The influence of impeller clearance on N_E is shown in Figure 4.3 for all studied impellers except for the HE3. Although, the test continued up to the speed of 20 rps for the HE3 impeller, no any bubble was observed within the tank. The point of air entrainment N_E is affected by both the type of impeller and the impeller clearance. The axial flow impellers mostly can be used for higher agitation speed. The surface aeration was observed after 16 rps for the Hydrofoil impeller, and for the PBTU and PBTB after 11.6 and 7 rps, respectively. For the radial flow impellers, the highest air entrainment speed was observed for the EB after 7.5 rps. The N_E values were observed in a range of 5 to 7 rps. The flow stream moves in two separate loops from the walls towards the shaft near the liquid surface for the radial flow impellers. The loops are created around the impeller blades in lower speed while they increase toward the tank wall and top surface, causing the sucking of air bubbles inside the liquid wall (Deshmukh & Joshi, 2006). In the case of axial flow impellers, the flow for the down flow impeller (PBTB)

is created one loop toward shaft near the liquid surface and discharges the flow in the downward direction. However, for the up flow impellers, PBTU and HE3, the flow is pumped upward along the shaft toward the surface and then circulates along the tank wall. This flow then loses its intensity and changes to a weak flow below the impeller. In the down flow impellers, the gas bubbles are drawn down into the central section of the tank and then distributed radially toward the tank wall and surface (Deshmukh & Joshi, 2006). Therefore, air entrainment for radial flow impellers and PBTU is different compared to PBTU and HE3 (Mali & Patwardhan, 2009).

A decrease in the clearance causes an increase in N_E . However, we considered an air entrainment point with the clearance level. Bhattacharya et al. (2007) reported that increasing the submergence caused a higher N_E which was in a good agreement with our obtained results. Decreasing the impeller clearance reduced the turbulent energy reaching the surface, resulting in a higher agitation speed to form bubbles at the liquid surface (Machado et al., 2012). In the present study, this trend was observed for all the given impellers except for the PBTU. A decrease in clearance causes reduction in power consumption. This can be attributed to its upward flow pattern which pumps flow stronger in lower clearances. The DCB impeller has a smaller N_E and is less sensitive to clearance. For the EB, CB and PB, the N_E shows a fairly similar values and trends. In the case of up-pumping impellers, a stronger discharge flow into the surface is generated than the down pumping impellers. Thus, the lower power consumption has been obtained at lower clearances for pitched blade up flow impeller. The high velocity under the down flow impellers causes the fluid to move along the bottom and then the top of the tank. Because of low pressure regions behind the impellers, the fluid does not move in a direct path to the surface, resulting in poor circulation and mixing in the top of the tank (Aubin et al., 2001).

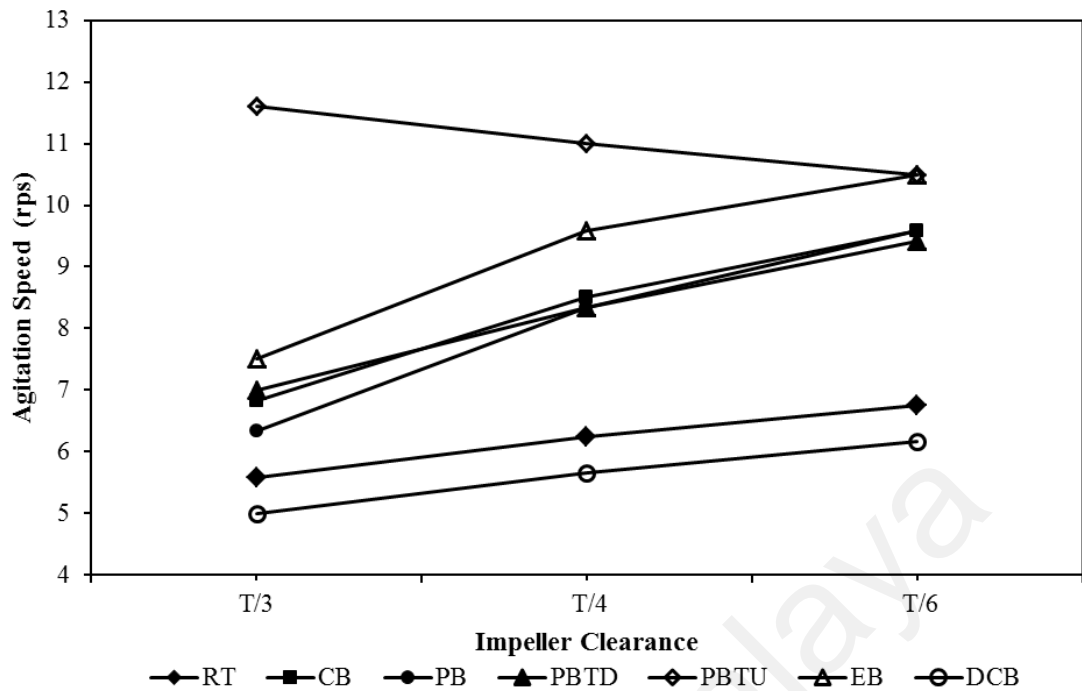


Figure 4.3: N_E as a function of the impeller clearance and agitation speed for RT (◆), CB (■), PBDT (▲), PBTU (◇), EB (△), PB (●) and DCB (○)

Figure 4.4 represents the mean energy dissipation rate for the impellers at the air entrainment point. As expected, the mean energy dissipation rate was increased with decreasing the clearance level, except for the PBTU. Although, the results for the PBTU at T/3 were higher than the PBDT, with decreasing the clearance, PBTU showed lower energy dissipation rate than the other impellers.

For the case where air entrainment is desired, N_E is a proper parameter to make a comparison between the impellers. Therefore, the PBDT gives the best performance with lowest N_E and smallest power consumption.

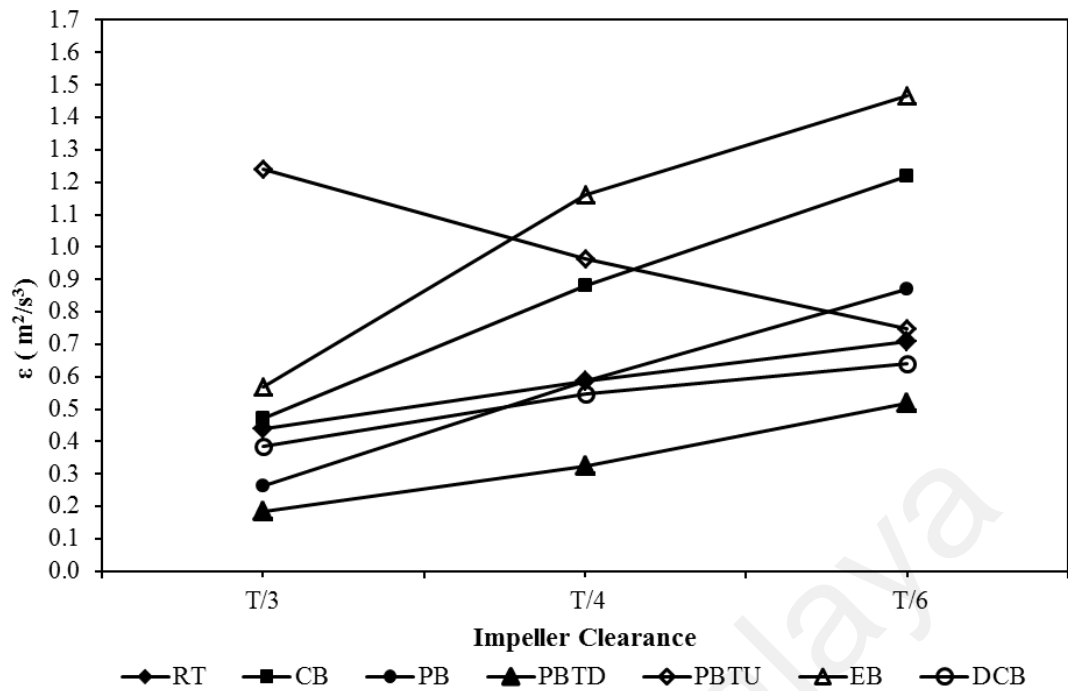


Figure 4.4: Mean energy dissipation rate at the point of air entrainment as a function of the impeller clearance for RT (◆), CB (■), PBD (▲), PBTU (◇), EB (△), PB (●) and DCB (○)

4.2.4 Mixing time

4.2.4.1 Effect of various impeller type on mixing time

The mixing times were obtained for impeller agitation speeds of 1.67 to 8.33 rps, corresponding to Reynolds numbers of 5.0×10^4 to 15.0×10^4 at clearance level of (T/3) for all the studied impellers. Due to high air entrainment within the tank, the experiments were stopped at 8.3 rps for all of the impellers, except for the DCB. For the DCB, the experiment was stopped at 6.6 rps because of high air entrainment within the tank above this speed. Figure 4.5 illustrates the results for mixing time against Reynolds number. The measurements proved the close mixing time values after $Re = 6.7 \times 10^4$ for all axial and radial impellers except for the hydrofoil impeller. Similar observation was made by (Biggs, 1963; Fentiman et al., 1998; Rewatkar & Joshi, 1991).

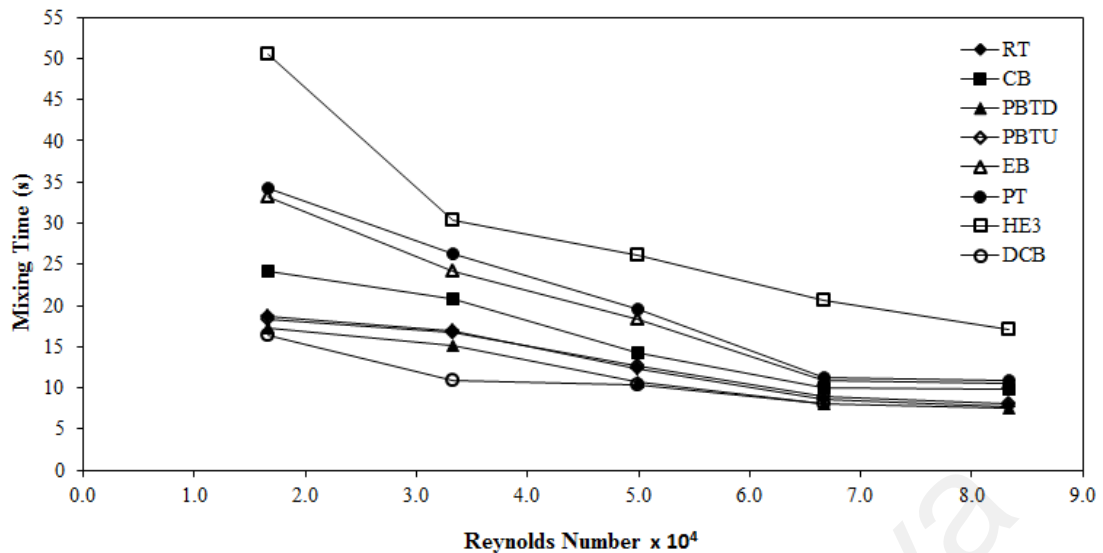


Figure 4.5: Mixing time against Reynolds number for various impellers

The results indicated that the mixing times decreased inversely with an increase in the agitation speed. The graph also illustrates that the DCB turbine can reach the desired mixing point at lower Reynolds numbers. On the other hand, the mixing time values for the Hydrofoil impeller were 2 to 4 times higher than the other impellers within the selected range of Reynolds number.

Increasing the agitation speed causes higher power consumption and a reduction in mixing time. A classification per decreasing order of power consumption has been shown as the DCB, RT, CB, EB, PT, PBTU, PBTU, PBTU and HE3 at all studied speeds. This trend was kept constant throughout the other clearance levels. The results were also verified that although the DCB impeller has the highest power consumption among the studied impellers, it can reach the highest uniformity at the smallest mixing time. Very close values were also obtained for the elliptical blade and curved blade impellers at the same power consumptions. The results clearly showed that, though the HE3 impeller has the lowest power consumption, the mixing time was the highest due to poor circulation action (Houcine et al., 2000). Therefore, longer mixing time was expected due to its specific design for slow bulk motion (Distelhoff et al., 1997). On the other

hand, shorter mixing times were predicted for the higher discharge rate impellers because of faster circulation within the tank. In the case of radial flow impellers, the mixing time values increased as the blade becomes more curved and therefore, mixing time values for the elliptical and parabolic blade turbines was higher in comparison with curved blade and Rushton turbine.

The experiments were conducted at the same power consumption to find out the effect of impeller design on the mixing time. Figure 4.6 represents the comparison of the mixing time for each impeller at the same power consumption per volume (P/V) at T/3. The figure indicates that the highest mixing time values at the same power consumption were obtained for the radial flow impellers while the lowest were found for the axial flow impellers. The results verified very close values for the radial and axial flow impellers in a range of 10.0 to 12.3 (s) and 7.6 to 8.9 (s). The best performance was observed for the PBDT. Therefore, the results prove the effect of flow diagram in the tanks influence the mixing efficiency.

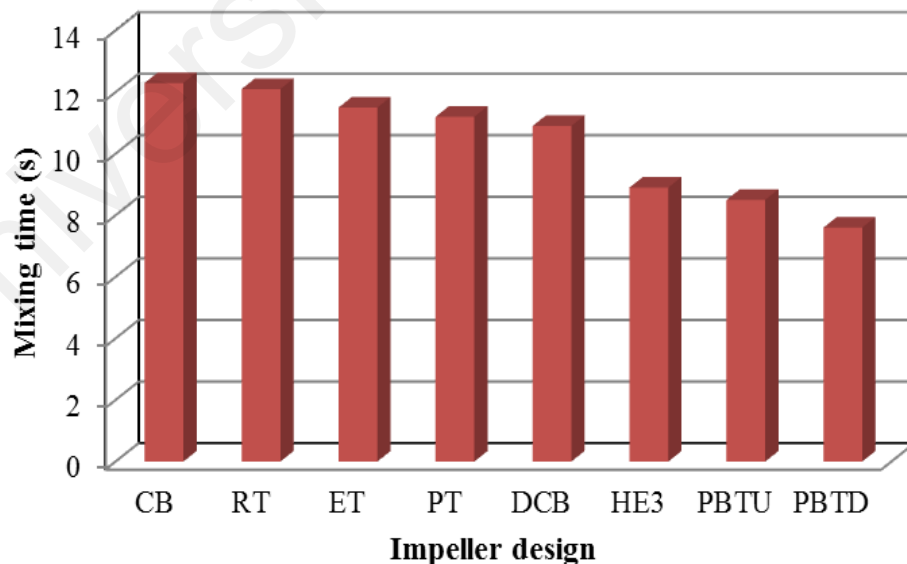


Figure 4.6: Comparison of the mixing time for different impellers at the same power consumption ($P/V=160 \text{ W/m}^3$)

4.2.4.2 Effect of clearance on mixing time

The effect of off-bottom clearance on mixing time in the mixing vessels was studied for each type of impellers through the T/3 to T/6 at 5 rps. As seen Figure 4.7, for the pitched blade down flow impeller and hydrofoil impeller, the value of mixing time increased with a decreasing clearance from T/3 to T/6. However, for the other impellers, the mixing time was found to decrease when the clearance was decreased from T/3 to T/6. The plot signified that the highest mixing time value was obtained for the HE3. In contrast, the PBDT shows better performance and it can be a good choice even in lower clearance due to the lower power consumption compared with radial flow impellers. In the case of HE3 and PBDT, decreasing clearance from T/3 to T/6 caused the generation of smooth flow and lower circulation velocity, which resulted in higher mixing time values. Decreasing the clearance for the PBTU leads to a larger circulation velocity and a better suction through tank and a lower mixing time value (Raghav Rao & Joshi, 1988). Decreasing the mixing time values in radial flow impellers with decreased in the clearance level can be described with a larger path length and flow rate in the area on the top of the impeller. The suction is divided by the disk and causes larger circulation velocities through upper and lower loops in the tank, resulting in smaller mixing times. Moreover, as the blade becomes more curved the slope of stream becomes smaller and causes a weaker radial jet. This resulted in higher mixing times in elliptical and parabolic blade turbines in comparison with curved blade and Rushton turbine (Zhao et al., 2011).

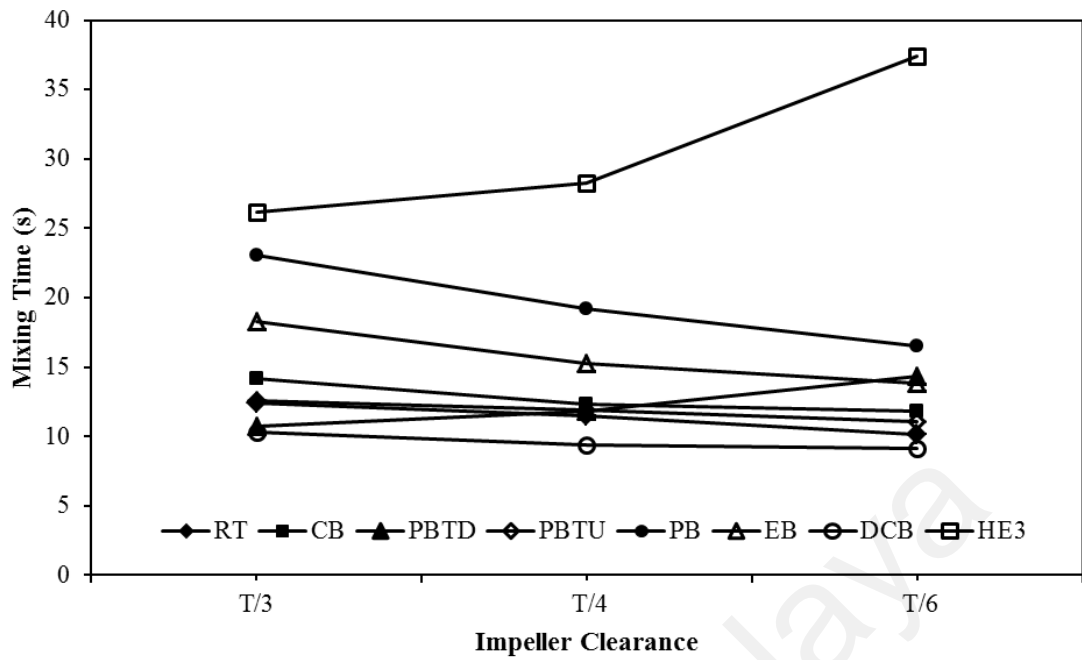


Figure 4.7: The effect of impeller clearance on mixing time at 5 rps

4.2.4.3 Mixing time correlation

As previously stated, the mean energy dissipation rate and the off-bottom clearance are two significant variables that affect the mixing time. Therefore, in the modeling of the mixing time in the present study we implemented an approach that takes into account the effect of variation in clearance as well as the variation in the mean energy dissipation rate due to the speed variation. The main distinguishing feature for selecting an appropriate model arises from the accuracy as well as simplicity of the equations. The general form of the relation between the mixing times, energy dissipation rate and impeller clearance in single phase liquid system was derived from the literature;

$$t_m = \alpha (\bar{\varepsilon})^\beta \left(\frac{C}{T} \right)^\gamma \quad (4.1)$$

The experimental mixing time data were fitted to the abovementioned mixing time model and the corresponding parameters for each impeller were then estimated.

For each studied impeller, a non-linear regression method was applied to independently determine the parameters corresponding to the aforementioned model (Equation 4.1). The optimal values of the model parameters are summarized in Table 4.3. To quantitatively compare the quality of the nonlinear regressions for the proposed model, the normalized standard deviation (Δq) and nonlinear regression coefficient (R^2) were calculated and presents in Table 4.1. As evident in this table, the model parameters for each impeller varied when the off-bottom clearance and the energy dissipation rate were changed.

On the basis of the calculated values of Δq and R^2 tabulated in Table 4.1, the proposed model was capable of fitting the experimental mixing time data over a broad range of experimental conditions for different impellers. Figure 4.8 illustrates the quality of the fit of this model to the experimental data for different impellers. The surface obtained from the global fitting of the aforementioned model to the experimental data shows that the experimental data are described well for all clearance levels and energy dissipation rates when the mixing time plotted according to the proposed model used.

Table 4.1: Calculated parameters of the proposed mixing time correlation and associated R^2 and Δq (%) for different impellers

| Impeller Design | α | β | γ | R^2 | Δq (%) |
|------------------------|----------------------------|---------------------------|----------------------------|-------------------------|----------------------------------|
| RT | 15.980 | -0.172 | 0.233 | 0.891 | 6.34 |
| CBT | 17.880 | -0.189 | 0.247 | 0.934 | 5.13 |
| PBTD | 3.680 | -0.151 | -0.292 | 0.882 | 5.64 |
| PBTU | 11.990 | -0.161 | 0.176 | 0.857 | 6.77 |
| EBT | 25.830 | -0.222 | 0.371 | 0.966 | 5.72 |
| PBT | 23.210 | -0.211 | 0.295 | 0.907 | 8.79 |
| DCB | 15.770 | -0.154 | 0.278 | 0.961 | 2.93 |
| HE3 | 4.061 | -0.221 | -0.429 | 0.977 | 2.89 |

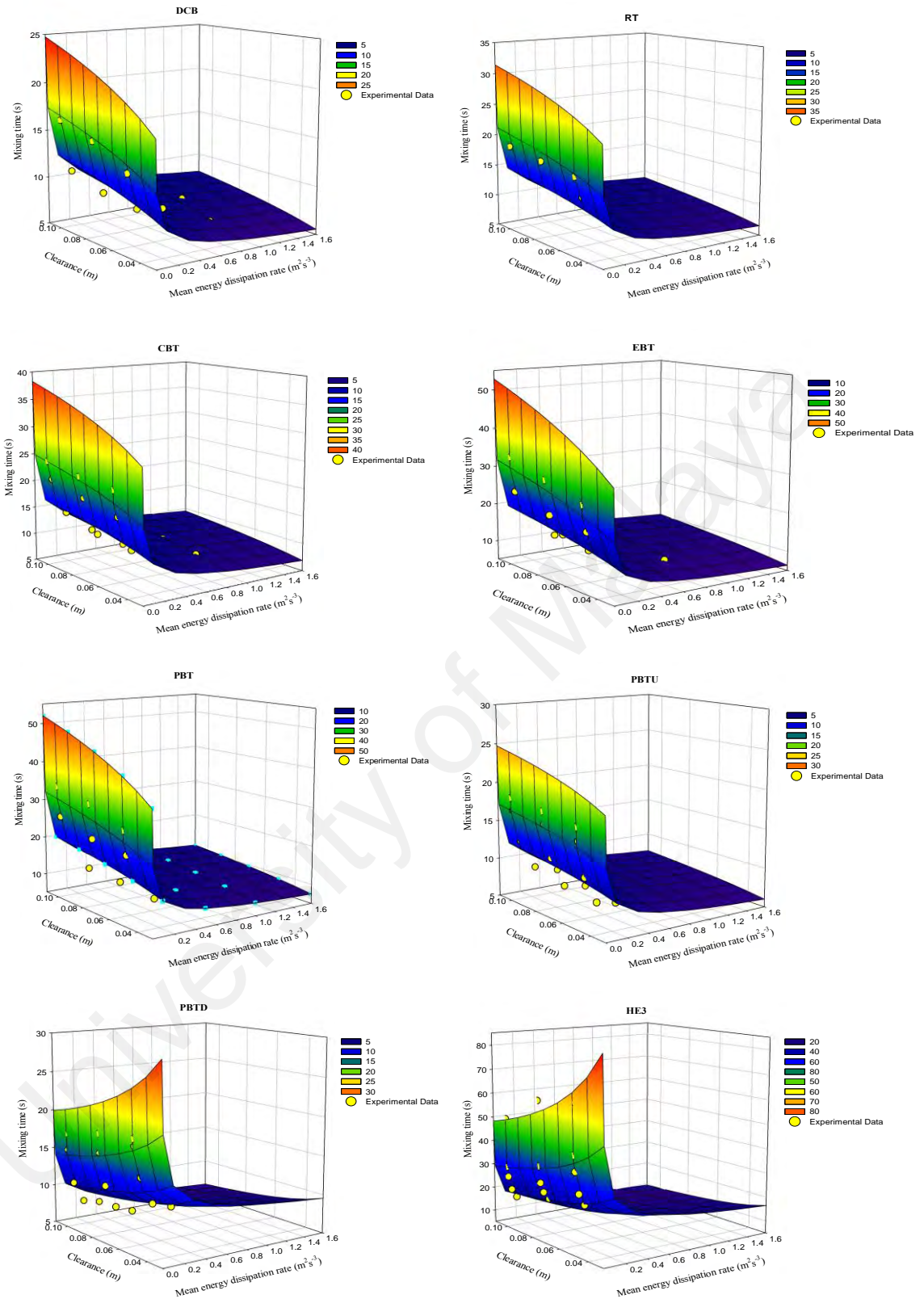


Figure 4.8: Graphical evaluation of the fit of the experimental data to the proposed mixing time correlation for different impellers

4.2.5 Mixing efficiency

The mixing efficiency (η) was evaluated with a consideration to both mixing time and the mean energy dissipation rate on different clearance and agitation speed. The mixing efficiency (η) for the single phase system can be evaluated through the following equation where t_m and ε_{av} respectively represents the mixing time and mean specific energy dissipation rate (Ochieng & Onyango, 2008):

$$\eta = \varepsilon_{av} t_m \quad (4.2)$$

Clearly, lower values of η , verify better efficiency within the mixing tank. Figure 4.9 shows the mixing efficiency values (η) against the P/V and the mixing time at the clearance of T/3. The graph shows that increasing the power consumption and mixing time lead to higher value for η . On the other hand, the efficient systems are considered to be those that can reach the desired level in lower mixing time and power consumption. Moreover, the same value of η for each impeller can be just seen at intersection point of two trend lines. Therefore, this point is assumed as an efficient point for each impeller. With this assumption, the best efficient points were attained for the axial flow impellers and especially for the hydrofoil and pitched blade down flow turbines. The lowest efficiencies were obtained for the RT, CB and DCB. The performance of elliptical and parabolic blade shape was nearly the same. The calculated results provide a good comparison in the form of mixing time and energy dissipation rate for industrial purposes. The results confirmed that the axial impellers like pitched blade impellers are more efficient in liquid mixing compared to the radial-flow turbines. Furthermore, the hydrofoil impeller can be a good choice for the process which needs slow bulk motion like as water treatment plant.

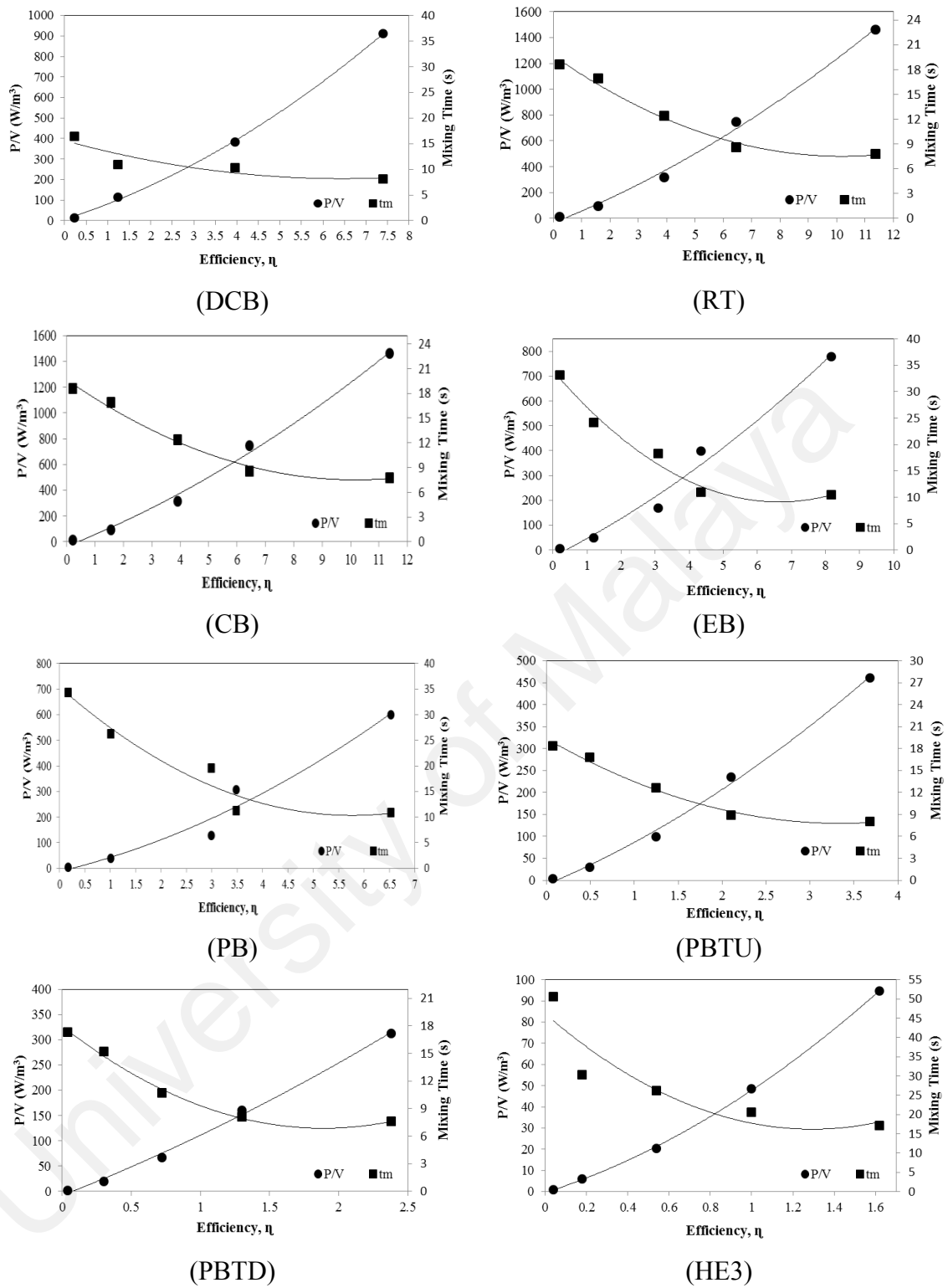


Figure 4.9: The efficiency of impellers in different agitation speed and clearance level

4.3 Drop size evaluation

4.3.1 Spatial uniformity of dispersions

The agitation speed close to the air entrainment point for each impeller was chosen to achieve the same energy dissipation rate for all impellers. Uniformity was considered through the measurement of drop size at two different positions. The first position was selected at the impeller region and the second at 0.05 m under the surface area. The system of 1% palm oil in water was chosen as a working media. The agitation speed was set for each impeller to avoid any air entrainment in the tank and give the same energy dissipation rate. The obtained mean drop size diameters (d_{32}) are presented in Table 4.2. The results verify that the d_{32} for all investigated impellers are independent of the sampling position. The obtained results are in a good agreement with Pacek et al (1999). The largest variance has been observed for the HE3 impeller with around 11% variation. Therefore, based on the presented results, the position around the impeller region was used as the sampling point in all other experiments.

Table 4.2: Mean drop size diameter in a mixture of 1% palm oil in water at $P/V=160 \text{ W/m}^3$

| Impeller type | d_{32} at 1 st sampling point ^a (μm) | d_{32} at 2 nd sampling point ^a (μm) |
|---------------|---|---|
| DCB | 86 | 91 |
| PBTD | 96 | 102 |
| RT | 102 | 107 |
| PBTU | 103 | 110 |
| CB | 109 | 115 |
| EB | 112 | 120 |
| PB | 121 | 132 |
| HE3 | 136 | 151 |

4.3.2 Equilibrium time

A dynamic equilibrium between drops is reached while there is no further change in mean droplet sizes during a breakage and coalescence in a mixing tank, showing the final drop size distribution (Hiraoka et al., 1990; Zainal Abidin et al., 2014).

Commonly, 1 to 3 hrs agitation is needed to reach a relative dynamic equilibrium based on the experimental conditions (Amer El-Hamouz, 2007; Pacek et al., 1999). Figure 4.10 illustrates the condition of drops for each impeller at 1, 3, 5 and 10 % dispersed phase hold-up and the same power consumption in different agitation periods. An increase in the dispersed phase volume fraction causes slight increase in the dynamic equilibrium time. For most of the studied impellers at $\phi=0.01$, drops reached to the equilibrium condition at around 70 minutes after mixing. In the case of $\phi=0.03$ and 0.05, the steady state was reached after around 80 and 90 minutes agitation for all studied impellers. The results proved that after 90 minutes of operation, the drop sizes were almost not dependent on time, and a steady state condition was provided.

4.3.3 The effect of impeller types on drop size

Most of the published works on liquid-liquid mixing accomplished with the Rushton turbine. A comparison between different type of impellers leads to an appropriate choice for a liquid-liquid mixing process. Furthermore, it is applicable to validate the drop size models. The results prove larger mean drop size diameters (d_{32}) for the hydrofoil impeller (HE3) at the same energy dissipation rate while the smallest mean drop sizes obtained for the DCB. The d_{32} for the HE3 impeller was taken at 136 μm and for the DCB was 37% smaller at the same energy dissipation rate. This can be explained by the larger swept volume of the DCB compared with other impellers. As might be expected at the equal energy dissipation rate the flow discharge and turbulence around the impeller zone for the DCB is greater than for the other impellers which leads in smaller droplet sizes.

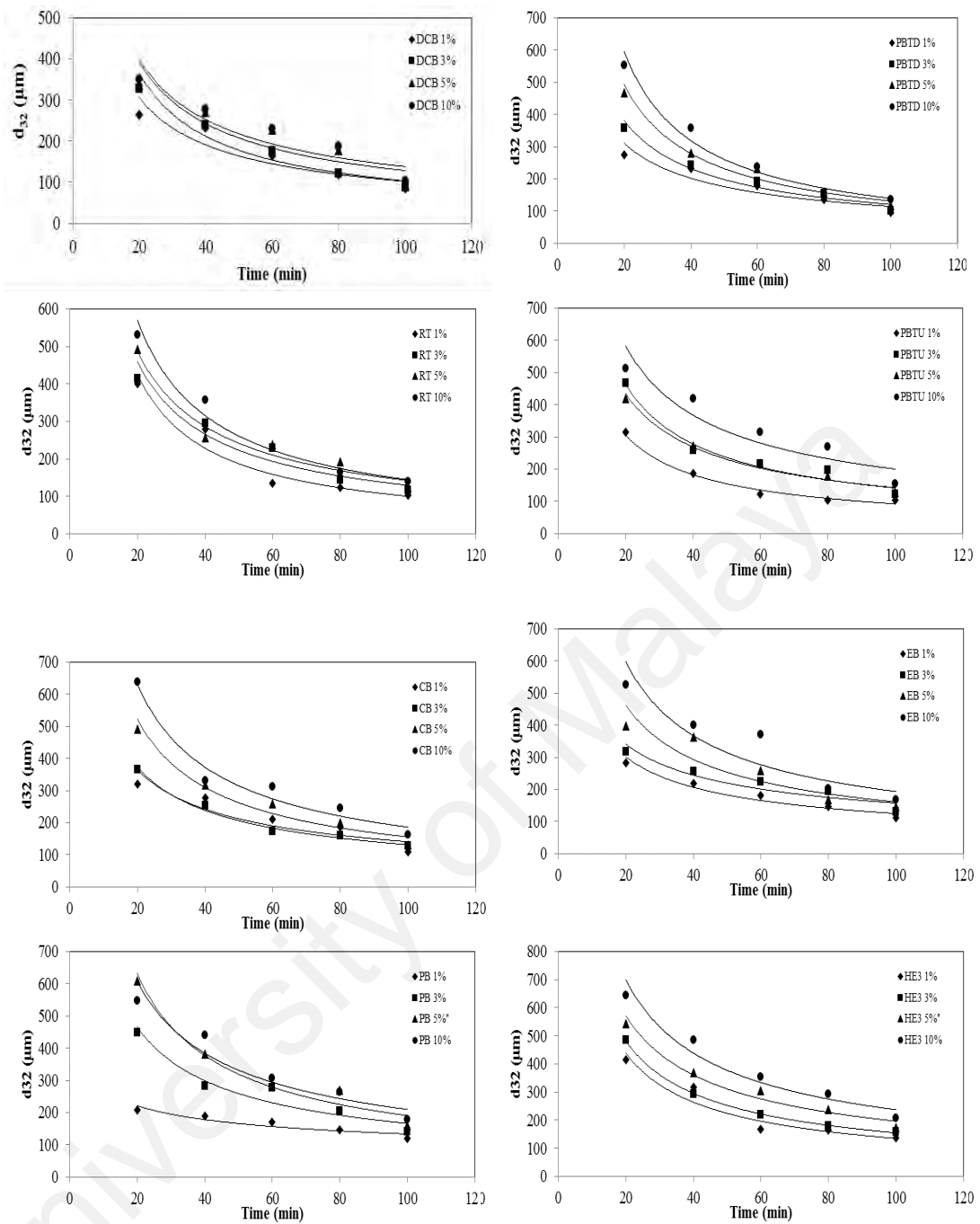


Figure 4.10: Drops equilibrium time for each impeller in different agitation times and dispersed phase hold up

In the case of radial flow impellers, the results showed smaller drop size values for the impellers with larger curvature angle. One of the differences between radial flow and axial flow impellers is on existence of disk blade for the radial flow impellers. This can generate the stronger flow stream in PBDT and consequences in higher drop breakage rate and smaller droplet size compared to the other axial flow impellers (Zhou and

Kresta, 1996; Giapos et al., 2005; Rajapakse, 2007). Turbulence around the PBTD is much more than the PBTU because of its flow direction and resulted in smaller droplet sizes. The reason for the larger droplet sizes produced by the HE3 is because of the blades number and flow direction which cause smaller turbulence and flow intensity around the impeller zone and consequence in lower drop breakage rate. These results clearly verified the effect of the blade shape design on the drop size breakage under the equal energy dissipation rate and experimental condition.

4.3.4 Effect of dispersed phase volume fraction

The effect of dispersed phase volume fraction for each impeller on mean drop size diameter is presented in Figure 4.11. Mixing characteristics are all influenced by the dispersed phase volume fraction. The significant effect of increasing the dispersed phase volume fraction is on the coalescence rate in mixing process (A. El-Hamouz, 2009). The viscosity measurement of the mixtures in this study was not shown any significant differences between viscosities. Therefore, increasing in the drop sizes is not related to increasing the coalescence due to the viscosity. The figure 4.11 shows a linear relation between the mean drop size and dispersed phase hold up. The results verify an increase in dispersed phase volume fraction results in larger d_{32} for all studied impellers. The trend is in a good agreement with Gabler et al. (2006), El-Hamouz (2009) and Khakpay and Abolghasemi (2010). This increase is expected due to higher collision rate between drops by increasing the dispersed phase volume fraction and subsequently increasing the drop coalescence process and larger drop (Kraume et al., 2004; Sechremeli et al., 2006). The difference between the Sauter mean diameters from 0.01 to 0.05 oil fractions is about 20 to 40 μm while the DCB impeller has the lowest changes among the impellers with 5 μm changes. Further increasing the dispersed phase volume fraction from 0.05 to 0.1 caused about 17 to 32 μm changes in drop sizes which show significant effect of dispersed phase volume fraction after 5% on drop sizes. The DCB impeller has

the lowest changes with 15 μm while the largest change is obtained for the HE3 with 32 μm from 0.05 to 0.1 hold up, which proves better efficiency of DCB in providing similar drops in all studied systems. Better performance of DCB in breakage rate of drops is due to higher flow intensity around the blades compared with other impellers.

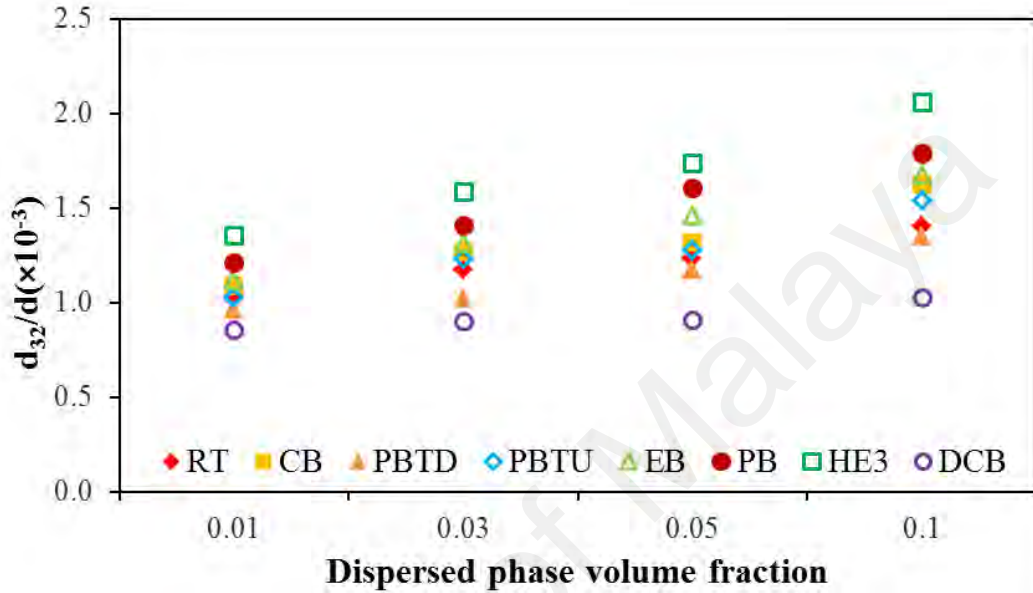


Figure 4.11: Effect of dispersed phase volume fraction on dimensionless drop size (d_{32}/D) for all impellers

4.3.5 Drop size correlation

The drop size and the power consumption were measured for each impeller at different dispersed phase. The relation between the drop size, Weber number and dispersed phase ratio can be correlated through the different semi empirical equation. Equation (4.3) is selected to correlate the dimensionless weber number and dispersed phase ratio with drop size due to not significant effect of viscosity in this work;

$$\frac{d_{32}}{d_1} = C_3(1 + C_4\phi_d) We^n \quad (4.3)$$

Therefore, the experimental drop size data were fitted to equation (4.3) and the corresponding parameters for each impeller were then estimated. The non-linear

regression method was also applied for this part. For each studied impeller, a non-linear regression method was applied to independently determine the parameters corresponding to the aforementioned model (Equation 4.3). The optimal values of the model parameters are summarized in Table 4.3. To quantitatively compare the quality of the nonlinear regressions for the proposed model, the normalized standard deviation (Δq) and nonlinear regression coefficient (R^2) were calculated and presents in Table 4.3. As evident in this table, the model parameters for each impeller varied when the dispersed phase ratio and the weber number were changed. As stated in the literature, C_4 and C_3 are depended on the coalescence tendency and the impeller type, respectively. C_4 is a coefficient particularly related to the liquid–liquid system (Angle & Hamza, 2006b). The values for C_3 have been reported in a range of 3 to 20 (Carlucci, 2010; Kraume et al., 2004; Pacek et al., 1994). The values for the C_4 have been reported in a range of 0.047 to 0.184 (Angle & Hamza, 2006b). The results for the C_3 and C_4 are in line with the reported literatures. The obtained values for the C_4 shows that the rate of coalescence in the system is relatively low for all studied impellers. The close value of C_4 for the DCB to 3 verifies less coalescence in the system while the higher coalescence rate can be concluded for the HE3 with C_4 equal to 8.19.

Table 4.3: Calculated parameters of the proposed drop size correlation and associated R^2 and Δq (%) of different impellers

| Impeller Type | n | C_3 | C_4 | R^2 | Δq (%) |
|---------------|------|--------|--------|-------|----------------|
| RT | -0.6 | 0.0543 | 6.1262 | 0.97 | 3.15 |
| CBT | -0.6 | 0.0562 | 7.9306 | 0.98 | 2.30 |
| PBTD | -0.6 | 0.0487 | 7.2358 | 0.98 | 3.96 |
| PBTU | -0.6 | 0.0542 | 7.7046 | 0.96 | 3.44 |
| EBT | -0.6 | 0.0591 | 7.8806 | 0.95 | 4.02 |
| PBT | -0.6 | 0.0643 | 7.644 | 0.91 | 5.02 |
| DCB | -0.6 | 0.0450 | 4.0728 | 0.99 | 0.74 |
| HE3 | -0.6 | 0.0708 | 8.1937 | 0.98 | 2.91 |

On the basis of the calculated values of Δq and R^2 tabulated in Table 4.3, the proposed model was capable of fitting the experimental drop size data over a broad range of experimental conditions for different impellers. Figure 4.12 illustrates the graphical evaluation of this model for different impellers. The surface obtained from the global fitting of the aforementioned model to the experimental data shows that the experimental data are described well for all dispersed phase fractions and impeller type when the dimensionless drop size plotted according to the proposed model used.

University of Malaya

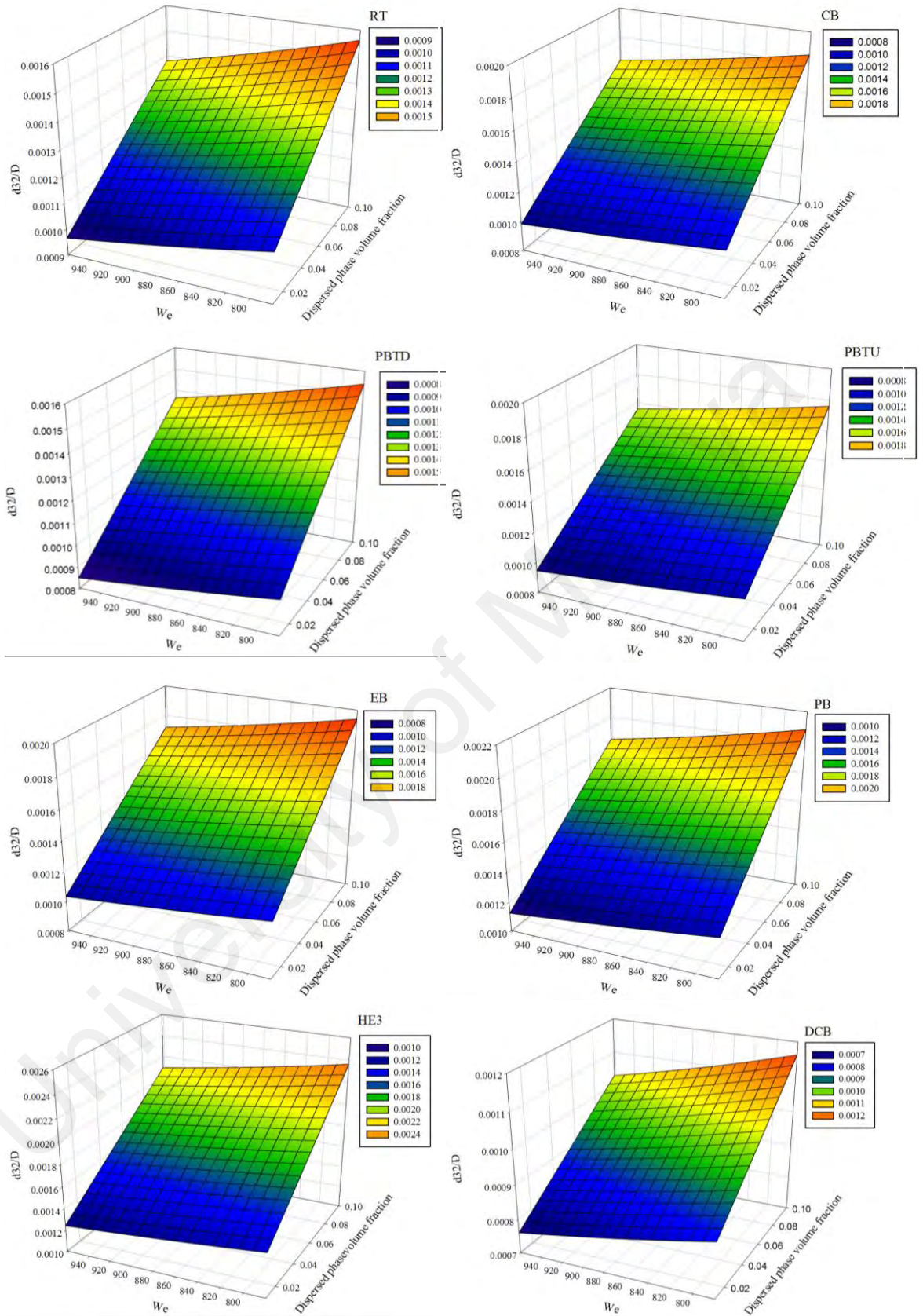


Figure 4.12: Graphical evaluation of the proposed drop size correlation for different impellers

4.4 Mass Transfer Study

4.4.1 Evaluation of mass transfer coefficient in non-reactive system

Figure 4.13 presents the effect of impeller blade design on the interfacial area, a , in different dispersed phase volume fraction. Radial flow impellers like Rushton turbine are commonly employed for liquid-liquid system due to their stronger radial flow which resulted in smaller droplet sizes and higher interfacial area (Jasinska et al., 2013). Therefore, the size of interfacial area for each impeller is explained by the size of droplets. The interfacial area for the DCB is much larger than the other impellers in all tested dispersed phase volume fractions due to smaller drop sizes while the HE3 was the lowest because of larger drop sizes. Hydrofoil impeller obtained 36-50% lower interfacial area compared to the DCB whereas for the PBTD was about 10-23% lower. The performance of CB was slightly better than the curved design elliptical and parabolic. In the case of a low dispersed phase volume fraction, the interfacial area is increased by increasing the dispersed phase volume fraction, though the drop size values are increased. The same trends were observed for the interfacial area in other dispersed phase volume fractions. The outcomes of this part clearly proved the suitability of double curved blade impeller in higher dispersed phase fractions while the hydrofoil impellers like HE3 are especially good for low dispersed phase systems.

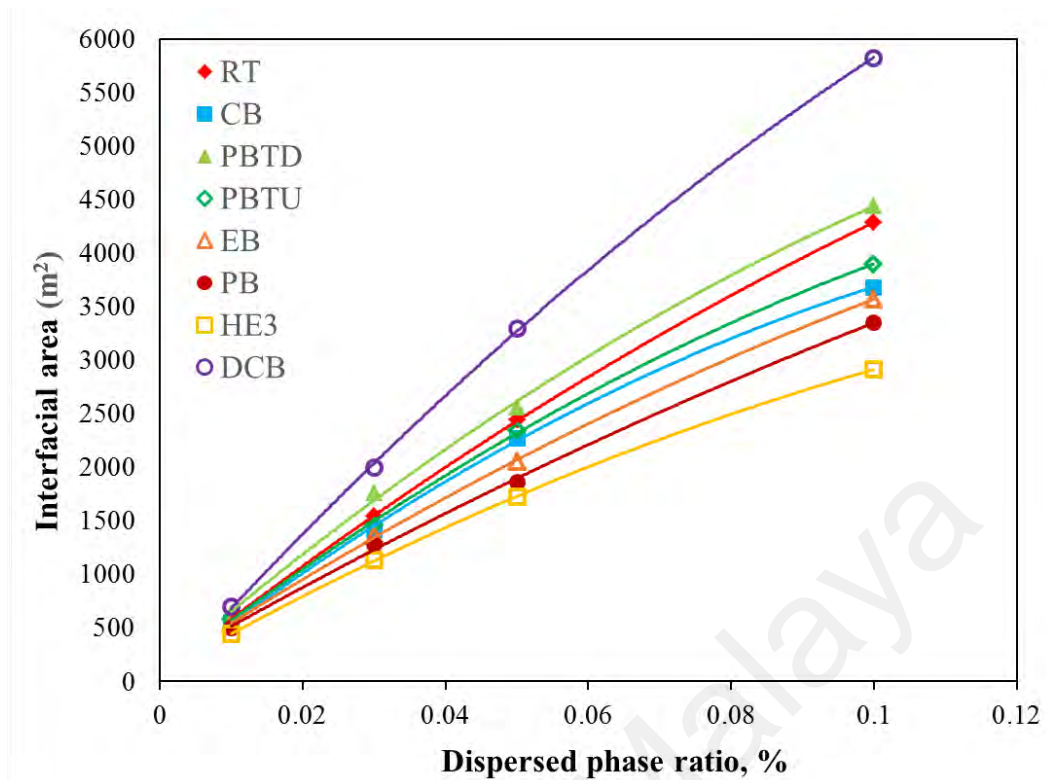


Figure 4.13: The effect of different impeller designs on interfacial area in oil-in-water system with different dispersed phase volume fraction at $\epsilon = 0.16 \text{ m}^2/\text{s}^3$

The values of mass transfer coefficients were calculated through correlation 2.29. Figure 4.14 presents the mass transfer coefficients (k_L) for all studied impeller in a system of oil-water with different ratio of dispersed phase volume fraction at the same energy dissipation rate ($\epsilon = 0.16 \text{ m}^2/\text{s}^3$). In this work the larger interfacial area for the DCB resulted in higher mass transfer coefficient while the lowest one obtained for the HE3. Mass transfer coefficient was obtained in a range of $0.84\text{-}1.08 \times 10^{-5} \text{ (m}\cdot\text{s}^{-1}\text{)}$ for all impellers at 1% oil volume fraction. The calculated mass transfer values were in a good agreement with the literature (Chapman et al., 1974; Zaldívar et al., 1996). The highest mass transfer coefficient was obtained for the DCB and PBTU at 1.08×10^{-5} and $1.011 \times 10^{-5} \text{ (m}\cdot\text{s}^{-1}\text{)}$, respectively. The k_L values for the RT, PBTU, CB, EB, PB and HE3 were 8.76%, 9.15%, 11.93%, 13.27%, 17.00%, and 21.95% lower, correspondingly. The same trends were obtained for the other dispersed phase fractions. The effect of interfacial area and droplet sizes are very significant due to the equal power

consumption and slight changes in physical properties in all experiments. The blade design has a considerable effect on the droplet size and interfacial area, subsequently. Moreover, Figure 4.14 represents considerable reduction in mass transfer coefficient after 3% volume fractions. The k_L values did not show significant differences between the impellers in 10% oil fractions. Although, the interfacial areas were larger in the higher volume fractions, the physical properties play an important role in mass transfer coefficient. The water-oil diffusivity were decreased slightly in higher dispersed phase volume fraction in addition to bigger drop size values which resulted in lower mass transfer coefficients.

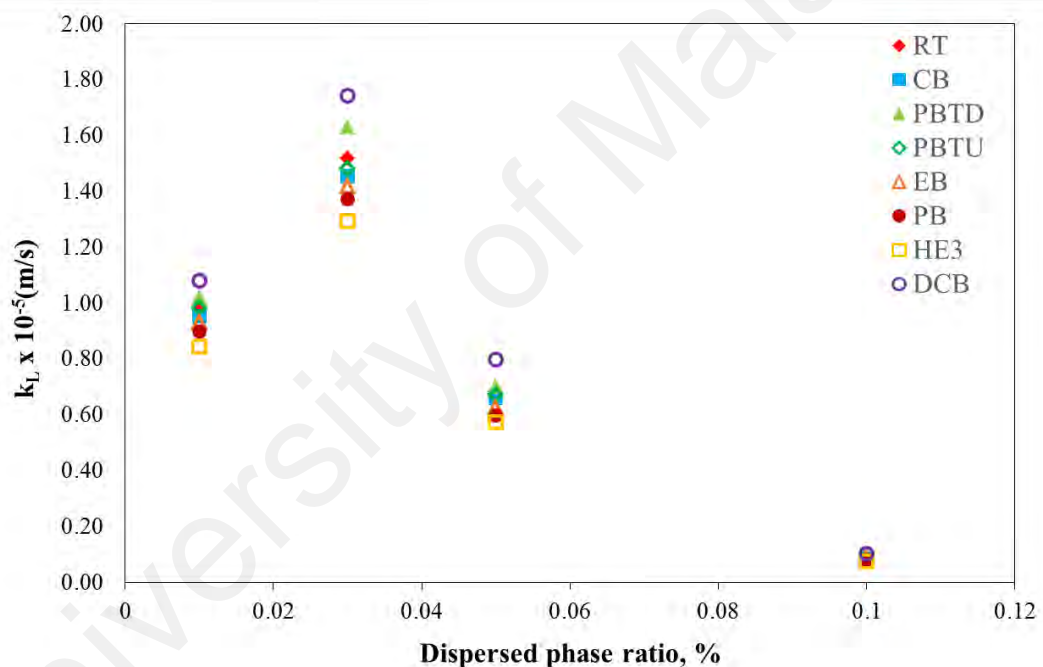


Figure 4.14: The effect of different impeller designs on mass transfer coefficient in oil-in-water system with different dispersed phase volume fraction at $\epsilon = 0.16 \text{ m}^2/\text{s}^3$

4.4.2 Impeller Performance in a Typical Reactive System

4.4.2.1 The effect of impeller type on the reaction rate

Figure 4.15 shows the effect of impeller type on the rate of FFA production in a tank. The values were obtained during two hours reaction in a mixture of 1% oil and water at the same energy dissipation rate, $\epsilon = 0.16 \text{ m}^2/\text{s}^3$. The power consumption for each

impeller was measured and controlled during the process. The agitation speeds for each impeller were set to perform the experiment under the same power consumption. The same energy dissipation rate was selected to follow the effect of impeller type and blade shape on production rate. The FFA concentration increased sharply until 70th minutes for most of the impellers but the rate of reaction increased slowly thereafter. The highest FFA concentration rate was obtained at 0.55×10^{-3} Kmol/m³ in 80 minutes for the double curved blade impeller. The Pitched blade down flow turbine was reached to nearly the same concentration in around 100 minutes. The same FFA concentration point was obtained for the RT and PBTU after 110 and 120 minutes, respectively. The CB, EB and PB are just reached to the concentration of 0.52×10^{-3} , 0.47×10^{-3} and 0.46×10^{-3} Kmol/m³ after 120 min reactions, respectively. The lowest FFA concentration was obtained for the HE3 at 0.39×10^{-3} Kmol/m³ after 120 min reactions. The double curved blade impeller has larger swept area and made longer residence time of vortices at impeller tip, the larger distance between the upper and lower vortices and the longer period. The bigger radial velocity and radial jet for the RT than all radial curved shape impellers caused higher production rate for the RT. In the case of hydrofoil impeller, the flow stream is not strong enough to transfer the reactant within the tank and resulted in lower production rate. Furthermore, the results clearly indicate a reduction in the FFA production rate for the radial flow impellers as the blade turns more curved. The trend of plot became linear for the PB and whereas it was quadratic for the other impellers. Therefore, it can be concluded that the reaction rate time for the DCB and PBTU is shorter than the other impellers.

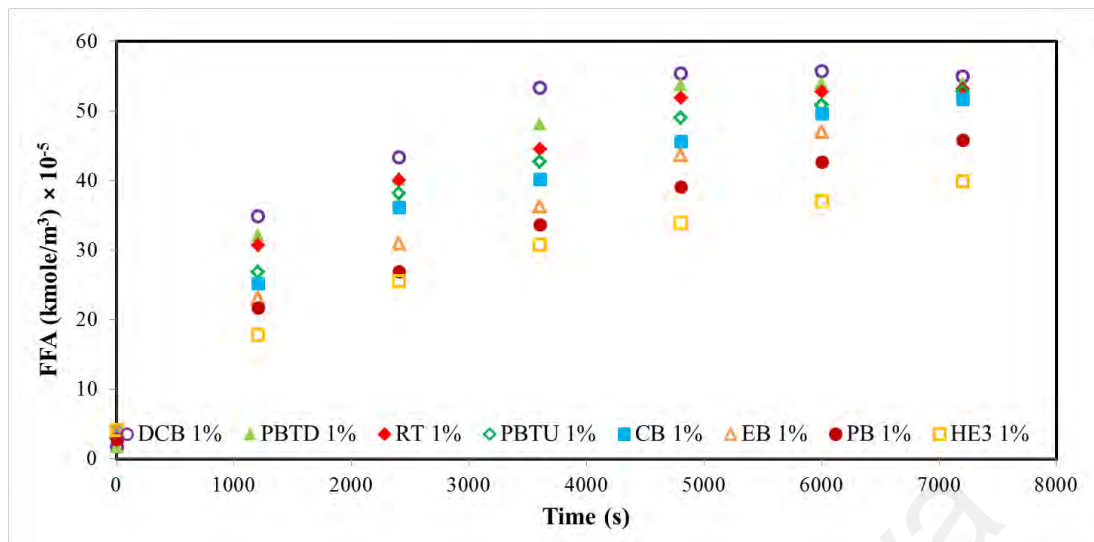


Figure 4.15: the rate of FFA production for 1% oil in water mixture; Vs. time for various impellers: ○ DCB; ▲ PBTD; ◆ RT; ◇ PBTU; ■ CB; △ EB; ● PB; □ HE3 at $\epsilon=0.16 \text{ m}^2/\text{s}^3$

4.4.2.2 The effect of dispersed phase volume fraction on the reaction rate

The effects of different dispersed phase volume fraction on the reaction rate for the impellers used are presented in Figure 4.16 and 4.17. Initially, the oil fraction was varied from 1% to 5%. In this range of dispersed phase volume fraction, the rate of hydrolysis changed linearly with oil volume fraction. The same trends were reported by Warner et al. (1984) for the hydrolysis of tallow, coconut oil and olive oil and later by Noor et al. (2003) (Linfield et al., 1984; Noor et al., 2003). The graphs clearly show an increase in hydrolysis rate with increasing the substrate volume fraction from 1% to 5% at a given energy dissipation rate. The increase in hydrolysis rate is explained by larger interfacial area due to the higher substrate concentration (Al-Zuhair et al., 2003). Comparing figure 4.15, 4.16 and 4.17 verifies the similar trend for all impellers at different oil fraction.

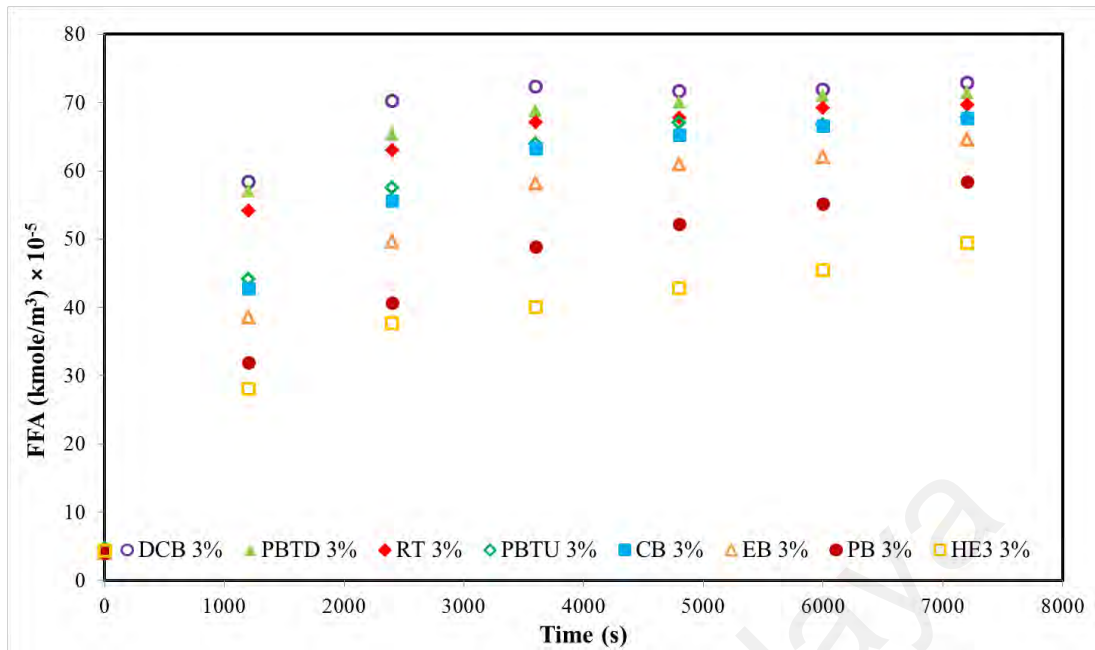


Figure 4.16: the rate of FFA production for 3% oil in water mixture; Vs. time for various impellers: ○ DCB; ▲ PBDT; ◆ RT; ◇ PBTU; ■ CB; △ EB; ● PB; □ HE3 at $\epsilon=0.16 \text{ m}^2/\text{s}^3$

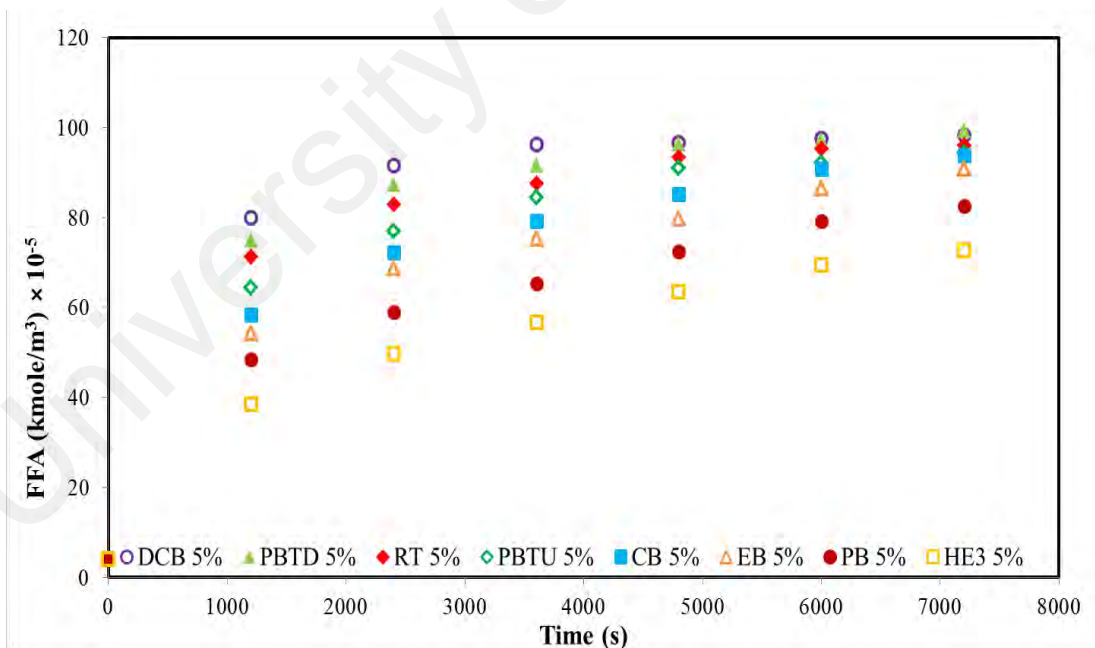


Figure 4.17: the rate of FFA production for 5% oil in water mixture; Vs. time for various impellers: ○ DCB; ▲ PBDT; ◆ RT; ◇ PBTU; ■ CB; △ EB; ● PB; □ HE3 at $\epsilon=0.16 \text{ m}^2/\text{s}^3$

4.4.3 Evaluation of mass transfer coefficient in reactive system

The values of mass transfer coefficients for the reactive system were also evaluated through correlation 2.29. Figure 4.18 demonstrates the mass transfer coefficients (k_L) for all studied impeller in a system with hydrolysis reaction. Different ratio of dispersed phase volume fraction in a range of 1-5% v/v were tested at the same energy dissipation rate ($\epsilon=0.16 \text{ m}^2/\text{s}^3$). The results proved 6-10% reduction in calculated mass transfer coefficients compared to the non-reactive systems. It could be predicted because of higher kinematic viscosity and density which causes reduction in diffusivity and lower mass transfer rate. The higher coefficient was calculated for DCB and the lowest one was obtained for the HE3 in a range of $0.78 \times 10^{-5} \text{ (m.s}^{-1}\text{)}$ to $0.11 \times 10^{-5} \text{ (m.s}^{-1}\text{)}$. This proves a considerable effect of blade design on mass transfer rate because of changes in the droplet size and interfacial area, subsequently. Figure 4.18 were also presents significant reduction in mass transfer coefficient after 3% volume fractions. This is because of reduction in diffusivity because of higher viscosity in higher dispersed phase fraction.

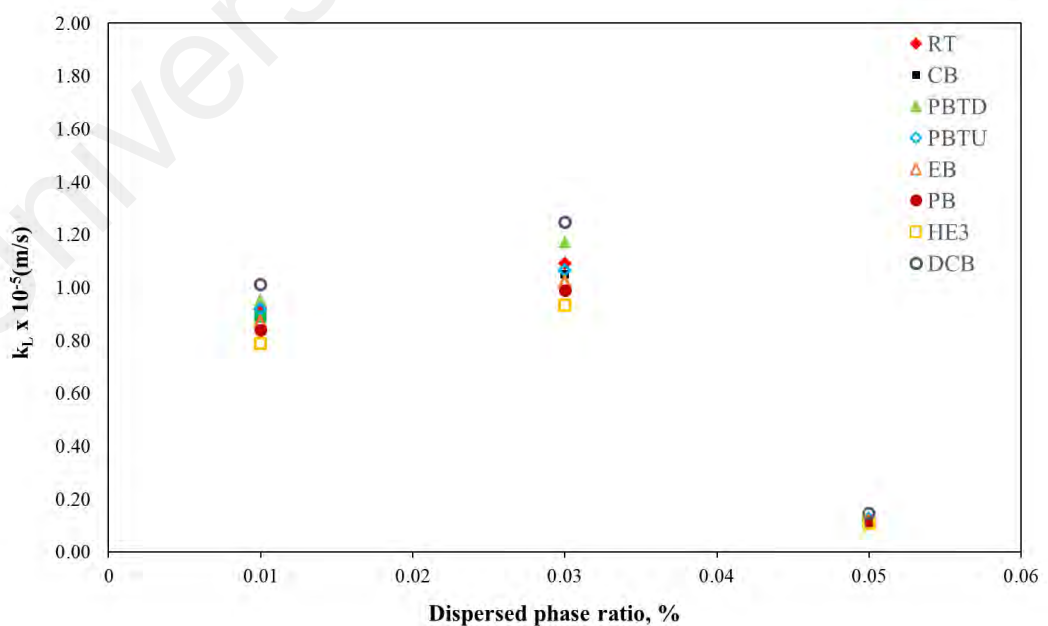


Figure 4.18: The effect of different impeller designs on mass transfer coefficient in a reactive system with different dispersed phase volume fraction at $\epsilon = 0.16 \text{ m}^2/\text{s}^3$

4.4.3.1 Kinetic Modeling

The reaction rate constants k_1 and k_2 , in the mathematical model are determined numerically from the experimental results. Table 4.4 presents the reaction rate constants for all studied impellers with varying oil volume fraction. The presented data show that the higher k_2 values comparing to the k_1 values cause decreasing in the reaction rate which is in a good agreement with experimental results. Figure 4.19 also represents the comparison between the model and experimental data for 1% dispersed phase volume fractions. As shown, good agreement between the experimental results and predicted results is achieved. The other graphs can be found through the appendix. The results for the reaction rate constant showed higher rate for the DCB and PBTB, respectively.

Table 4.4: The reaction rate constants for used impellers with varying oil volume fraction

| Oil fraction Impeller | 1% | | 3% | | 5% | |
|--------------------------|---------------------------|---------------------------|---------------------------|---------------------------|---------------------------|---------------------------|
| | k_1 (hr ⁻¹) | k_2 (hr ⁻¹) | k_1 (hr ⁻¹) | k_2 (hr ⁻¹) | k_1 (hr ⁻¹) | k_2 (hr ⁻¹) |
| DCB | 77092.63 | 32378.90 | 66079.40 | 62775.43 | 44052.93 | 49339.28 |
| PBTB | 66079.40 | 27753.35 | 55066.16 | 53414.18 | 44052.93 | 49339.28 |
| RT | 44052.93 | 18061.7 | 44052.93 | 44052.93 | 33039.70 | 37995.65 |
| PBTU | 39647.64 | 16652.01 | 37444.99 | 38568.34 | 22026.47 | 25770.96 |
| CB | 44052.93 | 19823.82 | 22026.47 | 22246.73 | 22026.47 | 26211.50 |
| EB | 22026.47 | 7709.26 | 22026.47 | 23348.05 | 68876.21 | 82651.46 |
| PB | 28634.41 | 13744.51 | 60773.13 | 69889.10 | 64824.67 | 86216.81 |
| HE3 | 26431.76 | 14801.78 | 64824.67 | 91402.79 | 40515.42 | 58747.36 |

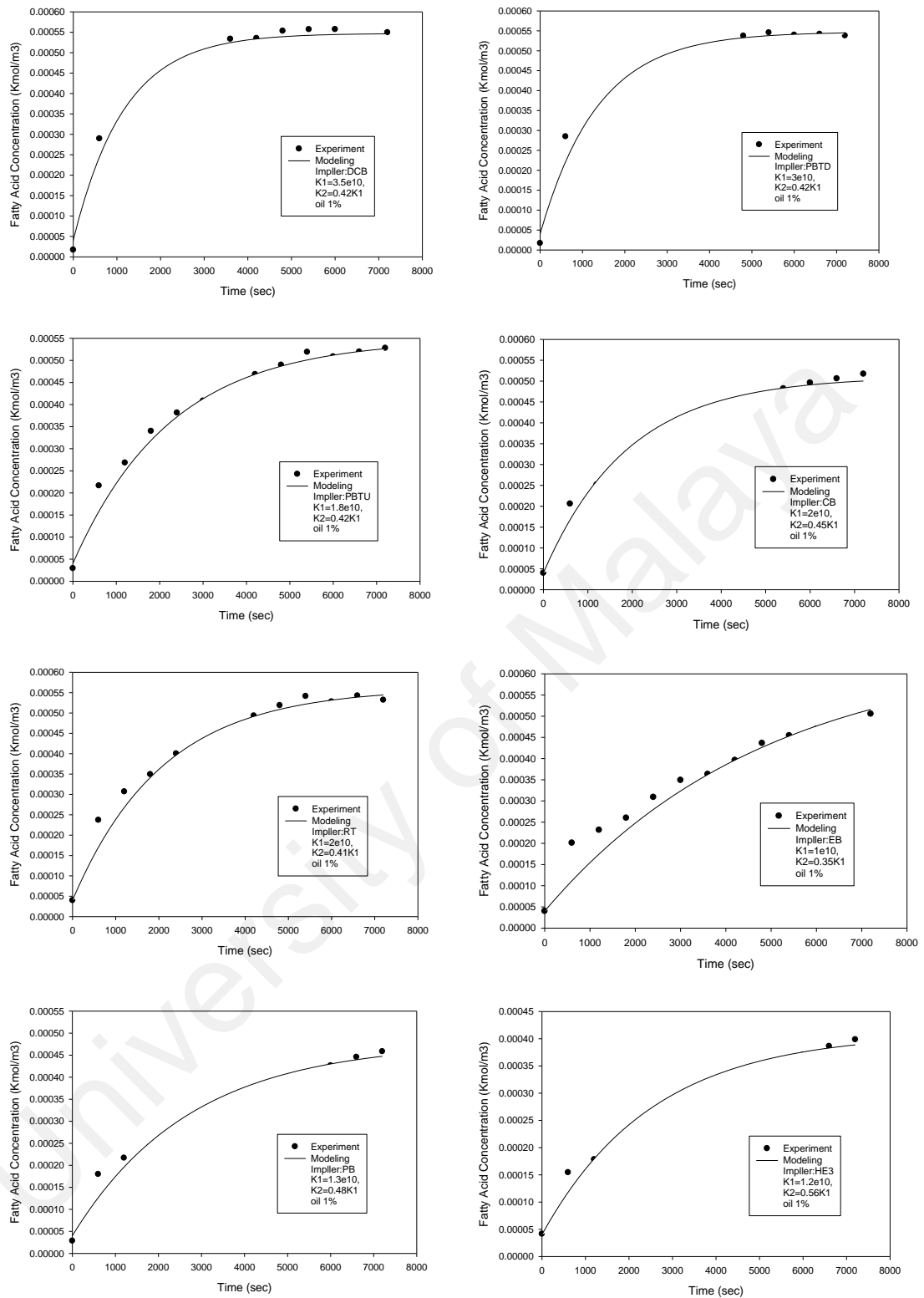


Figure 4.19: Comparison between experimental results and modeling for used impellers at 1% dispersed phase volume fraction

CHAPTER 5: CONCLUSION

5.1 Conclusion

Impeller design is one of the determinant factors in mixing performance for various processes. Therefore, dispersion characteristics of various impellers were studied through power consumption, air entrainment point, mixing time, drop size measurements and mass transfer. Four common impeller types in addition to three rarely used were chosen. A new curved blade impeller design was also developed for further studies. The impeller characterizations were carried out in a single liquid system and the effect of varying impeller speeds, Reynolds number and off-bottom clearance were examined. The water and palm-oil at 1-10% v/v oil content was chosen as a liquid-liquid system. The following conclusions can be extracted from the results:

Objective 1

1. The lowest values of power number (N_p) were obtained for the axial flow impellers including HE3, PBTD and PBTU while the highest power numbers were found for the Radial flow impellers. Moreover, reduction in power consumption was observed for the radial flow impellers as the blade's curvature increased. The lowest power numbers were obtained for the down flow impellers like HE3 and PBTD. Decreasing the off-bottom clearance from T/3 to T/6 led to lower power numbers for the up flow impellers, whereas an increase was observed for the downward flow impellers. In lower clearances, the impeller output flow hits the tank bottom and changes the flow direction significantly, consequently leading to higher energy dissipation rate in down flow impellers.
2. The result for air entrainment speed (N_E) showed that the DCB and RT reached to N_E very fast while HE3 did not reach to the N_E even after 20 rps. This is

because of strong flow in radial flow impellers. The Lowest required power to reach the N_E was obtained for the PBTD.

3. The mixing times decreased inversely with an increase in the agitation speed. The DCB turbine reached the desired mixing point at lower Reynolds numbers while this time was to 4 times higher than the HE3 due to lower discharge rate within the tank. In the case of radial flow impellers, when the blade becomes more curved a weaker radial jet and higher mixing times were obtained for the elliptical and parabolic blade turbines in comparison with curved blade and Rushton turbine. The mixing times increased with a decreasing in the clearance from $T/3$ to $T/6$, for the down flow impellers, due to generation of smooth flow and lower circulation velocity within the tank.
4. The results confirmed that the axial-flow impellers with downward flow direction like pitched blade down-flow turbine and hydrofoil impeller are more efficient in single phase liquid mixing compared to the radial-flow turbines.

Objective 2

1. A proposed model is capable of fitting the experimental mixing time data over a broad range of experimental conditions for different impellers.

Objective 3

1. The DCB and then PBTD reached the equilibrium points faster than the other impellers at the same power consumption.
2. In the case of radial flow impellers, 10% smaller drop sizes were obtained for the impellers with smaller curvature angle in radial flow impellers. Increasing the curvature angle causes larger swept volume, and more turbulence and flow

intensity around the blades zone. Increasing the dispersed phase volume fraction results in larger d_{32} due to higher collision rate between drops. The impellers with larger swept volumes and higher flow intensity like DCB, PBTD and RT can increase the rate of drop breakages.

3. General semi empirical correlation was developed to correlate impeller type, Webber number and dispersed phase volume fraction. The obtained values for the constants proved lower coalescence rate in a system with DCB while the HE3 showed higher coalescence rate.

Objective 3

1. Higher mass transfer rate was obtained for the DCB and PBTD at the same power consumption due to smaller drop sizes and larger interfacial area. The k_L values for the RT, PBTU, CB, EB, PB and HE3 were 8.76%, 9.15%, 11.93%, 13.27%, 17.00%, and 21.95% respectively lower than DCB.
2. In the case of reactive system, the highest production rate was obtained for the DCB and the PBTD. The FFA production rate for the radial flow impellers reduced with increasing curvature angle.
3. The close results for the DCB and PBTD are because of higher flow intensity around their blades zones. Double curved blade design provided larger swept volume and therefore, more turbulence around the impeller zone which resulted in better turbulence within the tank. Although, the swept volume in the PBTD is not as much as DCB, the high flow intensity under the impeller blades leads to better impeller pumping within the tank.
4. It can be stated that the axial down flow impellers are more energy efficient impellers, if they are providing the flow with enough kinetic energy within the

tank. Therefore, the HE3 impeller is just suitable for long term circulation in lower speeds and low dispersed phase volume fraction. It can also be a good choice for processes which need slow bulk motion. However, the novel double curved blade impeller can be a good alternative for processes with higher dispersed phase fraction.

5.2 Recommended future works

Designing the new type of impellers to achieve the highest performance in lower power consumption is compulsory for all processes involve with mixing systems. In this work one typical system was selected for the experimental studies. But, there are still many aspects which need to be further developed in the near future. Some of the recommendations for future works are as follow;

1. An investigation on the effects of impeller design on flow pattern can be carried out in order to find out the flow direction through the tank and also impeller swept volume. Moreover, computation fluid dynamic (CFD) can be applied to predict the mechanism of swept volume and flow pattern within the stirred vessels.
2. In this work, the experimental works were carried out and the obtained data was used to evaluate the mass transfer rate within the stirred tank. Mass transfer coefficient can be found out through the modeling study considering to all power consumption, drop size and physical properties.
3. Theoretical study to scale-up liquid-liquid system in a stirred-tank can be conducted to develop industrial mixing processes. This will be generated variable data to proceed successful industrial mixing process.

REFERENCES

- Abdul Aziz, A. R., Nik Meriam, N. S., Shaliza, I., & Vasanthi, S. (2007). Bubble size distribution: comparison between six-bladed curve blade impeller and Rushton Turbine. *Malaysian Journal of Chemical Engineering*, 1, 163-170.
- Ajeel, M. A., Aroua, M. K., & Daud, W. M. A. W. (2015). p-Benzoquinone Anodic Degradation by Carbon Black Diamond Composite Electrodes. *Electrochimica Acta*, 169, 46-51
- Al-Zuhair, S. (2006). Kinetics of hydrolysis of tributrine by lipase. *Journal of Engineering Science and Technology*, 1, 50-58.
- Al-Zuhair, S., Ramachandran, K. B., & Hasan, M. (2003). *Enzymatic Hydrolysis of Palm Oil in a Stirred Liquid-Liquid Reactor*. Paper presented at the Seminar Penyelidikan Jangka Pendek, University Malaya, Malaysia.
- Al-Zuhair, S., Ramachandran, K. B., & Hasan, M. (2004). High enzyme concentration model for the kinetics of hydrolysis of oils by lipase. *Chemical Engineering Journal*, 103, 7-11.
- Alopaeus, V. (2001). *Calculation of multicomponent mass transfer between dispersed and continuous phases*. (PhD), Helsinki University of Technology, Helsinki.
- Amanullah, A., Serrano-Carreón, L., Castro, B., Galindo, E., & Nienow, A. W. (1998). The influence of impeller type in pilot scale Xanthan fermentations. *Biotechnol. Bioeng.*, 57, 95-108.
- Angle, C. W., & Hamza, H. A. (2006a). Drop sizes during turbulent mixing of toluene-heavy oil fractions in water. *AIChE Journal*, 52, 2639-2650.
- Angle, C. W., & Hamza, H. A. (2006b). Predicting the sizes of toluene-diluted heavy oil emulsions in turbulent flow Part 2: Hinze-Kolmogorov based model adapted for increased oil fractions and energy dissipation in a stirred tank. *Chemical Engineering Science*, 61, 7325-7335.
- Arai, K., Konno, M., Matunga, Y., & Saito, S. (1977). Effect of dispersed-phase viscosity on the maximum stable drop size for break-up in turbulent flow. *Journal of Chemical Engineering Japan*, 10, 325-330.
- Ascanio, G., Castro, B., & Galindo, E. (2004). Measurement of Power Consumption in Stirred Vessels--A Review. *Chemical Engineering Research and Design*, 82, 1282-1290.
- Aubin, J., Mavros, P., Fletcher, D. F., Bertrand, J., & Xuereb, C. (2001). Effect of Axial Agitator Configuration (Up-Pumping, Down-Pumping, Reverse Rotation) on Flow Patterns Generated in Stirred Vessels. *Chemical Engineering Research and Design*, 79(8), 845-856.
- Azizi, F., & Al Taweel, A. M. (2012). Inter-phase mass transfer in turbulent liquid-liquid dispersions: A comparative analysis of models. *Chemical Engineering Journal*, 179, 231-241.

- Bart, H.-J. (2003). Reactive extraction in stirred columns - a review,. *Chemical Engineering Technology*, 26, 723-731.
- Beck, K. J. (1998). Mechanisms of drop break-up in stirred vessels using a sawtooth impeller. (PhD thesis), Cranfield University, UK.
- Bhattacharya, S., Hebert, D., & Kresta, S. M. (2007). Air Entrainment in Baffled Stirred Tanks. *Chemical Engineering Research and Design*, 85(5), 654-664.
- Biggs, R. D. (1963). Mixing rates in stirred tanks. *AIChE Journal*, 9(5), 636-640.
- Birch, D., & Ahmed, N. (1996). Gas sparging in vessels agitated by mixed flow impellers. *Powder Technology*, 88(1), 33-38.
- Bourne, J. R. (2003). Mixing and the Selectivity of Chemical Reactions. *Organic Process Research & Development*, 7(4), 471-508.
- Boxall, J. A., Koh, C. A., Sloan, E. D., Sum, A. K., & Wu, D. T. (2011). Droplet Size Scaling of Water-in-Oil Emulsions under Turbulent Flow. *Langmuir*, 28(1), 104-110.
- Boyadzhiev, L., & Elenkov, D. (1966). On the mechanism of liquid-liquid mass transfer in a turbulent flow field. *Chemical Engineering Science*, 21(11), 955-959
- Boye, A. M., Lo, M. Y. A., & Shamlou, P. A. (1996). The effect of two-liquid phase rheology on drop breakage in mechanically stirred vessels. *Chemical Engineering Communications*, 143(1), 149 - 167.
- Brown, D. E., & Pitt, K. (1974). Effect of impeller geometry on drop break-up in a stirred liquid-liquid contactor. *Chemical Engineering Science*, 29(2), 345-348.
- Bujalski, W., Nienow, A. W., Chatwin, S., & Cooke, M. (1987). The dependency on scale of power numbers of Rushton disc turbines. *Chemical Engineering Science*, 42(2), 317-326.
- Buwa, V., Dewan, A., Nassar, A. F., & Durst, F. (2006). Fluid dynamics and mixing of single-phase flow in a stirred vessel with a grid disc impeller: Experimental and numerical investigations. *Chemical Engineering Science*, 61(9), 2815-2822.
- Calabrese, R. V., Chang, T. P. K., & Dang, P. T. (1986). Drop breakup in turbulent stirred-tank contactors. Part I: Effect of dispersed-phase viscosity. *AIChE Journal*, 32(4), 657-666.
- Calabrese, R. V., Wang, C. Y., & Bryner, N. P. (1986). Drop breakup in turbulent stirred-tank contactors. Part III: Correlations for mean size and drop size distribution. *AIChE Journal*, 32(4), 677-681.
- Calderbank, P. H., & Korchinski, I. J. O. (1956). Circulation in liquid drops: (A heat-transfer study). *Chemical Engineering Science*, 6(2), 65-78.
- Calderbank, P. H., & Moo-Young, M. B. (1961). The continuous phase heat and mass transfer properties of dispersions. *Chemical Engineering Science*, 16, 39-54.

- Calderbank, P. H., & Moo-Young, M. B. (1995). The continuous phase heat and mass transfer properties of dispersions. *Chemical Engineering Science*, 50(24), 3921-3934.
- Camurdan, M. C., Baird, I. M. H., & Taylor, P. A. (1989). Steady state hydrodynamics and mass transfer characteristics of a Karr extraction column. *Canadian Journal of Chemical Engineering*, 67, 554-559.
- Carlucci, G. (2010). Drop size distributions in stirred liquid/liquid systems - Influence of the dispersed phase. (MSc), Technische Universität Berlin, Berlin.
- Chapman, J. W., Cox, P. R., & Strachan, A. N. (1974). Two phase nitration of toluene III. *Chemical Engineering Science*, 29, 1247-1251.
- Chatzi, E. G., Boutris, C. J., & Kiparissides, C. (1991). On-line monitoring of drop size distributions in agitated vessels: 2. Effect of stabilizer concentration. *Industrial & Engineering Chemistry Research*, 30(6), 1307-1313.
- Chen, J. P., Higgins, F. B., Chang, S.-Y., & Hung, Y.-T. (2005). Mixing *Physicochemical Treatment Processes*, 3, 47-101.
- Chen, Z. D., & Chen, J. J. J. (1999). Comparison of Mass Transfer Performance for Various Single and Twin Impellers. *Chemical Engineering Research and Design*, 77(2), 104-109.
- Chen, Z. D., & Chen, J. J. J. (2000). A study of agitated gas-liquid reactors with concave blade impellers. *Paper presented at the Mixing and crystalization, Malaysia*.
- Clift, R., Grace, J. R., & Weber, M. E. (1978). Bubbles, Drops, and Particles. *Academic Press: New York*.
- Coker, A. K. (2001). Fluid Mixing in Reactors *Modeling of Chemical Kinetics and Reactor Design* (552-662). Woburn: Gulf Professional Publishing.
- Cooke, M., & Heggs, P. J. (2005). Advantages of the hollow (concave) turbine for multi-phase agitation under intense operating conditions. *Chemical Engineering Science*, 60(20), 5529-5543.
- Crimaldi, J. (2008). Planar laser induced fluorescence in aqueous flows. *Experiments in Fluids*, 44(6), 851-863.
- Cussler, E. L. (1997). *Diffusion Mass Transfer in Fluid Systems* (Vol. 3). New York: Cambridge University Press.
- Daglas, D., & Stamatoudis, M. (2000). Effect of Impeller Vertical Position on Drop Sizes in Agitated Dispersions. *Chemical Engineering & Technology*, 23(5), 437-440.
- Danckwerts, P. V. (1951). Significance of Liquid-Film Coefficients in Gas Absorption. *Industrial & Engineering Chemistry*, 43(6), 1460-1467.
- Davies, J. T. (1985). Drop sizes of emulsions related to turbulent energy dissipation rates. *Chemical Engineering Science*, 40(5), 839-842.

- Deshmukh, N. A., & Joshi, J. B. (2006). Surface Aerators. *Chemical Engineering Research and Design*, 84(11), 977-992.
- Distelhoff, M. F. W., Marquis, A. J., Nouri, J. M., & Whitelaw, J. H. (1997). Scalar mixing measurements in batch operated stirred tanks. *The Canadian Journal of Chemical Engineering*, 75(4), 641-652.
- Doran, P. M. (1995). Fluid Flow and Mixing *Bioprocess Engineering Principles* (pp. 129-163). London: Academic Press.
- Edwards, M. F., Baker, M. R., Godfrey, J. C., N. Harnby, M. F. Edwards, & Nienow, A. W. (1997). Mixing of liquids in stirred tanks *Mixing in the Process Industries* (pp. 137-158). Oxford: Butterworth-Heinemann.
- El-Hamouz, A. (2007). Effect of Surfactant Concentration and Operating Temperature on the Drop Size Distribution of Silicon Oil Water Dispersion. *Journal of Dispersion Science and Technology*, 28(5), 797-804.
- El-Hamouz, A. (2009). Drop Size Distribution in a Standard Twin-Impeller Batch Mixer at High Dispersed-Phase Volume Fraction. *Chemical Engineering & Technology*, 32(8), 1203-1210.
- El-Hamouz, A., Cooke, M., Kowalski, A., & Sharratt, P. (2009). Dispersion of silicone oil in water surfactant solution: Effect of impeller speed, oil viscosity and addition point on drop size distribution. *Chemical Engineering and Processing*, 48(2), 633-642.
- Fentiman, N. J., St.Hill, N., Lee, K. C., Paul, G. R., & Yianneskis, M. (1998). A Novel Profiled Blade Impeller for Homogenization of Miscible Liquids in Stirred Vessels. *Chemical Engineering Research and Design*, 76(7), 835-842.
- Fernandes, J. B., & Sharma, M. M. (1967). Effective interfacial area in agitated liquid-liquid contactors. *Chemical Engineering Science*, 22(10), 1267-1282.
- Foo, K. Y., & Hameed, B. H. (2010). Insights into the modeling of adsorption isotherm systems. *Chemical Engineering Journal*, 156(1), 2-10.
- Gäbler, A., Wegener, M., Paschedag, A. R., & Kraume, M. (2006). The effect of pH on experimental and simulation results of transient drop size distributions in stirred liquid-liquid dispersions. *Chemical Engineering Science*, 61(9), 3018-3024.
- Gavhane, K. A. (2009). *Chemical Reaction Engineering II*: Nirali Prakashan.
- Giapos, A., Pachatouridis, C., & Stamatoudis, M. (2005). Effect of the Number of Impeller Blades on the Drop Sizes in Agitated Dispersions. *Chemical Engineering Research and Design*, 83(12), 1425-1430.
- Giles, J. W., Hanson, C., & Marshland, J. G. (1971). *Drop size distribution in agitated liquidliquid systems with simultaneous interphase mass transfer and chemical reaction*. Paper presented at the Proceedings of International Solvent Extraction Conference, The Hague, Netherlands.
- Glen, J. B. M. (1965). *Mass Transfer in Disperse Systems*. (Ph.D.), University of Canterbury, Christchurch, New Zealand.

- Grenville, R. K., & Nienow, A. W. (2004). Blending of Miscible Liquids *Handbook of Industrial Mixing* (pp. 507-542): John Wiley & Sons, Inc.
- Grober, H. (1925). *Vereines Deutscher Ingenieure.*, 69, 705.
- Haghdoust, A., Dehkordi, A. M., Darbandi, M., Shahalami, M., & Saien, J. (2011). Combined Model of Mass-Transfer Coefficients for Clean and Contaminated Liquid-Liquid Systems. *Industrial & Engineering Chemistry Research*, 50(8)
- Henschke, M., & Pfennig, A. (1999). Mass-transfer enhancement in single-drop extraction experiments. *AIChE Journal.*, 45, 2079-2086.
- Higbie, R. (1935). The rate of absorption of a pure gas into a still liquid a during short period of exposure. *Transactions of AIChE*, 31, 365-389.
- Hines, A. L., and Maddox, R. N. (1985). *Mass Transfer: Fundamentals and Applications*. New Jersey: Prentice Hall.
- Hinze, J. O. (1955). Fundamentals of the hydrodynamic mechanism of splitting in dispersion processes. *AIChE Journal*, 1(3), 289-295.
- Hiraoka, S., Yamada, I., Tada, Y., Mori, H., Narita, N., Suzuki, H., Aragaki, T. & Park, Y.T., (1990). Measurement of continues-phase mass transfer coefficient at droplet surface in liquid-liquid mixing vessel by chemical reaction method. *Journal of Chemical Engineering of Japan* , 23(2), 166-170.
- Houcine, I., Plasari, E., & David, R. (2000). Effects of the Stirred Tank's Design on Power Consumption and Mixing Time in Liquid Phase. *Chemical Engineering Technology*, 23(7), 605-613.
- Hu, B., Fishwick, R. P., Pacek, A. W., Winterbottom, J. M., Wood, J., Stitt, E. H., & Nienow, A. W. (2007). Simultaneous measurement of in situ bubble size and reaction rates with a heterogeneous catalytic hydrogenation reaction. *Chemical Engineering Science*, 62, 5392-5396.
- Hu, Y., Liu, Z., Yang, J., Jin, Y., & Cheng, Y. (2010). Study on the reactive mixing process in an unbaffled stirred tank using planar laser-induced fluorescence (PLIF) technique. *Chemical Engineering Science*, 65(15), 4511-4518.
- Ibemere, S. (2005). *Dissolution kinetics of liquid-liquid dispersions using local rates of turbulent dissipation*. (MSc dissertation), University of Alberta, Canada.
- Ibemere, S., & Kresta, S. (2007). Modelling the Mixing and Dissolution Kinetics of Partially Miscible Liquids. *Chemical Engineering Research and Design*, 85(5), 710-720.
- Jahoda, M., Mostek, M., Kukuková, A., & Machon, V. (2007). CFD Modelling of Liquid Homogenization in Stirred Tanks with One and Two Impellers Using Large Eddy Simulation. *Chemical Engineering Research and Design*, 85(5), 616-625.
- Jakobsen, H. A. (2008). Agitation and Fluid Mixing Technology *Chemical Reactor Modeling* (pp. 679-755): Springer Berlin Heidelberg.

- Jasinska, M., Baldyga, J., Cooke, M., & Kowalski, A. (2013). Investigations of mass transfer with chemical reactions in two-phase liquid-liquid systems. *Chemical Engineering Research and Design*.
- Jasińska, M., Bałdyga, J., Cooke, M., & Kowalski, A. J. (2012). *Investigations of mass transfer and micromixing effects in two-phase liquid-liquid systems with chemical reaction*. Paper presented at the 14th European Conference on Mixing Warszawa.
- Karcz, J., & Kaminska -Brzoska, J. (1994). *Heat transfer in a jacketed stirred tank equipped with baffles and concave disk impeller*. Paper presented at the Eighth European Conference on Mixing, UK.
- Karcz, J., & Major, M. (1998). An Effect of a Baffle Length on the Power Consumption in an Agitated Vessel. *Chemical Engineering and Processing*, 37(3), 249-256.
- Keey, R. B., & Glen, J. B. (1969). Area-free mass transfer coefficients for liquid extraction in a continuously worked mixer. *AIChE Journal*, 15(6), 942-947.
- Khang, S. J., & Levenspiel, O. (1976). New scale-up and design method for stirrer agitated batch mixing vessels. *Chemical Engineering Science*, 31(7), 569-577.
- Khare, A. S., & Niranjana, K. (1999). An experimental investigation into the effect of impeller design on gas hold-up in a highly viscous Newtonian liquid. *Chemical Engineering Science*, 54(8), 1093-1100.
- Kichatov, B. V., Korshunov, A. M., Boiko, I. V., & Assorova, P. V. (2003). Effect of Impeller Blade Geometry on Drop Size in Stirring of Immiscible Liquids. *Theoretical Foundations of Chemical Engineering*, 37(1), 19-24.
- Kolmogorov, A. N. (1949). The break-up of droplets in a turbulent stream. *Doklady Akademii Nauk*, 66, 825-828.
- Kraume, M., Gäbler, A., & Schulze, K. (2004). Influence of Physical Properties on Drop Size Distribution of Stirred Liquid-Liquid Dispersions. *Chemical Engineering & Technology*, 27(3), 330-334.
- Kreith, F., & Berger, S. A. (1999). *Fluid Mechanics- Mechanical Engineering Handbook*.
- Kumar, A. (1983). *Droplet behaviour in liquid/liquid extraction*. (PhD), Zurich.
- Kumar, A., & Hartland, S. (1999). Correlations for Prediction of Mass Transfer Coefficients in Single Drop Systems and Liquid-Liquid Extraction Columns. *Chemical Engineering Research and Design*, 77(5), 372-384.
- Kumar, S., Kumar, R., & Gandhi, K. S. (1991). Alternative mechanisms of drop breakage in stirred vessels. *Chemical Engineering Science*, 46(10), 2483-2489.
- Kumaresan, T., Nere, N. K., & Joshi, J. B. (2005). Effect of Internals on the Flow Pattern and Mixing in Stirred Tanks. *Industrial & Engineering Chemistry Research*, 44(26), 9951-9961.

- Laity, D. S., & Treybal, R. E. (1957). Dynamics of liquid agitation in the absence of an air-liquid interface. *AIChE Journal*, 3(2), 176-180.
- Lamberto, D. J., Alvarez, M. M., & Muzzio, F. J. (1999). Experimental and computational investigation of the laminar flow structure in a stirred tank. *Chemical Engineering Science*, 54(7), 919-942.
- Lamberto, D. J., Muzzio, F. J., Swanson, P. D., & Tonkovich, A. L. (1996). Using time-dependent RPM to enhance mixing in stirred vessels. *Chemical Engineering Science*, 51(5), 733-741.
- Lemenand, T., Della Valle, D., Zellouf, Y., & Peerhossaini, H. (2003). Droplets formation in turbulent mixing of two immiscible fluids in a new type of static mixer. *International Journal of Multiphase Flow*, 29(5), 813-840.
- Levenspiel, O. (1972). *Chemical Reaction Engineering*. New York: John Wiley and Sons.
- Linfield, W., Barauskas, R., Sivieri, L., Serota, S., & Stevenson, R. (1984). Enzymatic fat hydrolysis and synthesis. *Journal of the American Oil Chemists' Society*, 61(2), 191-195.
- Liu, S., & Li, D. (1999). Drop coalescence in turbulent dispersions. *Chemical Engineering Science*, 54(23), 5667-5675.
- Lovick, J., Mouza, A. A., Paras, S. V., Lye, G. J., & Angeli, P. (2005). Drop size distribution in highly concentrated liquid-liquid dispersions using a light back scattering method. *Journal of Chemical Technology and Biotechnology*, 80, 545-552.
- Maaß, S., Metz, F., Rehm, T., & Kraume, M. (2010). Prediction of drop sizes for liquid-liquid systems in stirred slim reactors—Part I: Single stage impellers. *Chemical Engineering Journal*, 162(2), 792-801.
- Maaß, S., Paul, N., & Kraume, M. (2012). Influence of the dispersed phase fraction on experimental and predicted drop size distributions in breakage dominated stirred systems. *Chemical Engineering Science*, 76(0), 140-153.
- Maaß, S., Wollny, S., Voigt, A., & Kraume, M. (2010). Experimental comparison of measurement techniques for drop size distributions in liquid/liquid dispersions. *Experiments in Fluids*, 50, 1-11.
- Machado, M. B., Nunhez, J. R., Nobes, D., & Kresta, S. M. (2012). Impeller characterization and selection: Balancing efficient hydrodynamics with process mixing requirements. *AIChE Journal*, 58(8), 2573-2588.
- Mali, R. G., & Patwardhan, A. W. (2009). Characterization of onset of entrainment in stirred tanks. *Chemical Engineering Research and Design*, 87(7), 951-961.
- Masiuk, S., & Rakoczy, R. (2007). Power consumption, mixing time, heat and mass transfer measurements for liquid vessels that are mixed using reciprocating multiplates agitators. *Chemical Engineering and Processing: Process Intensification*, 46(2), 89-98.

- Mayr, B., Horvat, P., & Moser, A. (1992). Engineering approach to mixing quantification in bioreactors. *Bioprocess and Biosystems Engineering*, 8(3), 137-143.
- McFarlane, C. M., & Nienow, A. W. (1996). Studies of High Solidity Ratio Hydrofoil Impellers for Aerated Bioreactors. 4. Comparison of Impeller Types. *Biotechnology Progress.*, 12(1), 9-15.
- Mhetras, M. B., Pandit, A. B., & Joshi, J. B. (1994). *Effect of agitator design on hydrodynamics and power consumption in mechanically agitated gas-liquid reactors*. Paper presented at the Eighth European Conference on Mixing, UK.
- Mok, Y. I., & Treybal, R. E. (1971). Continuous-phase mass transfer coefficients for liquid extraction in agitated vessels: II. *AIChE Journal*, 17(4), 916-920.
- Montante, G., Lee, K. C., Brucato, A., & Yianneskis, M. (2001). Numerical simulations of the dependency of flow pattern on impeller clearance in stirred vessels. *Chemical Engineering Science*, 56(12), 3751-3770.
- Montante, G., Mostek, M., Jahoda, M., & Magelli, F. (2005). CFD simulations and experimental validation of homogenisation curves and mixing time in stirred Newtonian and pseudoplastic liquids. *Chemical Engineering Science*, 60(8-9), 2427-2437.
- Moucha, T., Linek, V., & Prokopová, E. (2003). Gas hold-up, mixing time and gas-liquid volumetric mass transfer coefficient of various multiple-impeller configurations: Rushton turbine, pitched blade and techmix impeller and their combinations. *Chemical Engineering Science*, 58(9), 1839-1846.
- Musgrove, M., Ruszkowski, S., Akker, H. E. A. v. d., & Derksen, J. J. (2000). Influence of impeller type and agitation conditions on the drop size of immiscible liquid dispersions *10th European Conference on Mixing* (pp. 165-172). Amsterdam: Elsevier Science.
- Nagata, S. (1975). *Mixing Principles and Applications*. Tokyo: Kodansha Ltd.
- Nienow, A., W. (1996). *Gas-liquid mixing studies : A comparison of Rushton turbines with some modern impellers*. Amsterdam, PAYS-BAS: Elsevier.
- Nienow, A. W. (1997). On impeller circulation and mixing effectiveness in the turbulent flow regime. *Chemical Engineering Science*, 52(15), 2557-2565.
- Nienow, A. W. (2004). Break-up, coalescence and catastrophic phase inversion in turbulent contactors. *Advances in Colloid and Interface Science*, 108-109, 95-103.
- Noh, H. S., & Baird, I. M. H. (1984). Mass transfer and pressure drop in a cocurrent reciprocating plate extraction column. *AIChE Journal*, 30, 120-127.
- Noor, I. M., Hasan, M., & Ramachandran, K. B. (2003). Effect of operating variables on the hydrolysis rate of palm oil by lipase. *Process Biochemistry*, 39(1), 13-20.

- O'Rourke, A. M., & MacLoughlin, P. F. (2005). A comparison of measurement techniques used in the analysis of evolving liquid-liquid dispersions. *Chemical Engineering and Processing*, 44(8), 885-894.
- Ochieng, A., & Onyango, M. S. (2008). Homogenization energy in a stirred tank. *Chemical Engineering and Processing: Process Intensification*, 47(9-10), 1853-1860.
- Ochieng, A., Onyango, M. S., Kumar, A., Kiriamiti, K., & Musonge, P. (2008). Mixing in a tank stirred by a Rushton turbine at a low clearance. *Chemical Engineering and Processing: Process Intensification*, 47(5), 842-851.
- Okufi, S., De Ortiz, E. S. P., & Sawistowski, H. (1990). Scale-up of liquid-liquid dispersions in stirred tanks. *The Canadian Journal of Chemical Engineering*, 68(3), 400-406.
- Pacek, A. W., Chamsart, S., Nienow, A. W., & Bakker, A. (1999). The influence of impeller type on mean drop size and drop size distribution in an agitated vessel. *Chemical Engineering Science*, 54(19), 4211-4222.
- Pacek, A. W., Man, C. C., & Nienow, A. W. (1998). On the Sauter mean diameter and size distributions in turbulent liquid/liquid dispersions in a stirred vessel. *Chemical Engineering Science*, 53(11), 2005-2011.
- Pacek, A. W., Moore, I. P. T., Nienow, A. W., & Calabrese, R. V. (1994). Video technique for measuring dynamics of liquid-liquid dispersion during phase inversion. *AIChE Journal*, 40(12), 1940-1949.
- Papastefanos, N., & Stamatoudis, M. (1989). Effect of impeller and vessel size on impeller power number in closed vessels for Reynolds number between 40 and 65000. *Chemical Engineering Communications*, 80(1), 69 - 79.
- Patil, P., & Kumar, S. (2010). Breakup of drops around the edges of Rushton turbine. *The Canadian Journal of Chemical Engineering*, 88(6), 912-918.
- Patil, S. S., Deshmukh, N. A., & Joshi, J. B. (2004). Mass-Transfer Characteristics of Surface Aerators and Gas-Inducing Impellers. *Industrial & Engineering Chemistry Research*, 43(11), 2765-2774.
- Paul, E. L., Atiemo-Obeng, V. A., & Kresta, S. M. (2004). *Handbook of industrial mixing*: John Wiley & Sons, Inc.
- Podgórska, W. (2009). *Influence of the Impeller Type on Drop Size in Liquid-Liquid Dispersion* Paper presented at the 13th European Conference on Mixing, London.
- Quadros, P. A., & Baptista, C. M. S. G. (2003). Effective interfacial area in agitated liquid-liquid continuous reactors. *Chemical Engineering Science*, 58(17), 3935-3945.
- Raghav Rao, K. S. M. S., & Joshi, J. B. (1988). Liquid phase mixing in mechanically agitated vessels. *Chemical Engineering Communications*, 74(1), 1-25.

- Rajapakse, A. (2007). *Drop Size Distributions and Interfacial Area in Reactive Liquid-Liquid Dispersions*. (Phd), RMIT University, Australia.
- Ranade, V. V., Mishra, V. P., Saraph, V. S., Deshpande, G. B., & Joshi, J. B. (1992). Comparison of axial flow impellers using a laser Doppler anemometer. *Industrial Engineering Chemistry Research*, 31(10), 2370-2379.
- Ravikumar, S. V., & Ghosh, P. (2011). Mass transfer of chlorobenzene in concentrated sulfuric acid. *International Journal of Heat and Mass Transfer*, 54(11), 2245-2252.
- Rewatkar, V. B., & Joshi, J. B. (1991). Effect of impeller design on liquid phase mixing in mechanically agitated reactors. *Chemical Engineering Communications*, 102(1), 1-33.
- Rewatkar, V. B., Rao, K. S. M. S. R., & Joshi, J. B. (1990). Power consumption in mechanically agitated contactors using pitched bladed turbine impellers. *Chemical Engineering Communications*, 88(1), 69 - 90.
- Ribeiro, M. M. M., Guimarães, M. M. L., Madureira, C. M. N., & Cruz Pinto, J. J. C. (2004). Non-invasive system and procedures for the characterization of liquid-liquid dispersions. *Chemical Engineering Journal*, 97(2-3), 173-182.
- Rooney, D., & Weatherley, L. R. (2001). The effect of reaction conditions upon lipase catalysed hydrolysis of high oleate sunflower oil in a stirred liquid-liquid reactor. *Process Biochemistry*, 36(10), 947-953.
- Rushton, J. (1956). Principles of mixing in the fatty oil industries. *Journal of the American Oil Chemists' Society*, 33(11), 598-604.
- S. Maaß, A. Gäbler, M. Wegener, A. Zaccone, A. Paschedag, & M. Kraume. (2007). Drop breakage and daughter drop distributions in stirred liquid/liquid systems and their modelling within the population balance equation. *Chemical Engineering Research and Design*, 85, 703.
- Saito, F., Nienow, A. W., Chatwin, S., & Moore, I. P. T. (1992). Power, gas dispersion and homogenisation characteristics of SCABA SRGT and Rushton turbine impellers. *Journal of Chemical Engineering Japan*, 25, 281-287.
- Sathyagal, A. N., Ramkrishna, D., & Narsimhan, G. (1996). Droplet breakage in stirred dispersions. Breakage functions from experimental drop-size distributions. *Chemical Engineering Science*, 51(9), 1377-1391.
- Schindler, H. D., & Treybal, R. E. (1968). Continuous-phase mass-transfer coefficients for liquid extraction in agitated vessels. *AIChE Journal*, 14(5), 790-798
- Sechremeli, D., Stampouli, A., & Stamatoudis, M. (2006). Comparison of mean drop sizes and drop size distributions in agitated liquid-liquid dispersions produced by disk and open type impellers. *Chemical Engineering Journal*, 117(2), 117-122.
- Shafeeyan, M. S., Daud, W. M. A. W., Shamiri, A., & Aghamohammadi, N. (2015). Adsorption equilibrium of carbon dioxide on ammonia-modified activated carbon. *Chemical Engineering Research and Design*, 104, 42-52.

- Shafeeyan, M. S., Wan Daud, W. M. A., Houshmand, A., & Arami-Niya, A. (2012). The application of response surface methodology to optimize the amination of activated carbon for the preparation of carbon dioxide adsorbents. *Fuel*, *94*, 465-472.
- Shaw, J. A. (1994). Understanding the effects of impeller type, diameter and power on mixing time. *Chemical Engineering Progress.*, 45-48.
- Shiue, S. J., & Wong, C. W. (1984). Studies on homogenization efficiency of various agitators in liquid blending. *Canadian Journal of Chemical Engineering*. *62*, 602-609.
- Sis, H., & Chander, S. (2004). Kinetics of emulsification of dodecane in the absence and presence of nonionic surfactants. *Colloids and Surfaces A: Physicochemical and Engineering Aspects*, *235*, 113-120.
- Sis, H., Kelbaliyev, G., & Chander, S. (2005). Kinetics of Drop Breakage in Stirred Vessels under Turbulent Conditions. *Journal of Dispersion Science and Technology*, *26*(5), 565-573.
- Skelland, A. H. P., & Kanel, J. S. (1992). Simulation of mass transfer in a batch agitated liquid-liquid dispersion. *Industrial & Engineering Chemistry Research*, *31*(3), 908-920.
- Skelland, A. H. P., & Lee, J. M. (1981). Drop size and continuous-phase mass transfer in agitated vessels. *AIChE Journal*, *27*(1), 99-111.
- Skelland, A. H. P., & Moeti, L. T. (1990). Mechanism of continuous-phase mass transfer in agitated liquid-liquid systems. *Industrial & Engineering Chemistry Research*, *29*(11), 2258-2267.
- Skelland, A. H. P., & Xien, H. (1990). Dispersed-phase mass transfer in agitated liquid-liquid systems. *Industrial & Engineering Chemistry Research*, *29*, 415-420.
- Sprow, F. B. (1967). Distribution of drop sizes produced in turbulent liquid-liquid dispersion. *Chemical Engineering Science*, *22*(3), 435-442.
- Srivastava, P., Hahr, O., Buchholz, R., & Worden, R. M. (2000). Enhancement of mass transfer using colloidal liquid aphrons: Measurement of mass transfer coefficients in liquid-liquid extraction. *Biotechnology and Bioengineering*, *70*(5), 525-532.
- Szalai, E. S., Arratia, P., Johnson, K., & Muzzio, F. J. (2004). Mixing analysis in a tank stirred with Ekato Intermig® impellers. *Chemical Engineering Science*, *59*(18), 3793-3805.
- Ting, W. J., Tung, K. Y., Giridhar, R., & Wu, W. T. (2006). Application of binary immobilized *Candida rugosa* lipase for hydrolysis of soybean oil. *Journal of Molecular Catalysis B: Enzymatic*, *42*(1-2), 32-38.
- van't Riet, K., & Smith, J. M. (1973). The behaviour of gas-liquid mixtures near Rushton turbine blades. *Chemical Engineering Science*, *28*(4), 1031-1037.
- van't Riet, K., & Tramper, J. (1991). *Basic Bioreactor Design*, Marcel Dekker.

- van de Vusse, J. G. (1955). Mixing by agitation of miscible liquids Part I. *Chemical Engineering Science*, 4(4), 178-200.
- van Woezik, B. A. A., & Westerterp, K. R. (2000). Measurement of interfacial areas with the chemical method for a system with alternating dispersed phases. *Chemical Engineering and Processing*, 39(4), 299-314.
- Vasquez, V., & Bautista, R. G. (1997). Mass Transfer Correlation Coefficients for Two-Phase Systems: A General Review for Liquid-Liquid. *Mineral Processing and Extractive Metallurgy Review*, 17(1-4), 239-255.
- Wales, S. M. (1989). *Reaction Kinetics for Chemical Engineers*. Boston: Butterworth.
- Wang, C. Y., & Calabrese, R. V. (1986). Drop breakup in turbulent stirred-tank contactors, Part II: Relative influence of viscosity and interfacial tension. *AIChE Journal*, 32, 677-676.
- Warmoeskerken, & Smith, J. M. (1989). The Hollow Blade Agitator for Dispersion and Mass Transfer. *Chem. Eng. Res. Des.*, 67, 193-198.
- Weetman, R. J. a. O., J. Y. (1988). *Power, flow and shear characteristics of mixing impellers*. Paper presented at the Proc 6th Europ Conf on Mixing, Pavia, Italy.
- Wesselingh, J. A. (1975). Mixing of liquids in cylindrical storage tanks with side-entering propellers. *Chemical Engineering Science*, 30(8), 973-981.
- Woziwodzki, S. (2011). Unsteady Mixing Characteristics in a Vessel with Forward-Reverse Rotating Impeller. *Chemical Engineering & Technology*, 34(5), 767-774.
- Woziwodzki, S., Broniarz-Press, L., & Ochowiak, M. (2010). Transitional Mixing of Shear-Thinning Fluids in Vessels with Multiple Impellers. *Chemical Engineering & Technology*, 33(7), 1099-1106.
- Wu, J., Zhu, Y., & Pullum, L. (2001). Impeller Geometry Effect on Velocity and Solids Suspension. *Chemical Engineering Research and Design*, 79(8), 989-997.
- Yapici, K., Karasozen, B., Schäfer, M., & Uludag, Y. (2008). Numerical investigation of the effect of the Rushton type turbine design factors on agitated tank flow characteristics. *Chemical Engineering and Processing: Process Intensification*, 47(8), 1340-1349.
- Yeo, L. Y., Matar, O. K., Perez de Ortiz, E. S., & Hewitt, G. F. (2002). Simulation Studies of Phase Inversion in Agitated Vessels Using a Monte Carlo Technique. *Journal of Colloid and Interface Science*, 248(2), 443-454.
- Young C.H., Korchinsky, W.J. (1989). Modelling drop-side mass transfer in agitated polydispersed liquid-liquid systems. *Chemical Engineering Science*, 44: 2355 – 2361.
- Zadghaffari, R., Moghaddas, J. S., & Revstedt, J. (2009). A mixing study in a double-Rushton stirred tank. *Computers & Chemical Engineering*, 33(7), 1240-1246.

- Zainal Abidin, M. I. I., Abdul Raman, A. A., & Mohamad Nor, M. I. (2014). Experimental Investigations in Liquid-Liquid Dispersion System: Effects of Dispersed Phase Viscosity and Impeller Speed. *Industrial & Engineering Chemistry Research*, 53 6554–6561. doi: 10.1021/ie5002845
- Zaldívar, J. M., Molga, E., Alós, M. A., Hernández, H., & Westerterp, K. R. (1996). Aromatic nitrations by mixed acid. Fast liquid-liquid reaction regime. *Chemical Engineering and Processing*, 35(2), 91-105.
- Zhang, Q., Yong, Y., Mao, Z.-S., Yang, C., & Zhao, C. (2009). Experimental determination and numerical simulation of mixing time in a gas–liquid stirred tank. *Chemical Engineering Science*, 64(12), 2926-2933.
- Zhao, J., Gao, Z., & Bao, Y. (2011). Effects of the Blade Shape on the Trailing Vortices in Liquid Flow Generated by Disc Turbines. *Chinese Journal of Chemical Engineering*, 19(2), 232-242.
- Zhao, W. Q., Pu, B. Y., & Hartland, S. (1993). Measurement of drop size distribution in liquid/liquid dispersion by encapsulation. *Chemical Engineering Science*, 48(2), 219-227.
- Zhao, Y., Li, X., Cheng, J., Yang, C., & Mao, Z.-S. (2011). Experimental Study on Liquid-Liquid Macromixing in a Stirred Tank. *Industrial & Engineering Chemistry Research*, 50(10), 5952-5958.
- Zhou, G., & Kresta, S. M. (1998). Evolution of drop size distribution in liquid-liquid dispersions for various impellers. *Chemical Engineering Science*, 53(11), 2099-2113.

LIST OF PUBLICATION AND PAPERS PRESENTED

Publications

R. Afshar Ghotli, A. R. Abdul Aziz, S. Ibrahim. (2017). Effect of Various Curved-Blade Impeller Geometries on Drop Size in Liquid-Liquid Stirred Vessel. *Chemical Engineering Communications Journal*, 204(8), 884-896. (ISI-Cited Publication, **Impact Factor: 1.297**)

R. Afshar Ghotli, A. R. Abdul Aziz, S. Ibrahim. (2016). The effect of various designs of six-curved blade impellers on reaction rate analysis in liquid-liquid mixing vessel, *Measurement Journal*, 91, 440-450. (ISI-Cited Publication, **Impact Factor: 2.359**)

R. Afshar Ghotli, A. R. Abdul Aziz, S. Ibrahim (2015). A review on liquid-liquid mass transfer studies in various stirred vessel designs, *Reviews in chemical engineering*, 31(4) 329-343. (ISI-Cited Publication, **Impact Factor: 3.157**)

Reza Afshar Ghotli, Shaliza Ibrahim, A.R. Abdul Aziz, Saeid Baroutian, Arash Arami-Niya (2013). Study Of Various Effects Of Curved-Blade Impellers Geometries On Power Consumption In Stirred Vessel Using Response Surface Methodology, *Journal of the Taiwan Institute of Chemical Engineers*, 44(2): 192-201. (ISI-Cited Publication, **Impact Factor: 4.217**)

S.A. Asgharzadehahmadi, M. Davoody, **R. Afshar Ghotli**, A.R. Abdul Aziz, R. Parthasarathy (2015), Effect of ultrasonic irradiations on gas-liquid mass transfer coefficient (KLa); Experiments and modeling. *Measurement Journal*, 79, 119–129. (ISI-Cited Publication, **Impact Factor: 2.359**)

Under Progress Manuscripts

Huiwen,L., **Afshar Ghotli, R.**, Shah, R.S.S.R.E., Abdul Aziz, A. R., Effect of Disc-blade Intercepting Angle on Mixing Performance in Multiphase Stirred Vessel, *Journal of Dispersion Science and Technology*, (ISI-Cited Publication, **Impact Factor: 1.59**), Being drafted.

R. Afshar Ghotli, A. R. Abdul Aziz, S. Ibrahim (2015). Macromixing Study in Liquid phase for Various Designs of Impellers in Stirred Vessel, *Chemical Engineering Research and Design*, (ISI-Cited Publication, **Impact Factor: 2.358**), Being drafted,

Conference proceeding

R. Afshar Ghotli, A.R. Abdul Aziz, Shaliza Ibrahim, The Effect of Curvature Angles and Central Disk Sizes of Six curved Blade Impellers on Liquid-liquid Reaction Through Stirred Vessel, *International Symposium on Mixing in Industrial Processes VIII Conference (ISMIP8), 2014, Melbourne, Australia.*

S. Asgharzadehahmadi, **R. Afshar Ghotli**, A.R. Abdul Aziz, R. Parthasarathy, Gas-Liquid Mass Transfer Study Using Ultrasonic Irradiation Assistance and Response Surface Methodology, *International Symposium on Mixing in Industrial Processes VIII Conference (ISMIP8), 2014, Melbourne, Australia.*

University of Malaya